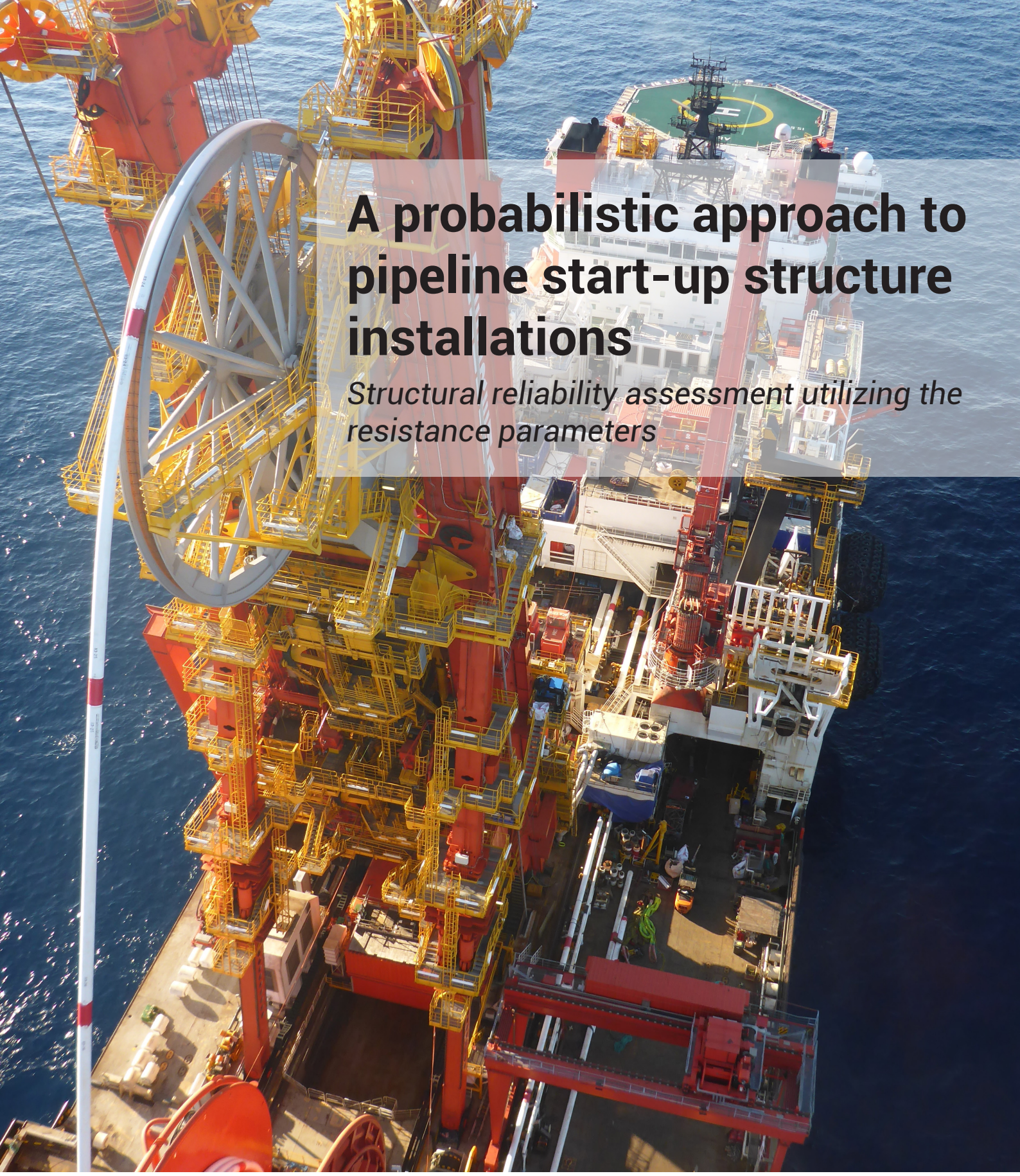

A probabilistic approach to pipeline start-up structure installations

Structural reliability assessment utilizing the resistance parameters

K.A.T.J Franken

Master of Science Thesis TU Delft
In collaboration with Heerema Marine Contractors

HEEREMA MARINE CONTRACTORS

TU Delft

A probabilistic approach to pipeline start-up structure installations

Structural reliability assessment utilizing the resistance parameters

by

K.A.T.J. Franken

to obtain the degree of Master of Science in Offshore & Dredging Engineering,
at the Delft University of Technology

Offshore Engineering Department
Faculty of Mechanical, Maritime and Materials Engineering
Faculty of Civil Engineering and Geosciences

Student number:	4095014	
Project duration:	March 5, 2018 – December 18, 2018	
Thesis committee:	Ir. A.C.M. van der Stap,	TU Delft
	Dr. ir. O. Morales Napoles,	TU Delft
	Ir. J.S. Hoving,	TU Delft
	Ir. H. Smienk,	Heerema Marine Contractors
	Ir. C.F.C. Hoekstra,	Heerema Marine Contractors

An electronic version of this thesis is available at http://repository.tudelft.nl/.

TU Delft

Abstract

Subsea pipeline are extensively used for the transport of hydrocarbons from offshore wells, to platforms, pump stations and to onshore facilities. Because the installation of pipelines is time consuming it is responsible for a significant amount of the total costs of a project. Thus the workability of the installation is of great importance.

When installing a subsea pipeline one always begins with a start-up structure, a FLET (flowline end termination) or PLET (pipeline end termination). The start-up structure is lowered through the moonpool via the pipelay tower until it reaches the seafloor. When it's close to the sea floor the start-up rigging is coupled to the start-up pile with the use of a remote operated vehicle (ROV). Often the moment the start-up structure transitions from a vertical to a horizontal position with respect to the sea floor the loads on the stem pipe become critical with regards to the structural integrity of the pipe. And as such dictates the workability limits of the start-up structure installation. Pipe integrity is maintained via the use of a unity check equation which is described by the design standard DNVGL-ST-F101 issued by Det Norske Veritas Germanischer Loyd (DNVGL). In this equation, the combined loading criterion, the combination of the effective axial tension, the bending moment load and the water depth is evaluated for the structural integrity of the pipe string. The purpose of this thesis is to decrease the conservatism of the equation by probabilistic modelling of the resistance parameters – yield stress, ultimate tensile strength, wall thickness, outer diameter and ovality – instead of using deterministic nominal values and in the end allowing for higher sea states to operate in which in most situations increases the workability. For start-up structure installations DNVGL aims for a target probability of failure of 10^{-3}.

To achieve this first a well-documented load case was found in the Ichthys project. In HMC's pipeline database the 18" Ichthys pipeline project offered 1106 geometrical and material strength pipe line data points. This data set was filtered analysed and used two describe the (bivariate) probability distributions of the resistance parameters. Analysing the data set it was found that the wall thickness and outer diameter and the yield strength and ultimate tensile strength showed a significance correlation. Dependence models have been defined by the use of copula's. A performed sensitivity analysis showed that in the shallow water case, which the Ichthys project is, modelling the ovality as a stochastic variable has no significance influence on the outcome of the unity check. To assess the benefits of probabilistic modelling of the resistance parameters in a more general sense the base case Ichthys situation is altered to four different load scenario's. Two shallow water cases and two deep water cases. For shallow and deep water, one case with the original sea state, in which the unity check is below 1. And one case in which the significant wave height is increased to push the unity check value to its limit of 1. After the input, the (bi-variate) probability distributions, and the test cases were defined the sample size for the Monte Carlo was determined to be $3 \cdot 10^6$ samples to guarantee the accuracy similar to what is used in current installation analyses.

Performing the Monte Carlo simulations the results showed the expected conservatism in the current method. Where DNVGL aims for a probability of failure of 10^{-3}, the probability of failure in the base case was calculated to be 10^{-5}. Which allowed for fine tuning and decreasing the safety class resistance factor used in the equation by 3% in the shallow water case and up to 5% in the deep water case. Which makes it possible to operate in heavier sea states and thus increases the workability of a start-up structure installation in certain situations.

Contents

Glossary

API	American Petroleum Institute
BIC	Bayesian information criterion
CDF	Cumulative distribution function
CRA	Corrosion resistant alloy
DCC	Displacement controlled condition
DCV	Deep water construction vessel
DNVGL	Det Norske Veritas Germanischer Loyd
FEM	Finite element method
FLET	Flowline end termination
HMC	Heerema Marine Contractors
ISO	International Organization for Standardization
KDE	Kernel density estimation
KWRL	Key weather risk list
LCC	Load controlled condition
LRFD	Load resistance factor design
LSD	Limit state design
ODE	Offshore & Dredging Engineering
pdf	Probability density function
PoF	Probability of failure
RP	Recommended practice
SMTS	Specified minimum tensile strength
SMYS	Specified minimum yield stress
SAF	Strain amplification factor
SCR	Steel catenary riser
SRA	Structural reliability assessment

Nomenclature

α_c	Flow stress parameter (DNVGL)
α_U	Material strength factor (DNVGL)
α_{fab}	Fabrication factor (DNVGL)
β	Factor used in combined loading criteria (DNVGL)
δ	Ovality (API)
γ_A	Load effect factor for accidental load (DNVGL)
γ_c	Condition load factor (DNVGL)
γ_E	Load effect factor for environmental load (DNVGL)
γ_F	Load effect factor for functional load (DNVGL)
γ_m	Material resistance factor (DNVGL)
$\gamma_{SC,LB}$	Partial safety factor, local buckling (DNVGL)
ν	Poisson ratio
σ_l	Longitudinal stress (ISO)
σ_y	Specified minimum yield strength (SMYS) at maximum design temperature (ISO)
σ_a	Axial stress in the pipe wall (API)
σ_{hp}	Circumferential stress, or hoop stress, due to fluid pressure only (ISO)
σ_h	Circumferential stress (ISO)
τ	Shear stress (ISO)
ε	Allowable bending strain in the pipe (API)
ε_1	Maximum installation bending strain (API)
ε_b	Buckling strain under pure bending (API)
A	Cross-sectional area of pipe steel (API)
A_i	Internal cross-sectional area of the pipe (API)
A_o	External cross-sectional area of the pipe (API)
D	Pipe diameter (DNVGL)
D_o	Nominal outside diameter (ISO)
E	Young's modulus
f_1	Bending safety factor for installation bending plus external pressure (API)
f_h	Hoop-stress design factor (ISO)
f_u	Characteristic material tensile strength (DNVGL)

f_y	Characteristic material yield stress (DNVGL)
f_c	Collapse factor for use with combined pressure and bending loads (API)
f_o	Collapse factor (API)
$f_{u,temp}$	De-rating value of tensile strength due to temperature (DNVGL)
$f_{y,temp}$	De-rating value of yield stress due to temperature (DNVGL)
$g(\delta)$	Collapse reduction factor (API)
H_s	Significant wave height
M_A	Accidental load moment (DNVGL)
M_E	Environmental load moment (DNVGL)
M_F	Functional load moment (DNVGL)
M_I	Interference load moment (DNVGL)
$M_p(t)$	Plastic capacity against bending moment (DNVGL)
M_{Sd}	Design moment load effect (DNVGL)
O_0	Ovality (DNVGL)
P_c	Collapse pressure (API)
$p_c(t)$	Characteristic collapse pressure (DNVGL)
P_e	Elastic collapse pressure (API)
p_e	External pressure (DNVGL)
$p_p(t)$	Plastic collapse pressure (DNVGL)
P_y	Yield pressure at collapse (API)
P_c	Collapse pressure of the pipe (API)
$p_{el}(t)$	Elastic collapse pressure (DNVGL)
p_{id}	Design pressure (ISO)
P_i	Internal pressure in the pipe (API)
P_i	Internal pressure in the pipe(API)
p_{min}	Minimum internal pressure (DNVGL)
p_{od}	Minimum external hydrostatic pressure (ISO)
P_o	External hydrostatic pressure (API)
S_A	Accidental load effective axial force (DNVGL)
S_E	Environmental load effective axial force(DNVGL)
S_F	Functional load effective axial force (DNVGL)
S_I	Interference load effective axial force (DNVGL)
$S_p(t)$	Plastic capacity against effective axial force (DNVGL)
$S_{Sd}(p_i)$	Design effective axial force load effect (DNVGL)

$SMTS$	Specified minimum tensile strength (DNVGL)
$SMYS$	Specified minimum yield stress (DNVGL)
t	Wall thickness (DNVGL)
T_a	Axial (material) tension in pipe (API)
T_{eff}	Effective tension in pipe (API)
t_{min}	Specified minimum wall thickness (ISO)
T_p	Peak wave period
T_y	Yield tension of the pipe (API)

List of Figures

List of Tables

1

Introduction

1.1. General background

Heerema Marine Contractors is a world leading marine construction company for the oil, gas and renewable energy industry and is specialized in design, transportation, installation and removal of all types of fixed and floating offshore structures. HMC owns and operates her own fleet including the world's largest semi-submersible crane vessel Thialf, deep water construction vessel (DCV) Aegir, DCV Balder, anchor handling tugs, supply vessels, cargo/launch barges and other equipment required for offshore activities. Both DCV Aegir and DCV Balder are equipped with deep water pipe lay equipment and are depicted in figure 1.1.

(a) DCV Aegir (b) DCV Balder

Figure 1.1: HMC's pipelaying vessels

With the DCV Aegir and the DCV Balder, Heerema is capable to install subsea pipes with a diameter size of up to 32" and reach depths of 3500m.

Considering the current offshore market conditions, a relatively low oil price and a setback in investments of 44% from 2014 to 2016 [11] it is a necessity to research possibilities to increase the company's competitiveness. To support cost calculations and to guarantee the safety during the entire offshore process, weather conditions are incorporated in workability predictions for the pipe-lay vessel. In related literature different definitions of the term workability can be found. In this report however, it is defined as the statistically expected percentage of time in which a certain offshore operation can be executed safely under the given conditions of a certain location. The workability is dependent on the operability limits. Operability is the ability to keep a piece of equipment, a system or a whole industrial installation in reliable functioning conditions, according to pre-defined operational requirement. The operability limits are based on limitations of pipe integrity, equipment limits and deck handling. In offshore situations these operability limits are characterized by operable

weather conditions and pipe integrity limits are translated to limiting weather conditions. More specifically HMC calculates vessel operability limits using a combination of significant wave height (H_s) and peak wave wave period (T_p). Given a project's location the workability can be determined. The first step in this process is gathering the project dependant data; metocean data of the location, equipment limits and client specific specifications. The metocean data is then deduced to a representative simplification of the situation which consists of combinations of significant wave heights, peak wave periods and wave directions. This is used as input for the dynamic and static analyses to calculate and optimize the operability limits for every step of the installation process. Pipeline installation analyses generally involve the use of finite element method (FEM) based software packages specialized on stress calculations in pipelines. In this analyses the sea states determine if the pipe integrity or equipment limits are exceeded - what these limits are is defined by the design standard that is used and will be discussed in chapter 2. If the limits are exceeded the values of H_s and T_p are lowered until all values are acceptable. The results of these analyses get summarized in the key weather risk list (KWRL) in which, for each step of the installation, a maximum H_s and T_p is defined. So in combination with the metocean scatterplot of the project's location - which gives a percentage of occurrence of a H_s/T_p combination per month or year - the workability of each operation can be determined. With a low workability the number of 'waiting on weather days' will be high and this results in a higher price for the operation. Increasing operability limits will in most cases increase the workability of an operation and will thus result in increasing the competitiveness of HMC's business. A block diagram of the workability calculation is depicted in figure 1.2, note that optimization of this process often occurs.

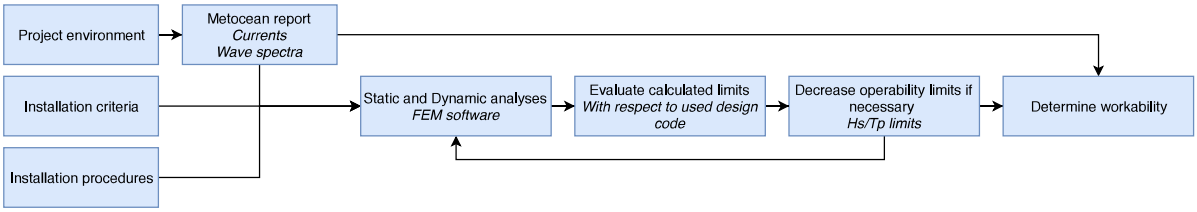

Figure 1.2: Block diagram workability calculation

1.2. Problem description

The installation of a pipeline consists of different phases. Having installed many of these pipelines it is known that from the entire installation, the start-up structure installation is often one of the most critical steps in the process. Therefore this research focuses on methods to increase the installation workability for pipeline start-up structure installations, also known as 1st end structure installations. A start-up structure, or 1st-end structure, is a pipeline end manifold (PLEM), pipeline end termination (PLET) or flowline end termination (FLET) and a integral part of the pipeline system. The difference between a manifold and termination depends on if the structure splits the product flow into multiple routes or if it terminates the flowline or pipeline and serves as a an attachment point for a subsea jumper, a short pipe connector that connects two subsea components.

The purpose of this master thesis is to develop a structural reliability assessment (SRA) for a pipeline start-up structure installation analysis. And hereby determine a less conservative approach opposed to current methods. From experience it is known that these installations are often limited by the pipeline integrity in which fatigue and local buckling limit states are governing. With regards to local buckling the peak loading occurs in the stem pipe, the first part of the pipeline after the start-up structure, the step the start-up structure is lowered through the splash zone or during the transition from lowering and installing the start-up structure to normal pipe lay. These two situations are depicted in figure 1.3a. The critical steps with respect to local buckling are during phase 1 or during the transition from phase 3 to normal lay. In 1.3b a close up of this transition can be found.

The limit state, the condition of the pipeline beyond which it is no longer fulfills the design criteria, for local buckling is dictated by the design standard that is used. Even in the most

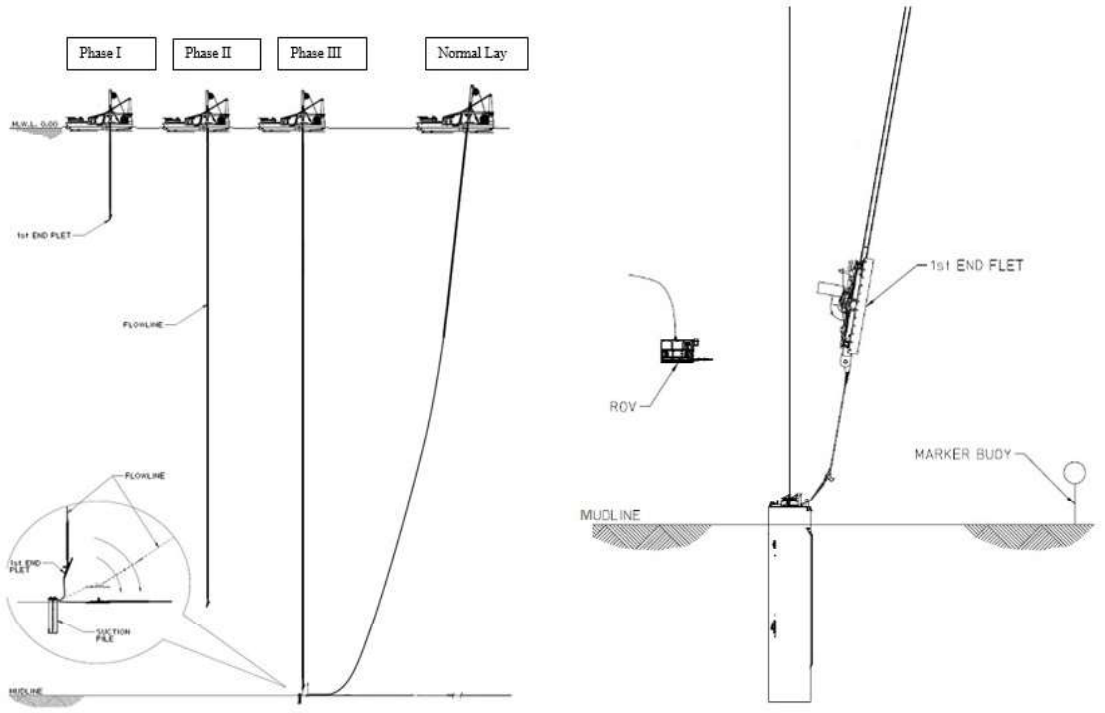

(a) Lowering of the start-up structure (b) Close-up of 1st end flet hooked onto the start-up pile

Figure 1.3: Schematic start- up structure installation

installation analysis the pipeline capacity is only based on a general approach for pipeline integrity which should be applicable for all situations. Therefore being conservative in certain situations. Reducing the conservatism in the dictated approach will increase operability limits and could increase installation workability without violating the pipeline integrity for an acceptable probability of failure (PoF), which is defined by the design code.

1.3. Research Objective

The goal of this graduation thesis is to develop a structural reliability assessment for pipeline start-up structure installations and determine the benefit of the increased workability compared to the existing methodology for the pipeline integrity check.

1.3.1. Research question

Aiming for a less conservative methodology the following general research question can be stated:

What is the benefit of a structural reliability analyses regarding the workability of a pipeline start-up structure installation with respect to the general methodologies?

Which in turn raises the following support questions:

- What phase during the start-up structure installation is critical for the considered limit state local buckling?
- How can the start-up structure installation analyses benefit from probabilistic modelling of the resistance parameters?

1.4. Problem approach

To reach the goal of this research, improving the workability of start-up structure installations, the following approach is taken towards the problem.

1. Understand and study current methodology used by HMC to perform the start-up structure installations analyses.
2. Investigate the possibilities of improving the existing method by using the data from previous projects which are gathered in HMC's pipeline database.
3. Select a study case which can serve as the load case for the research to make sure there is sufficient data for a full statistical analyses and for which results can be compared.
4. Develop a SRA and implement the findings from point 2.
5. Verify and compare the SRA with the conventional method and specify the benefits.

1.5. Report outline

In the following chapter the results of the literature study can be found and the main topics regarding subsea pipeline installation and the statistical concepts used in this research are discussed. In the third chapter the current methods regarding start-up structure installation analyses are explained and the study case is elaborated on. The data set corresponding to the determined study case is examined in the fourth chapter. In this part of the report the input for the structural reliability assessment will be defined. In the fifth chapter the structural reliability assessment is carried out. The results and conclusions and recommendations can be found in chapter six and seven respectively.

2

Literature study

In the following chapter all knowledge gathered during the literature study is presented. Two main topics can be distinguished, in sections 2.1 to 2.3 the main topics regarding sub-sea pipeline installation are discussed, installation methods, failure mechanisms and design standards. Section 2.4 to 2.10 contain information about the statistical and probabilistic concepts used in the rest of the report.

2.1. Pipeline installation methods

The most commonly used installation methods for offshore pipelines are the following:

- S-lay (shallow to deep)
- J-lay (intermediate to deep)
- Reel-lay (intermediate to deep)

The major difference between the three methods is the way in new pipe sections get connected to the pipeline and how these enter the water. In the following subsections each method will be discussed.

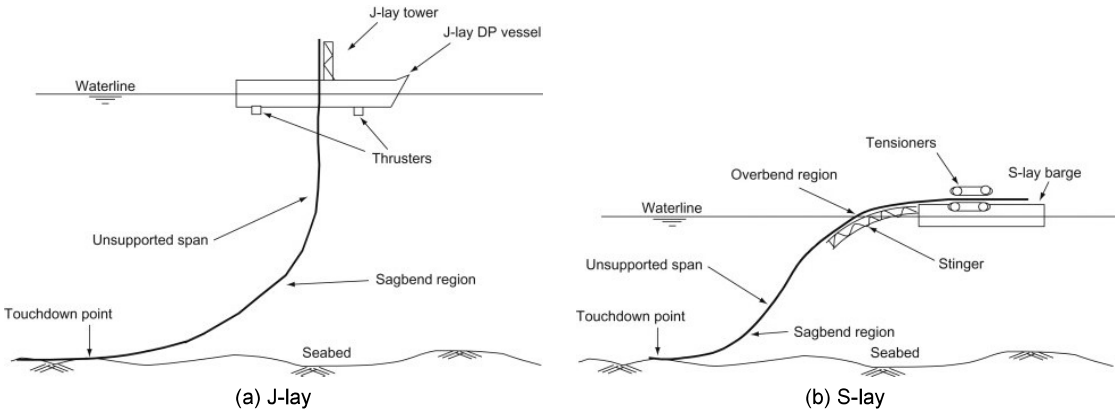

Figure 2.1: Installation methods [8]

2.1.1. S-lay method

Using the S-lay method pipe joints are welded to the pipeline in a horizontal position. The pipeline is guided to the seabed via a stinger in which the bending radius is controlled. This maintains pipe bending in the elastic range. The pipe is lowered using tensioners. The main advantages of the S-lay configuration is that the horizontal set-up allows for multiple work stations which increases the production rate. Opposed to reel-lay in S-lay no plastic bending

of the pipe will occur. Disadvantages of the S-lay method are the necessary long stinger that's required, especially with large diameter pipes and/or when laying in deep water. Besides the stinger the vessel also needs a large thrust when laying in deep water which results in high fuel costs for the operation. The vessels of HMC are not equipped with S-lay configuration equipment.

2.1.2. J-lay method

In the J-lay configuration new pipe sections get welded to the pipeline in an inclined position, corresponding to the top angle of the pipe catenary to the seabed. The pipe is lowered with a traveling block using friction clamps (light J-lay) or collars (heavy J-lay). If friction clamps are sufficient to hold the pipe depends on the pipe diameter, wall thickness and the water depth. Advantages of the J-lay method are the fact that no or a significantly smaller stinger is used. And similar to S-lay the pipe only bends in the elastic region. Because of single stage welding and coating the production rate of a J-lay pipe vessel is significantly lower. Another disadvantage of J-lay are the needed collars on the pipe or friction clamps which result in higher costs. In shallow water the tower angle needs to be adjusted to make sure that the pipe in the sagbend area only bends in the elastic region. This results in a higher pulling force from the pipeline and requires more trust and thus fuel for a shallow water pipelay operation opposed to deep water. Both HMC's DCV Balder as well as DCV Aegir are equipped with a J-lay pipelay tower.

2.1.3. Reel-lay method

Large lengths of pipe are welded onshore and spooled onto vertical reels directly on board the vessel, or the reels can be changed and transferred from the spool base to the vessel. During pipelay the pipe is unspooled from the reel and before it enters the water it gets straightened. Hardly any welding, coating and non destructive testing s performed on board, only when the reels are changed, which results in a very high production rate. Another advantage of the reel-lay method is the fact that all welding onshore is done under very easy to control circumstances in comparison to welding offshore. The disadvantage of reel-lay are the need for a dedicated spool base for pipe preparation, the fact that the pipe is bend plastically and the incapability of laying concrete coated pipes. Only the DCV Aegir is capable of pipelaying with the reel-lay method for HMC.

2.2. Failure mechanisms

A pipeline system during it's entire lifetime is subjected to threats that can cause failure of the pipeline, such as external impact, for example dropping anchors or trawling fishnets, mechanical defects that cause fracture or rupture, corrosion and natural hazards. Because of the large variety of threats and naming all in this research would result in trivial sections this report focuses on failure mechanisms that occur during offshore pipeline installation. When all the failure mechanisms that need to be taken into account for pipeline installation, considering the different design standards, are summarized the following mechanisms come into play.

DNVGL

- Fatigue
- Fracture
- System collapse
- Local buckling

API

- Combined bending and tension during installation

- Buckling and collapse due to combined bending and external pressure
- Pipeline stability against horizontal and vertical displacement
- Fatigue affects during construction

ISO

- Yielding
- Buckling
- Fatigue

2.2.1. Buckling

Local buckling of a pipeline is the buckling behaviour within the pipeline's cross section. Buckling is defined as the state of a structure for which a relatively small increment in load leads to a relatively large increment in displacement.

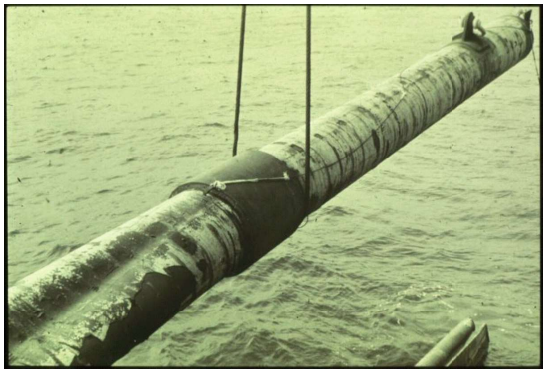

Figure 2.2: Buckled pipe

2.2.2. Fatigue failure

Fatigue is the weakening of a specific material caused by cyclic loading. Fatigue occurs when a material is subjected to repeated loading and unloading and if these loads are above a certain threshold, eventually microscopic cracks will start to occur. Overtime, when cyclic loading continues, the crack will propagate until a critical size is reached at which the material fractures.

From HMC's extensive background in pipelaying it is known that fatigue and local buckling are the two types of failure mechanisms that will govern the installation process. Which one of these mechanisms is indeed limiting depends on the project details. For instance, in shallow water the wall thickness of a pipeline can be smaller than in deeper water because it does not need to sustain the high external pressures that are inherent to the deep sea. Given the smaller wall thickness however, it is more prone to fatigue since the amount of stress cycles it can sustain will be a lot smaller than in the deep water case. **In this research the situations in which local buckling is governing are optimized.**

2.3. Design standards

Several internationally accepted design codes are used for the design of subsea pipelines. These include but are not limited to:

- API RP 1111; Design, Construction, Operation and Maintenance of Offshore Hydrocarbon Pipelines (Limit State Design) [2]
- ISO 13623; Petroleum and natural gas industries - Pipeline transportation systems [12]

- DNVGL-ST-F101; Submarine pipeline systems [6]

Which are written by the American Petroleum Institute (API), the International Organization for Standardization (ISO) and Det Norske Veritas Germanischer Loyd (DNVGL) respectively. API is a US based national trade association representing all facets of the oil and natural gas industry. One of it's missions is to promote safety across the industry globally and it is doing so by developing petroleum, natural gas and petrochemical equipment and operating standards. ISO is an independent, non-governmental organization based in Geneva with a membership of 162 national standards bodies. To support innovation and provide solutions to global challenges it brings together experts to share knowledge and develop voluntary, consensus-based, market relevant International Standards. DNVGL is a global quality assurance and risk management company and provides classification, technical assurance, software and data management services to customers across a wide range of industries. Which one of these standards is used depends on the clients wishes. All standards are constantly revised and updated to improve the quality and to stay up to date with the latest innovations in the industry. HMC is one of the contributors to the present 2017 DNVGL-ST-F101 version and has been contributing since the first version in 1996. In the following subsections the different design standards will be discussed.

2.3.1. API RP 1111

The recommended practice (RP) published by API; API RP 1111 sets out criteria for the design, construction, testing, operation, and maintenance of offshore steel pipelines in the production, production support, or transportation of hydrocarbons. The criteria contained in the RP are intended to permit the economical transportation of hydrocarbons while providing for the safety of life and property and the protection of the environment. The RP uses a limit state design (LSD) methodology. Which is also known as load and resistance factor design (LRFD). A limit state is a state beyond which the structure no longer fulfills the relevant design criteria [5]. A structure that is designed with this methodology is fit to sustain all actions likely to occur during its design life and to remain fit for use with an appropriate level of reliability for each limit state.

The API RP distinguishes three specific limits that are important to take into account whilst designing for installation. Namely, the longitudinal load design, collapse due to external pressure and buckling due to combined bending and external pressure.

Longitudinal load design

In paragraph 4.3.1.2 of API RP 1111 the effective tension exceedance value is stated, in this report stated as equation 2.1.

$$T_{eff} \leq 0.60 T_y \tag{2.1}$$

$$T_{eff} = T_a - P_i A_i + P_o A_o \tag{2.2}$$

$$T_a = \sigma_a A \tag{2.3}$$

$$T_y = SA \tag{2.4}$$

$$A = A_o - A_i = \frac{\pi}{4}(D^2 - D_i^2) \tag{2.5}$$

Where:

A is the cross-sectional area of pipe steel
A_i is the internal cross-sectional area of the pipe
A_o is the external cross-sectional area of the pipe
P_o is the external hydrostatic pressure
P_i is the internal pressure in the pipe
T_a is the axial (material) tension in pipe
T_{eff} is the effective tension in pipe
T_y is the yield tension of the pipe
σ_a is the axial stress in the pipe wall

External pressure design

Regarding the external pressure the design needs to comply with the following two limits, equations 2.6 and 2.10. The former secures that the external pressure does not exceed the collapse pressure of the pipeline and the latter safeguards the combined bending strain and external pressure limit. Respectively the two equations are discussed in paragraph 4.3.2.2 and 4.3.2.2 of API RP 1111.

$$f_o P_c \geq (P_o - P_i) \tag{2.6}$$

$$P_c = \frac{P_y P_c}{\sqrt{P_y^2 + P_c^2}} \tag{2.7}$$

$$P_y = 2S(\frac{t}{D}) \tag{2.8}$$

$$P_e = 2E\frac{\frac{t}{D}^3}{(1-v)^2} \tag{2.9}$$

Where:
E is the modulus of elasticity
f_o is the collapse factor
P_c is the collapse pressure
P_e is the elastic collapse pressure
P_y is the yield pressure at collapse

$$\frac{\varepsilon}{\varepsilon_b} + \frac{P_o - P_i}{f_c P_c} \leq g(\delta) \tag{2.10}$$

Given that:

$D/t \leq 50$

$$g(\delta) = (1 + 20\delta)^{-1} \tag{2.11}$$

$$\delta = \frac{D_{max} - D_{min}}{D_{max} + D_{min}} \tag{2.12}$$

$$\varepsilon_b = \frac{t}{2D} \tag{2.13}$$

Where:
ε is the allowable bending strain in the pipe (in the presence of external pressure)
ε_b is the buckling strain under pure bending
f_c is the collapse factor for use with combined pressure and bending loads
$g(\delta)$ is the collapse reduction factor
δ is the ovality

To avoid buckling, bending strains should be limited following equation 2.14.

$$\varepsilon \geq f_1 \varepsilon_1 \tag{2.14}$$

Where:
ε_1 is the maximum installation bending strain
f_1 is the bending safety factor for installation bending plus external pressure

However ε_1 and f_1 don't have preset values. ε_1 is calculated with the multiplication of the nominal bending strain and the strain amplification factor (SAF). And typically a more detailed analyses needs to be conducted to determine an appropriate value for the SAF. Also f_1 should be determined by the designer with appropriate consideration of the magnitude of increase that may occur in ε_1 for installation bending strain.

2.3.2. ISO 13623

The International Standard ISO 13623 is not a design manual; rather it is intended for use in combination with sound engineering practice judgement. It allows the use of innovative techniques and procedures such as reliability based limit state design methods, as long as the minimum requirements of the International Standard are satisfied the design can still be ISO certified. The standard specifies functional requirements, gives recommendations and via such provides a basis for their safe design, construction, testing, operation, maintenance, and abandonment of pipeline systems used for transportation in the petroleum and natural gas industries. Amongst others it applies to the rigid metallic pipelines considered in this research. Pipelines should be designed for the following mechanical failure modes and deformations:

- yielding
- buckling
- fatigue
- ovality

Regarding the buckling failure mode the following buckling modes need to be considered:

- local buckling due toe external pressure, axial tension or compression, bending and torsion, or a combination of these loads;
- buckle propagation
- restrained buckling due to axial compressive forces induced by high operating temperatures and pressures

With regards to the yielding or bursting failure mode ISO 13623 dictates that the hoop stress σ_{hp} due to internal pressure shall be determined in accordance with equation 2.15

$$\sigma_{hp} \leq f_h \cdot \sigma_y \tag{2.15}$$

$$\sigma_{hp} = (p_{id} - p_{od}) \cdot \frac{(D_o - t_{min})}{2t_{min}} \tag{2.16}$$

Where:
D_o is the nominal outside diameter
f_h is the hoop-stress design factor
p_{id} is the design pressure
p_{od} is the minimum external hydrostatic pressure
t_{min} is the specified minimum wall thickness
σ_{hp} is the circumferential stress, or hoop stress, due to fluid pressure only
σ_y is the specified minimum yield strength (SMYS) at maximum design temperature

Circumferential, longitudinal, shear and equivalent stresses shall be calculated taking into account stresses from all relevant functional, environmental and construction loads.

Functional loads are loads that arise from the intended use of a pipeline system, think of the weight of the pipeline including components and fluid, loads due to marine growth and external hydrostatic pressure. Environmental loads are loads from waves, currents, tides and wind etcetera. Loads that are necessary for installation and commissioning are classified as construction loads. Besides functional, environmental, and construction loads there are also accidental loads. These are loads occurring to the pipeline under unplanned however, possible circumstances. Loads from falling objects, sudden decompression or explosions are considered accidental.

When equivalent stresses or strains are calculated the most unfavourable combination of above mentioned loads that can be predicted to occur simultaneously need to be considered. Equivalent stresses, σ_{eq}, shall be calculated using the von Mises equation as given in equation 2.17. Nominal values of diameter and wall thickness can be used in equivalent stress calculations.

$$\sigma_{eq} = (\sigma_h^2 + \sigma_l^2 - \sigma_h\sigma_l + 3\tau^2)^{1/2} \tag{2.17}$$

Where:

σ_h is the circumferential stress
σ_l is the longitudinal stress
τ is the shear stress

The maximum equivalent stress needs to be determined in accordance with equation 2.18.

$$\sigma_{eq} \leq f_{eq} \cdot \sigma_y \tag{2.18}$$

The design factors f_h and f_eq can be found in tables 3 and 4 in ISO13623 respectively.

2.3.3. DNVGL-ST-F101

The DNVGL-ST-F101 standard gives criteria and recommendations on concept development, design, construction operation and abandonment of submarine pipeline systems. The standard applies to single rigid metallic submarine pipelines systems for the use of hydrocarbon transport. Similar to the API RP the DNVGL standard is based on limit state design.

The DNVGL standard describes two limits regarding local buckling. One in which only external overpressure occurs and a combined loading criterion in which also the bending moment and effective tension comes into play. Since this research focuses on the installation of start-up structures only the latter will be discussed here. For the combined loading criteria a differentiation is made between a load controlled condition (LCC) and displacement controlled condition (DCC). In a LCC the structural response is primarily governed by the imposed loads, for instance the manner in which a pipeline bends in the sagbend. In a DCC situation the structural response is primarily governed by imposed geometric displacements, for instance how a pipeline bends over a S-lay stinger in the overbend area, strictly following the geometry of the rollers in the stinger or how a reeled pipe gets straightened after it gets reeled of the spool. Also the local buckling criteria is only applicable to pipelines that are straight in stress free condition. Pipe members subjected to bending moment, effective axial force and external overpressure shall be designed to satisfy the criterion given by equation 2.19 at all cross-sections, in the DNVGL design code referred to as equation 5.28.

$$\left[\gamma_m \cdot \gamma_{SC,LB} \cdot \frac{|M_{Sd}|}{\alpha_c \cdot M_p\,(t_2)} + \left(\gamma_m \cdot \gamma_{SC,LB} \cdot \frac{S_{Sd}(p_i)}{\alpha_c \cdot S_p\,(t_2)}\right)^2\right]^2 + \left[\gamma_m \cdot \gamma_{SC,LB} \cdot \frac{p_e - p_{min}}{p_c(t_2)}\right]^2 \leq 1 \tag{2.19}$$

Given that:

$15 \leq D/t_2 \leq 45$

$p_{min} < p_e$

$|S_{Sd}|/S_p < 0.4$

Where:

γ_m	is the material resistance factor
$\gamma_{SC,LB}$	is the safety class resistance factor
M_{Sd}	is the design moment load effect
$S_{Sd}(p_i)$	is the design effective axial force load effect
α_c	is the flow stress parameter
$M_p(t_2)$	is the plastic capacity of the pipe, given by equation 2.21
$S_p(t_2)$	is the plastic capacity of the pipe, given by equation 2.23
p_e	is the external pressure
p_{min}	is the minimum internal pressure
$p_c(t_2)$	is the characteristic collapse pressure, given by equation 2.28
D	is the pipe outer diameter
t_2	is the characteristic wall thickness

The material and safety class resistance factor are dependent on limit state categories and safety class. Values can be found in Table 5-1 and 5-2 of the DNVGL standard. In accordance of equations 2.20 to 2.31 the different parameters that serve as input for the combined loading criteria can be calculated.

$$M_{Sd} = M_f \cdot \gamma_F \cdot \gamma_c + M_E \cdot \gamma_E + M_I \cdot \gamma_F \cdot \gamma_c + M_A \cdot \gamma_A \cdot \gamma_c \tag{2.20}$$

$$M_p\,(t) = f_y \cdot (D - t)^2 \cdot\ t \tag{2.21}$$

$$S_{Sd} = S_f \cdot \gamma_F \cdot \gamma_c + S_E \cdot \gamma_E + S_I \cdot \gamma_F \cdot \gamma_c + S_A \cdot \gamma_A \cdot \gamma_c \tag{2.22}$$

$$S_p\,(t) = f_y \cdot \pi \cdot (D - t) \cdot\ t \tag{2.23}$$

$$f_y = (SMYS - f_{y,temp}) \cdot \alpha_U \tag{2.24}$$

$$f_u = (SMTS - f_{u,temp}) \cdot \alpha_U \tag{2.25}$$

$$\alpha_c = (1 - \beta) + \beta \cdot \frac{f_u}{f_y} \tag{2.26}$$

$$\beta = \frac{60 - \frac{D}{t_2}}{90} \tag{2.27}$$

$$[p_c\,(t) - p_{el}(t)]\left[p_c\,(t)^2 - p_p(t)^2\right] = p_c\,(t) \cdot p_{el}\,(t) \cdot p_p\,(t) \cdot O_0 \cdot \frac{D}{t} \tag{2.28}$$

$$p_{el}\,(t) = \frac{2\ \cdot E \cdot \left(\frac{t}{D}\right)^3}{1 - v^2} \tag{2.29}$$

$$p_p\,(t) = f_y \cdot \alpha_{fab} \cdot \frac{2 \cdot t}{D} \tag{2.30}$$

$$O_0 = \frac{D_{max} - D_{min}}{D} \tag{2.31}$$

Where:

M_F is the functional load moment
M_E is the environmental load moment
M_I is the interference load moment
M_A is the accidental load moment
γ_F is the functional load effect factor
γ_E is the environmental load effect factor
γ_A is the accidental load effect factor
γ_c is the condition load factor
S_F is the effective axial functional force
S_E is the effective axial environmental force
S_I is the effective axial interference force
S_A is the effective axial accidental force
f_y is the characteristic material yield stress
f_u is the characteristic material tensile strength
$f_{y,temp}$ is the de-rating value of yield stress due to temperature
$f_{u,temp}$ is the de-rating value of tensile strength due to temperature
α_c is the flow stress parameter
$p_c(t)$ is the characteristic collapse pressure
$p_{el}(t)$ is the elastic collapse pressure
$p_p(t)$ is the plastic collapse pressure
α_{fab} is the fabrication factor
α_U is the material strength factor
O_0 Ovality

Note that for start-up structure installations the temperature during the installation is assumed to be low enough not for temperature de-rating to occur. De-rating of yield stress and tensile strength only occurs during operation when the pipe material gets heated by the transported hydrocarbons. Which results in the following definitions for the characteristic material yield stress and tensile strength.

$$f_y = SMYS \cdot \alpha_U \tag{2.32}$$

$$f_u = SMTS \cdot \alpha_U \tag{2.33}$$

The load factors, γ_F, γ_E, γ_A and γ_c are stated in tables 4-4 and 4-5 of the DNVGL code. α_{fab} depends on the fabrication process of the used pipes and is defined in table 5-4. The material strength factor, α_U, is defined in table 5-3 and has a value of 0.96 for all loading scenario's except the system pressure test. However, when the supplementary requirement U is met the material strength factor can be upgraded to a value of 1.0. In section 7.9.5 of the DNVGL design code the exact requirements are stated. One of the options to fulfill the requirements is to show with retrospective documentation that from 50 test units the average yield strength is at least 2.0 standard deviations above SMYS. For further details see section 7.9.5 of the design code. Note that all mentioned DNVGL tables can be found in appendix A. Regarding the combined loading criterion one more topic needs to be addressed. DNVGL defines two different checks for the local buckling ultimate limit state. ULSa when system effects are present and ULSb, which is a local check for which the load factors differ. According to the DNVGL code both checks need to be evaluated when conducting a installation analyses. An analytical solution for the collapse pressure can be found in appendix B.

From sections 2.1 to 2.3 it is now known that there are several different types of failure mechanisms that can occur and threaten the pipe's structural integrity and that there are different types of design codes in which these typical threats are described. Taking the objective of this research into account it is important to make a distinction between what codes and which situation offers the most significant improvement. In the API RP and the ISO standard a very general design approach is provided whereas the DNVGL code is more specific and gives per limit state a more detailed description. In the case of combined loading, no different limits are to be checked but there is just one combined

loading criterion in which all relevant loads; functional, environmental, moments, tensions and pressure are taken into account. **Therefore the DNVGL equation 5.28, in this report equation 2.19, will be the topic for optimization.**

2.4. Probabilistic assessment

Probabilistic reliability assessment of structures allows to take the uncertainty in the governing parameters in to account. So instead of using deterministic values, for each variable the joint probability density functions (pdf) needs to be known. Using the pdf's makes it possible to express the systems performance in terms of probability of failure (PoF) or in other words, reliability. The required PoF or safety margin of a system depends on the function of the system and the consequences of system failure. As already mentioned in chapter 1 in the case of start-up structure installations the PoF is determined by the design standard that is used.

2.5. Evaluation of probability of failure

In the majority of the situations the reliability of a system can be assessed by comparing the resistance of a system R, to the load that it experiences, S. Thus the safety of a system can be assessed by verifying that the resistance is larger than the load, such that no failure occurs.

In the simplest form failure can be expressed as the load (S) on the system being greater than the resistance of the system (R). Mathematically this relation is captured by equation 2.34, a limit state function.

$$Z = R - S \tag{2.34}$$

Where the system is defined safe or reliable when $R < S$, so when $Z \geq 0$ and the system fails when $Z < 0$. The probability of failure equals $P_f = P[Z < 0] = P[S > R]$. In the probabilistic approach resistance and load effects are not regarded as deterministic quantities, but as random variables, each can be described by a certain distribution type and accompanying parameters. Which means that the resistance will vary from element to element and that the load will show spatial as well as time variation. In case of one-dimensional problems and simple distribution functions for the load and resistance, P_f can be easily calculated - often using analytical methods. However, in practice multiple basic variables influence the limit sate, making it difficult and most often impossible to evaluate the multidimensional integrals exactly. Therefore, several methods to perform reliability analysis are available [13].

A general formulation for limit state design is given by equation 2.35.

$$g(\underline{X}) = Z = 0 \tag{2.35}$$

Where the vector $\underline{X}$ consists of n basic variables such as:

- material properties
- actions (loads)
- geometrical properties
- model uncertainties

All basic variables need to be described by an appropriate probabilistic model, or distribution. In case a basic variable has negligible variation in time or space, the variable can be considered as deterministic.

Now the failure probability, P_f, of the system can be calculated by solving the n-dimensional probability density function of the n variables in vector $\underline{X}$ of the limit state function $g(\underline{X})$, equation 2.36. The PoF of a system is then equal to the area, in case of $n = 1$, or equal to the volume of the joint probability function in the area defined by $g(\underline{X}) < 0$.

$$P_f = \int_{g(\underline{X})<0} f_{\underline{X}}(\underline{x}) d\underline{x} \tag{2.36}$$

2.5.1. Probability of failure for installation

As discussed the rules that a contractor needs to adhere to are dependant on the design code that is chosen to apply during a certain project. Since in this research the DNVGL-ST-F101 code is chosen as the design standard, further referred to as DNVGL code or standard, to optimize the probability of failure that this code asks for is elaborated on in this section. As discussed, the DNVGL code ensures the safety of a system by a safety class methodology. This means that the pipeline system is classified in one or more safety classes which are based on the failure consequences. Which are dependent on the content and location of the system. For each safety class, a set of partial safety factors is assigned to each limit state.

According to table 2-4 in the DNVGL design code installation until pre-commissioning should be classified as safety class low. Which is defined as the safety class where failure implies insignificant risk of human injury and minor environmental and economic consequences. The combined loading scenario during installation is specified as a ultimate limit state according to table 5-7 of the same design code and knowing this the nominal annual target failure probability can be found in table 2-5. For the ultimate limit state category and safety class low the target failure probability is $10^{-}3$ per pipeline. Note that the above mentioned tables can be found in appendix **??**.

2.6. Reliability analysis levels

There are five different levels of assessment regarding reliability analysis. Depending on the complexity of the system and the required accuracy, the level of assessment can be determined.

2.6.1. Level 0 methods

These are deterministic methods which use deterministic or nominal values of the basic variables and one (empirical) global safety factor.

2.6.2. Level 1 methods

Level 1 methods are semi-probabilistic and are based on the application of partial safety factors. The variables whose probabilistic distributions have to be taken in to account are represented by characteristic values that correspond to a low and high percentile for strength or resistance distributions and action or load distributions respectively. With the use of the partial safety factors the desired PoF can be obtained without performing a full probabilistic assessment.

2.6.3. Level 2 methods

In case of level 2 methods the uncertain parameters are modelled by the mean values and standard deviations and correlations coefficients between the stochastic variables. The joint probability density function is simplified and taken as a normal distribution and the limit state function is linearized in the design point, the most probable failure point i.e. the point on $g(\underline{X}) = 0$ with the highest probability density.

2.6.4. Level 3 methods

When a reliability method of level 3 is applied, the probabilistic formulation for P_f is calculated exactly, using numerical integration, analytical formulations or a Monte Carlo simulation. Using analytical formulations to solve a problem is only possible in a limited number of simple cases; numerical integration is only practical when the number of basic variables n is small [13]. During a Monte Carlo simulation random sampling is used to simulate physical phenomena. Level 3 methods evaluate equation 2.36 explicitly.

2.6.5. Level 4 methods

Level 4 methods take in to account the consequences of failure (costs, loss of life etc.) and risk (which is defined as consequence times probability of failure) is used as a measure of reliability. Level 4 methods allow for economic comparison, taking into account cost and benefit for certain designs or situations.

Taking the aim of this thesis into account, calculating the probability of failure exactly is desirable and thus level 3 methods will need to be used. From the different options explained in subsection 2.6.4, Monte Carlo simulation has the least limitations. **Therefore in this research the Monte Carlo simulation method will be used for the structural reliability assessment**

2.7. Correlation

In statistics, correlation is any statistical dependence of two or more random variables, whether causal or not. If the correlations between random variables in a model are not known and not taken into account it can cause major flaws in the results. Therefore assessing the correlation of the observed data is necessary to model situations correctly.

A correlation coefficient is a statistical measure of the degree of correlation. Several different correlation coefficients exists, the Pearson product-moment correlation coefficient being the most common. However, it is only sensitive to linear relationships between two variables. A more robust type of correlation coefficients are rank correlation coefficients like Spearman's rank- and Kendall tau rank correlation coefficients. Being more robust means that they are more sensitive to other types of dependencies, or non-linear relationships. In the following subsections Pearson's product-moment correlation coefficient and Spearman's rank correlation coefficient will be discussed.

2.7.1. Pearson's moment correlation coefficient

Pearsons's moment correlation coefficient or linear correlation coefficient, given by equation 2.37, assesses linear relationships between two variables. Positive values give positive relations and negative values give negative relations. For instance if a certain data-set has a $\rho_{X,Y}$ value of 1 it will be plotted as a straight line, opposed to a cloud of points, with a positive direction coefficient.

$$\rho_{X,Y} = \frac{cov\,(XY)}{\sigma\,(X)\,\sigma\,(Y)} = E\left\{\frac{X - E\,(X)}{\sigma\,(X)} \cdot \frac{Y - E\,(Y)}{\sigma\,(Y)}\right\} \tag{2.37}$$

Where:

$cov(XY)$ is the covariance between X and Y
$\sigma(X)$ is the standard deviation of X
$E(X)$ is the expected value of X

The covariance between two different variables also depicts a degree of dependence however the value of covariance is hard to interpret since it depends on the values of the assessed variables. In the Pearson moment correlation coefficient the covariance is normalized and thus gives a comparable rate of correlation. The expected value is the mean or weighted average of a random variable. And the standard deviation of a random variable is a measure to depict the variation or dispersion in a dataset and is calculated as the square root of the expected value of the squared deviation from the mean of the variable as shown in equation 2.38.

$$\sigma^2(X) = E[(X - E[X])^2] \tag{2.38}$$

2.7.2. Spearman's rank correlation coefficient

Spearman's rank correlation coefficient, given by equation 2.39 assesses monotonic relationships, whether linear or not. This means that when a dataset has a Spearman's correlation coefficient of 1 all data points above a given x-value will have greater y-values as well.

$$r_{X,Y} = \rho(F_X(X), F_Y(Y)) \tag{2.39}$$

Where:

$F_X(X)$ is the ranked variable X

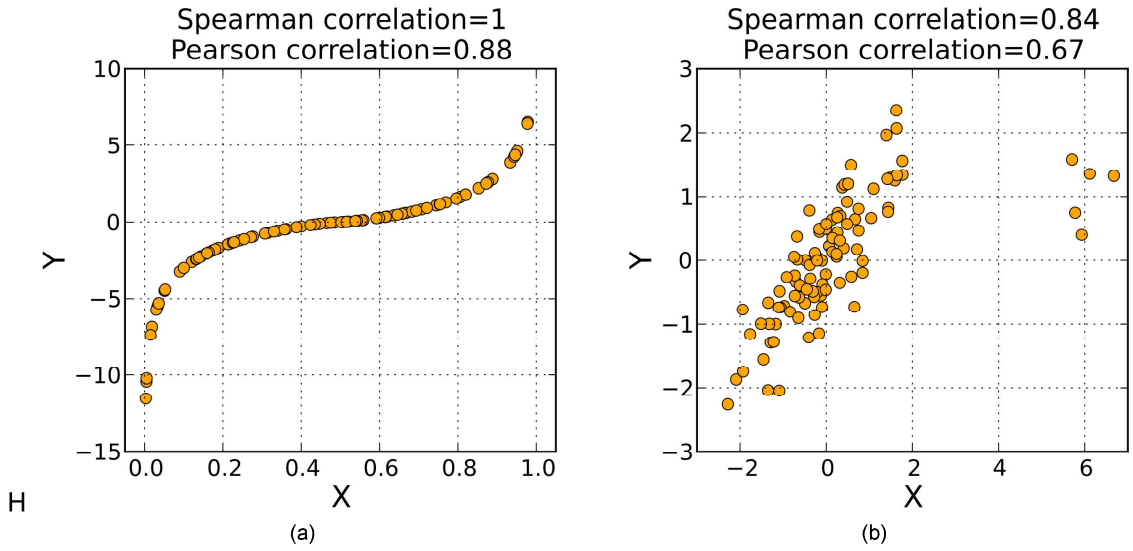

Figure 2.3: Difference Pearson and Spearman correlation

Figures 2.3a and b give a good indication on the differences of both correlations coefficients. Figure 2.3a shows how the Spearman correlation coefficient picks up the monotonic relationship of the data and that the Pearson moment correlation coefficient has a lower value since the relation is not strictly linear. Figure 2.3b shows that the Spearman rank correlation is less sensitive to outliers in the tails of the sample. This is causes by the fact that in the Spearman rank correlation coefficient the outlier is valued to its rank.

2.8. Kernel density estimation

Kernel density estimation (KDE) is a non-parametric way to estimate the probability density function of a random variable.

$$\hat{f}_h(x) = \frac{1}{nh}\sum_{i=1}^{n} K\left(\frac{x - x_i}{h}\right) \tag{2.40}$$

Where x_1, x_2, …, x_n are random samples from an unknown distribution, n is the sample-size, K is the Kernel function and h is the bandwidth. The center of the Kernel is placed over each datapoint of the assessed random variable. The influence of each data point is spread about its neighbourhood via the bandwidth and in this manner controls the smoothness of a density estimate. The contribution of each point is summed to the overall density estimate. Different types of Kernel functions can be used [18]:

- Uniform Kernel
- Gaussian Kernel
- Triangular Kernel
- Epanechnikov Kernel

2.9. Copula's & Sklar's theorem

A random variable is characterized by its cumulative distribution function (CDF) as in equation 2.41. For a collection of random variables $X_1, \ldots, X_n$, the marginal CDF's $F_1, \ldots, F_n$ describe the individual behaviour of the variables however, they provide no information about their joint behaviour. Copulas are joint distribution functions constructed from any number of

standard uniform marginal distributions and they couple these marginal distributions with a specification of the dependence between the random variables [14].

$$F(x) = P(X \leq x) \tag{2.41}$$

A copula is a distribution on the unit square with uniform marginal distributions. Random distributions X and Y are joined by copula C if there joint distribution can be written according to equation 2.42. Which is also known as Sklar's theorem. For each given continuous joint distribution a corresponding unique copula can be found.

$$F_{X,Y} = C\left(F_X(x), F_Y(y)\right) \tag{2.42}$$

What makes copulas so flexible and widely used in Monte Carlo simulations is that it is possible to generate a particular dependence pattern and then induce the marginal distribution that is desirable. Or keep the marginal distributions the same while inducing different dependence models.

Later in this report five types of copula's will be examined to fit the empirical data. In figure 2.4 the scatterplots of 3000 randomly generated samples from each model can be found. The Gumbel, Clayton and Frank copula models from the Archimedean copula family and the T and Gaussian copula models from the Elliptical copula family. The Spearman's rank correlation for these samples is arbitrarily chosen as 0.75 to show the different characteristics of each model. Table 2.1 shows the different properties of each copula that already have been showed by the figures. These copula models are chosen since all of them, except for the T copula only, have one copula parameter which controls the degree of dependence and are thus easily described. Furthermore they cover a wide range of properties. Note that the Gumbel and Clayton copula are not capable of modelling negative dependence however, certain transformations can be made which give some extra options if necessary. In appendix C the mathematical descriptions of the copula models can be found.

Upper and lower tail dependence occurs if the limit in equation 2.43 and 2.44 respectively exists.

$$\lim_{u \to 1} P(U > \bar{u} | V > \bar{u}) > 0 \tag{2.43}$$

$$\lim_{u \to 0} P(U < \bar{u} | V < \bar{u}) > 0 \tag{2.44}$$

Table 2.1: Characteristics different copula models

Copula type	Elliptical copula		Archimedean copula		
	Gaussian	**T**	**Gumbel**	**Clayton**	**Frank**
Tail symmetry	Symmetric	Symmetric	Asymmetric	Asymmetric	Symmetric
Tail dependence	No	Yes	Yes, upper tail	Yes, lower tail	No
Negative dependence	Yes	Yes	No	No	Yes

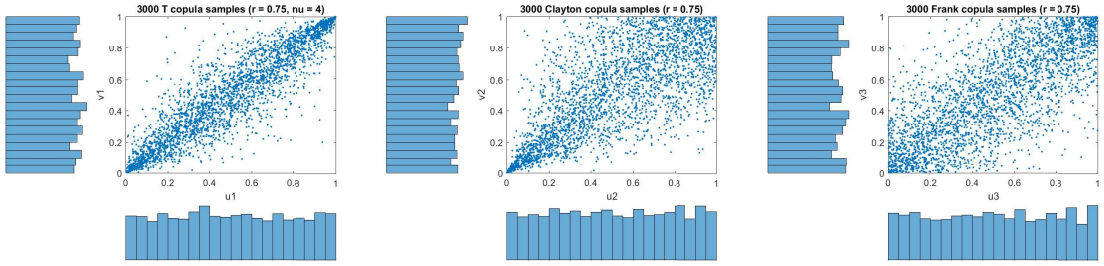

(a) T copula (b) Clayton copula (c) Frank copula

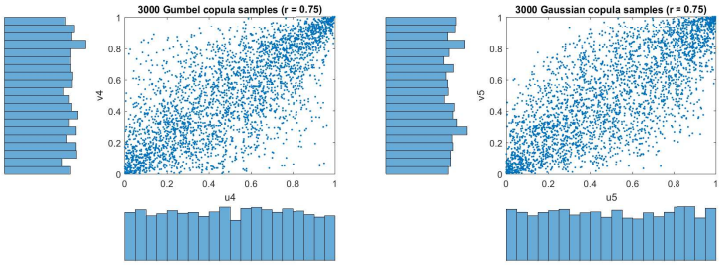

(d) Gumbel copula (e) Gaussian

Figure 2.4: Scatterplots assessed copula models

2.10. Goodness-of-fit

Since over or under estimating the variable can have a large impact on the overall reliability in reliability calculations it is necessary to asses the goodness of fit to test if a chosen model fits the observed data there are several methods to test the goodness of fit. In this report the goodness of fit test for the multivariate copula's will be a semi correlations comparison and the Cramér von Mises statistic analysis. In the instance that a distribution is fitted for a non dependant variable, e.a. a regular univariate probability distribution, the Bayesian information criterion will be used. The goodness of fit is important to formally decide whether a certain theoretical model is capable of representing the empirical data that has been collected.

2.10.1. Bayesian information criterion

The Bayesian Information Criterion (BIC) is a statistical measure for model selection. From a finite set of candidate models and the given empirical data the BIC for each model can be determined. The model with the lowest BIC value is preferred and represents the given data the best of all assessed candidate models.

$$BIC = ln(n)k - 2ln(\hat{L}) \tag{2.45}$$

- n is the sample size
- k is the number of parameters estimated by the model
- $\hat{L}$ is the maximized value of the likelihood function

The difference between the Bayesian Information Criterion calculated for the fit of two theoretical probability distributions gives an indication on the difference of representation. Table 2.2 gives an implication of the value of this difference [15].

Table 2.2: Implication of BIC value

Δ BIC	Implication
0 to 2	Distributions do not differ significantly
2 to 6	Distributions slightly differ
6 to 10	Significant difference in distributions
> 10	Very significant difference in distributions

2.10.2. Kolmogorov-Smirnov test

The Kolmogorov-Smirnov test (K-S test), is a statistical test based on the Kolmogorov-Smirnov statistic value given by 2.46, a measure for the difference in two distributions. There is a one-sample test and a two-sample test. The one-sample test investigates the null hypothesis, $H_0 : F = F_0$, that the tested sample from the unknown distribution function F is sampled from the known, reference distribution function F_0. And thus functions as a goodness-off-fit test. If the K-S test rejects the null hypothesis in favor of the alternative hypothesis, $H_1 : F \neq F_0$, the conclusion is that the sample doesn't come from the reference distribution and if it doesn't reject the null hypothesis it does. The two-sample test investigates if two different samples are drawn from the same, unknown, distribution. If the D value is greater than the critical D-value then it can be concluded that the null hypothesis is rejected, otherwise there is not enough evidence to prove the difference. The critical D-value is dependent on the adopted significance level [16].

$$D_n = \sup_x |F_n(x) - F_0(x)| \tag{2.46}$$

2.10.3. Semi-correlations

The semi-correlation test can be used to asses the goodness-of-fit of a theoretical copula model and empirical data by calculating the Pearson product moment correlation coefficient of specific parts of the empirical data set and compare these to the correlations of the theoretical copula model. To make the semi correlation comparison the first step is to transform the observed data to standard normal and divide the domain in four quadrants around zero. Then on each quadrant (north west, north east, south east and south west) the linear correlation coefficient can be calculated. Random samples of the copula models of which the goodness of fit will be assessed need to be generated while using the appropriate similar rank correlation coefficient ass the empirical data. These samples then also need to be transformed to standard normal and the linear correlation coefficients per quadrant need to be calculated. The value for each quadrant can then be compared. Note that high values for the Pearson moment correlation coefficient give an indication of tail dependence. Also for the specific project that the copula models will be used for it is important to determine which quadrant is the most important and will be the quadrant of interested regarding the semi-correlation comparison.

2.10.4. Cramér von Mises statistic

A formal way of assessing and quantifying the goodness of fit is calculating the Cramer von Mises statistic value. Equation CM_n is the Cramér von Mises statistic value and $C_n(u, v)$ is the empirical copula [7]. The empirical copula is a generalization of the empirical cumulative distribution function to two dimensions.

$$CM_n = n\sum_{i=1}^{n}\left\{C_n\left(\frac{R_i}{n+1}, \frac{S_i}{n+1}\right) - C_{\theta n}\left(\frac{R_i}{n+1}, \frac{S_i}{n+1}\right)\right\}^2 \tag{2.47}$$

$$C_n(u,v) = \frac{1}{n}\sum_{i=1}^{n} 1\left(\frac{R_i}{n+1} \leq u\ , \frac{S_i}{n+1} \leq v\right) \tag{2.48}$$

The Cramer von Mises statistic value is the summed, squared difference of the theoretical model minus the empirical model. Plotting the absolute difference of the Cramer von Mises statistic value also visualizes where the bigger differences regarding the two models are. This additional information can be helpful when making the decision what model fits best when it is known in what part of the model the best representation of the empirical data is needed.

3

Current methods and study case

In the first section of this chapter an introduction on installation analyses procedures as conducted by HMC will be given. The second section covers the examined study case of this research. Section 3 discusses the production process of the pipes in question and section 4 reviews a big assumption that has been made in this specific study case.

3.1. HMC analysis reports

The installation of a subsea pipeline is divided in different installation procedures. The start-up structure installation being one of them. Every installation procedure is also divided into different phases and steps. All of which get assessed separately. During a start-up structure installation the different phases are generally as follows:

- I FLET installed in J-lay tower
- II 1 Quad-joint installed on top of FLET stem
- III FLET in water column
- IV Hook-up of FLET to start-up pile through to landing the FLET mudmat on the seabed
- V Landing FLET frame on mudmat throug to 'normal' pipelay

For all phases a static analysis, dynamic and fatigue analysis is conducted. The goal of dynamic analysis is to determine operational limits for installation of the FLET and to assess the effect of the dominant sea-state on the flowline and FLET during installation. To achieve this, for each installation phase the limiting sea-states in which the FLET can be safely installed within vessel capabilities and pipe structural capacity are calculated. Note that this is an iterative process. From the metocean report for the project location the sea-states that need to be reviewed are defined. For each wave period the maximum significant wave height is determined. A fatigue analysis is performed to assess fatigue damaged to the FLET and flowline due to cyclic loading during installation. If results from simulations with all the fatigue analysis sea-states show sufficient fatigue life and acceptable contingency times, the limiting sea-states with respect to installation fatigue have been determined. Otherwise installation sea-states must be reduced. Limiting installation sea-states with respect to fatigue should be in line with the limiting sea-states for dynamic installation loads. The limiting sea-states should be reduced depending on which analysis is governing.

For the limit state of local buckling phase III and phase V are the most governing. For phase III the biggest loads occur just after the moment that the FLET is lowered through the moon pool. Where it is subjected to the current and wave loads, which both gradually decrease when the FLET is lowered further. In phase V the FLET lands on the seabottom and the pipe gets subjected to the functional load of the FLET caused by the weight and

configuration of this step of the installation. And environmental loads caused by vessel motions which are mainly heave driven.

In the analysis report all installation analyses calculations are summarized and the critical steps in the installation have been determined. Together with the metocean report of the project location the workability can be calculated. In the metocean report the wave scatter plot can be found in which the occurrence of a certain combination of significant wave height and wave period per year or month is stated. Note that because of this the workability of a start-up structure installation is incredibly dependant on the location and, depending on the type of information that is available, also on the time of the year in which the installation is planned. Therefore it is impossible to make a general quantitative statement about the improvement of the workability if the structural reliability assessment improves the situation as expected.

3.1.1. Flexcom software

Flexcom is a Finite Element Method (FEM) software package for numerically solving engineering problems. It is a highly versatile software package, capable of simulating risers, mooring lines, umbilicals, floating bodies, offloading lines and installation processes to name a few[22]. Within HMC Flexcom is used to analyze the installation of pipelines and risers both statically and dynamically.

3.2. Load case description

After examination of HMC's pipeline database and mapping the different amount of data that has been collected during previous projects. It was found that there was only a small number of projects that had been fully documented. Only three projects have more than 100 full data points however, one of them clearly stands out with 1106 material and geometrical data points. Which is the Ichthys 18" project. Because of probabilistic approach and thus the statistical nature of this research the size of the data set is important. Because the Ichthys project is the best documented pipe lay project in the HMC's pipeline database the start-up structure installations of this project serve as the reference case for this research.

For every point this dataset includes the following parameters:

- Length
- Weight
- Internal diameter pipe end A
- Internal diameter pipe end B
- Internal diameter Body
- Wall thickness pipe end A
- Wall thickness pipe end B
- Out of roundness pipe end A
- Out of roundness pipe end B
- Out of roundness body
- Peaking pipe end A
- Peaking pipe end B
- Peaking Body
- Straightness Full
- Straightness pipe end A

- Straightness pipe end B
- Yield stress
- Ultimate tensile strength
- Elongation

While using the DNVGL code the wall thickness, internal diameters, yield stress, ultimate tensile strength and out of roundness are of interest for this research.

3.2.1. Ichthys Field

INPEX Australia discovered the immense Ichthys gas and condensate field in the year 2000. It is located in the Browse basin about 200 km offshore Western Australia. It is the largest discovery of hydrocarbons in Australia in 40 years. The project has an expected operational lifetime of 40 years or more. Australia aims to be one of the largest LNG exporters by 2020. The Ichthys field is estimated to contain more than 12 trillion cubic feet of gas and 500 million barrels of condensate [10]. In the Ichthys field six 18" start-up structures have been installed in three different locations. Figure 3.1a shows the field layout of the Ichthys project and figure 3.1b shows the project location.

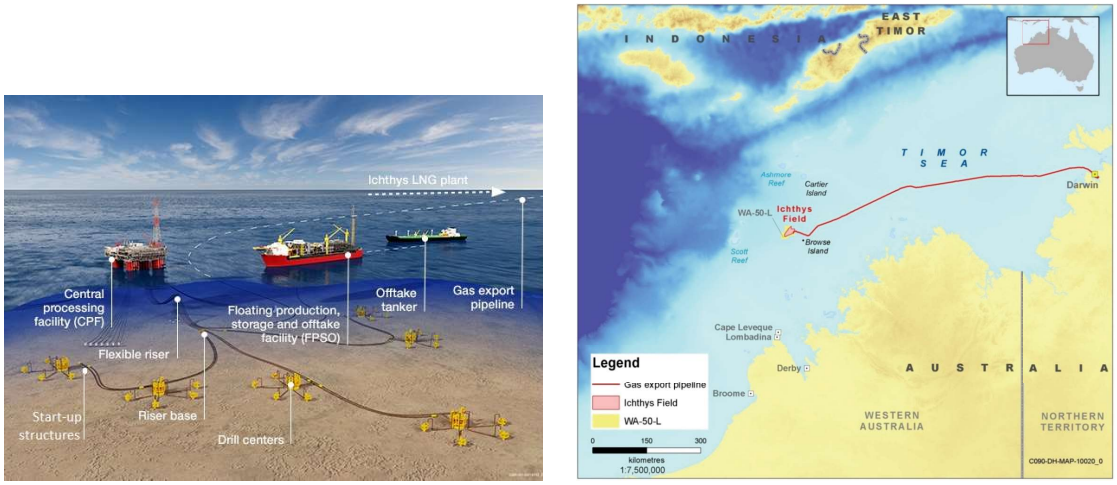

(a) Field layout (b) Field location

Figure 3.1: Ichthys location & field layout

3.2.2. Ichthys start-up structures

During the Ichthys project the largest start-up structures in the industry have been installed. Because of the large weight of the structures some precautions have been made to reduce the functional loads during installation. To decrease the amount of stress in the stem pipe of the pipeline system there are several design options available to apply. In the Ichthys project the following have been utilized.

- Hingable yoke
- Hingable mudmat
- Installation buoy
- Alterations in start-up rigging
- Change of tower angle

The first two measures decrease loads because they increase the possible range of motion. An installation buoy decreases the functional loads because of its buoyancy force and counteracts the weight of the start-up structure. With the length of the start-up rigging the shape of the pipe catenary can be influenced and in this manner loads can be minimized. The tower angle has a similar effect. Note that the tower angle can also have a large impact on the fuel consumption.

3.2.3. Start-up structure installation Ichthys project

As discussed he start-up structure installation that is examined during this research is part of the Ichthys project. In table 3.1 all input parameters of this case can be found. These are used to calculate the unity check value.

Table 3.1: Input parameters Ichthys start-up structure installation analysis

Property	Symbol	Value	
Specified minimum yield strength	$SMYS$	450	[MPa]
Specified minimum tensile strenght	$SMTS$	535	[MPa]
Youngs's modulus	E	200	[GPa]
Poisson's ratio	v	0.3	[-]
Gravity constant	g	9.81	[m/s^2]
Ovality	$f0$	1.5	[%]
Wall thickness	t	24.9	mm
Outer diameter	D	457.2	mm
Density internal fluid	ρ_{int}	1025	[kg/m^3]
Density external fluid	ρ_{ext}	1025	[kg/m^3]
Yield stress derated value due to temperature	$F_{y,temp}$	0	[-]
Ultimate tensile stength derated value due to temperature	$F_{u,temp}$	0	[-]
Material resistance factor	γ_m	1.15	[-]
Safety class resistance factor, local buckling	γ_{sc}	1.04	[-]
Material strength factor	α_u	0.96	[-]
Fabrication factor	α_{fab}	0.85	[-]
Functional load effect factor, ULSa	$\gamma_{F,ULSa}$	1.2	[-]
Environmental load effect factor, ULSa	$\gamma_{E,ULSa}$	0.7	[-]
Functional load effect factor, ULSb	$\gamma_{F,ULSb}$	1.1	[-]
Environmental load effect factor, ULSb	$\gamma_{E,ULSb}$	1.3	[-]
Functional load effect factor, ALS	$\gamma_{F,ALS}$	1	[-]
Environmental load effect factor, ALS	$\gamma_{E,ALS}$	1	[-]
Condition load effect factor	γ_c	1	[-]
Water depth	WD	251	[m]
Effective axial functional force	S_F	130.3	[kN]
Effective axial environmental force	S_E	26.295	[kN]
Functional load moment	M_F	1180	[kNm]
Environmental load moment	M_E	243.788	[kNm]

Note that the water depth, fluid density, forces and loads come from the Ichthys project installation analysis report [9]. The functional and environmental functional forces and functional and environmental load moments are calculated with Flexcom and are specific for this step, in the installation. The pipe specific parameters; SMYS, SMTS, Young's Modulus, Poisson's ratio, ovality, wall thickness and outer diameter come from the same report. The material resistance factor, safety class resistance factor, material strength factor and fabrication factor are stated in table 5-1 to 5-4 of the DNVGL design code [6]. The load effect factors and condition load factor are also dictated by DNVGL and are stated in the same report in table 4-4 and 4-5 respectively.

3.3. Production process Ichthys pipe joints

There are several types of subsea pipelines when differentiating between the specific production processes. The first distinction can be made between welded and seamless pipes. In this section only welded pipes are considered. For welded pipes the most commonly used weld processes are;

- Longitudinal submerged arc welding (LSAW)
- Spiral submerged arc welding (Spiral SAW)
- Electric resistance welding (ERW)

In the LSAW process the butt joint is welded from the inside as well as the outside. The welds are made by heating with an electrode arc between the bare metal electrodes. The electrodes provide the weld material. The Spiral SAW method allows large diameter pipes to be produced from more narrow plates. During ERW a high frequency electrical current is transmitted to the material by means of copper sliding contacts so that the edges of the plate initiate fusion as they come into contact when they are pressed together [19].

The lined pipes that have been used in the Ichthys project are classified as *DNV SAWL 450 DSF317L* pipes. This means that they are produced according to DNV standards with a longitudinal submerged arc welded process and have a specified minimum yield stress of 450 MPa. The letters DSF identify that the line pipe is build following supplementary requirements D, S and F. Which account for more stringent dimensional requirements, H_2S service or sour service, and fracture arrest properties respectively. Full specifications and test regimes regarding the supplementary requirements can be found in [6]. The pipe has a carbon manganese (C-Mn) backing pipe a stainless steel liner. The liner material is of 317 L grade stainless steel and is mechanically bonded to the backing pipe.

Table 3.2: Pipe requirements

Property	Range	
Wall thickness	23.9 - 27.9	[mm]
Outer diameter	454 - 460.4	[mm]
Yield stress	450 - 570	[MPa]
Ultimate tensile strength	535 - 760	[MPa]
Ovality	$\leq$ 1.5	[%]

In table 3.2 the requirements for the Ichthys 18 inch pipe are stated, note that the yield strenght and ultimate tensile stress are properties of the C-Mn backing steel. Geometrical requirements are stated in the in the production delivery report [3] of a line pipe delivery from Butting Germany, the fabrication company. The material strength requirements come from table 7-5 in [6] where the mechanical property requirements of C-Mn steel pipes are stated.

The backing pipe is produced by implementing the JCO process. In this type of pipe manufacturing a steel plate is formed by a brake press, the first step is to round one end to shape a ”J”, then the second end gets bend to shape a ”C”, and finaly through the center to seal the pipe into an ”O” shape after which it can be welded.

The pipes are of the BuBi type which stands for **BU**TTING **Bi**-metal pipe and means that a corrosion resistant alloy (CRA) pipe is lined into a pipe of high strength carbon manganese steel. The inner pipe and the outer pipe are expanded together with the use of a hydroforming press. Because of the normally more elastic resilience of the outer pipe, the inner pipe is placed under residual compressive stress. In this manner a secure mechanical tight fit is produced [4]. Figure 3.2 gives a schematic overview of the hydro forming process.

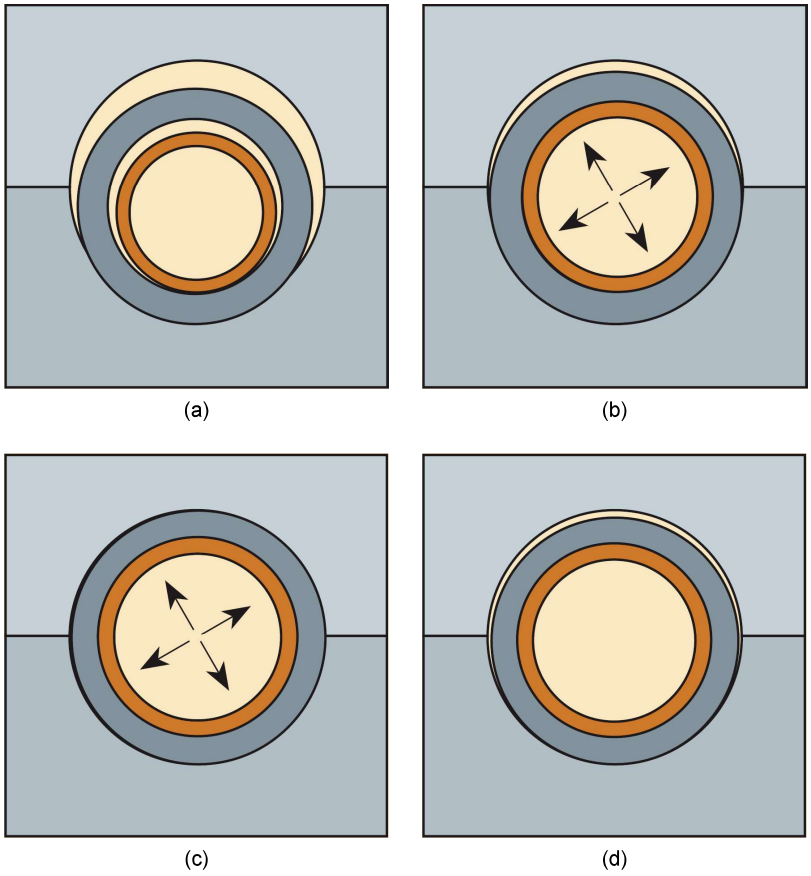

Figure 3.2: Hydroforming of the lined pipe

3.4. Assumptions

An important assumption that needs explanation is the fact that during the Ichthys project the liner material is included in the material thickness for the DNVGL calculation of allowable bending moment. Which means that the 21.9mm of C-Mn steel backing pipe together with the 3mm stainless steel liner pipe are considered one 24.9mm C-Mn steel pipe during all calculations. This assumption was researched by HMC [17] and was approved by DNVGL [1]. As discussed the lined BuBi pipes conists of a C-Mn backing pipe and a CRA liner. The bond between the liner and carbon steel is mechanical. When subjected to bending the liner can wrinkle which can lead to damage and reduction of the bending moment capacity. The onset of liner wrinkling can be influenced by the initial ovality of the pipes as well as initial liner imperfections (small gaps between the backing material and the liner). In the HMC research both a perfect liner and a liner with an imperfection are regarded. Using a finite element model in which the backing pipe and liner are modelled separately with an initial ovality of 1.5%. In all cases that HMC evaluated in this research, which have been described in consultation with DNVGL, the onset of liner wrinkling happened after reaching the maximum allowable moment. While in the FE analysis the actual CRA liner properties where used and the maximum allowable moments were calculated with the Carbon steel material properties. Thus it was concluded that the liner thickness can be included in the calculation of the allowable bending strain.

4

Statistical analyses

In this chapter the Ichthys pipeline data set will be examined. In the first section the data gets filtered and the correlation between different variables is measured. Also the physical meaning of the dependencies of the different parameters is discussed. In the second section the sensitivity regarding the combined loading criteria in the Ichthys load case is analyzed. After this analysis it is clear which parameters need to be modelled stochastically in the Monte Carlo simulation and if these parameters can be modelled as independent random variables or that a certain dependence model, using a copula, is necessary. In section 4 the dependence models are described and the final input for the structural reliability assessments is made.

4.1. Examining the data set

As discussed in chapter 3 there are 18 parameters documented for the Ichthys project. Considering the combined loading criteria equation not all parameters can be utilized in this research and some of them need some computations to be able to serve as input. Some of the parameters are location specific and are measured at the two pipe ends and the body or middle of the pipe. The parameters that will be used and are location specific are the internal diameter, wall thickness and out of roundness. Furthermore the yield stress and the ultimate tensile strength will be utilized.

4.1.1. Filtering

Because large outliers and non realistic values were found in the data-set it was necessary to filter the data to make sure that later fitted models would represent the reality correctly. The requirements by which the data has been filtered was taken similar to the project's pipe requirements depicted in table 3.2. To be able to use these requirements some computations had to be made first. The outer diameter is calculated using the location specific internal pipe diameter combined with twice the wall thickness of the same location. The ovality is calculated by dividing the location specific out of roundness by the nominal diameter according to equation 2.31. Whilst assessing the entire set, from the 1106 samples 14 points were found not to be valid. In appendix D the cut out data points are stated.

4.1.2. Material strength factor α_u

The DNVGL standard allows for a reduction in conservatism by adjusting the material strength factor value to 1, when material strength properties are tested and found to be fulfilling the requirements described in section 7.9.5 in the design standard. As mentioned in subsection 2.3.3 one of the procedures to fulfill the requirements is to show with retrospective documentation that from 50 test units the average yield stress is at least 2.0 standard deviations above SMYS. Whilst assessing the data this requirement is found to be fulfilled, in table 4.1 the properties needed for the evaluation of the requirement are shown.

This means that in the Ichthys case the material strength factor α_u could have been upgraded to a value of 1.

Table 4.1: Supplementary requirement U

SMYS	435	[MPa]
Mean yield stress	503.8	[MPa]
Standard deviation yield stress	12.5	[MPa]
Mean YS - 2 standard deviations	478.8	[MPa]

4.1.3. Implementation of parameters

After a first check of the Pearson correlation coefficients in the original data, it was expected that the outer diameter and wall thickness and the yield stress and ultimate tensile strength would be dependent of each other. However, while the examined dataset distinguishes wall thickness at both sides of a pipe joint and diameter at both sides as well as the body, DNVGL equation 5.28 or equation 2.19 in this report, only asks for one diameter and wall thickness for the entire pipe string since in regular practice the nominal value is used. From a statistical point of view it is preferable to keep the sample size of the variable sets similar to maintain the possibility of fitting a copula, since this can not be done with different sample sizes. Nonetheless this would only be necessary in the case of significant dependence between outer diameter, wall thickness and any arbitrary other sensitive variable to allow for the possibility of fitting a multivariate copula. Therefore three different options are examined. In figures 4.1, 4.2 and 4.3 the properties of these three options are stated.

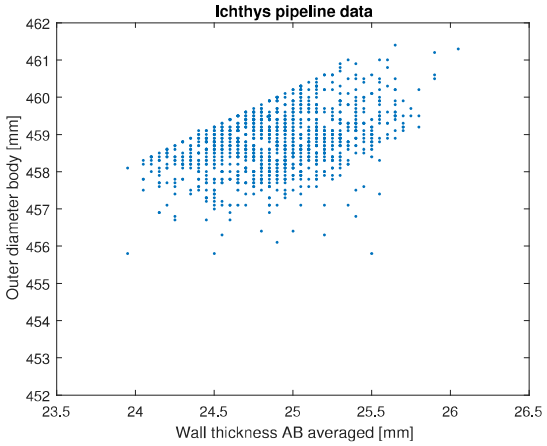

(a)

Mean averaged wall thickness	24.90	[mm]
Mean outer diameter body	458.74	[mm]
Standard dev. averaged wall thickness	0.37	[mm]
Standard dev. outer diameter body	1.05	[mm]
Pearson correlation	0.32	[-]
Sample size	1091	[-]

(b)

Figure 4.1: Properties of the outer diameter body - averaged wall thickness model - option 1

In the first option, depicted above the outer diameter, of the body is combined with the averaged wall thickness of both pipe ends of the same pipe. The outer diameter of the body is calculated by adding twice the averaged wall thickness to the internal diameter of the body, this because wall thicknesses of the body are not available. Note the 'sharp' line in the upper part of the figure 4.1a. An explanation of what is happening in this situation has to do with the production process. During the hydroforming press process, discussed in section 3.3, the pipe is pushed outward into the mold of the press and via this process plastically deforms the pipe and ensures a mechanical bond between the liner and the backing material. The springback when the hydroforming press is released is expected to be larger in the case of smaller wall thicknesses. Which results in smaller outer diameters.

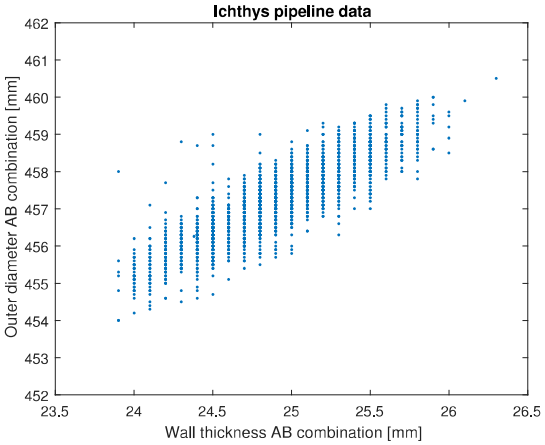

(a)

Mean averaged wall thickness	24.90	[mm]
Mean outer diameter AB combined	457.23	[mm]
Standard dev. wall thickness AB combined	0.42	[mm]
Standard dev. outer diameter AB combined	1.10	[mm]
Pearson correlation	0.86	[-]
Sample size	2182	[-]

(b)

Figure 4.2: Properties of the outer diameter AB combined - wall thickness AB combined model - option 2

In option two the outer diameters and wall thicknesses of each pipe end are combined in one larger dataset. In this manner twice as many data points are used to fit a certain model. Also because none of the values are averaged the spread of this is largest and with regards to the uncertainty this gives the best representation of the situation.

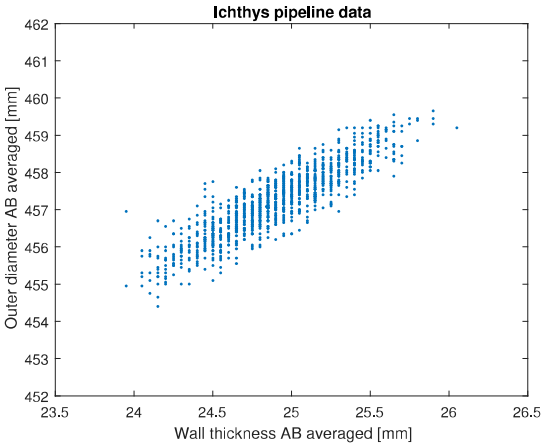

(a)

Mean averaged wall thickness	24.90	[mm]
Mean averaged outer diameter	457.23	[mm]
Standard dev. averaged wall thickness	0.37	[mm]
Standard dev. averaged outer diameter	0.92	[mm]
Pearson correlation	0.89	[-]
Sample size	1091	

(b)

Figure 4.3: Properties of the averaged outer diameter - averaged wall thickness model - option 3

In the third option both the outer diameter as well ass the wall thickness is averaged. In this manner the sample size is kept the same however, the spread of the set gets smaller while the Pearson correlation coefficient overestimates the linear relationship of the situation, both because of the averaging.

In the next section the correlations between all different parameters are checked and a decision can be made on what option will be used. Note that when no significant dependence is shown between the wall thickness and outer diameter and any of the other variables the second option is preferred. This is because the spread of the parameters is the biggest, which can be seen from the larger standard deviations. Keeping in mind that equation 2.19 needs to be satisfied at every point in the pipeline, or the entire pipe string the larger sample size gives a better representation of the real life situation. Also it is the less conservative option which in this case has to be chosen since all values do occur in the final pipeline.

4.1.4. Correlations

In the following table the correlations between the different variables of the dataset can be found. The list has been reduced to the variables with a correlation highter than 10%, the

complete list of inter variable correlations can be found in appendix D.

The significant negative correlation seen with the internal diameter of the body and the wall thickness has to do with production process of the pipe. Because of the expanding of the pipe against a mold a bigger wall thickness causes a smaller internal diameter. The fact that the correlation is not as large with the internal diameters of the pipe ends has to do with the fact than because of the stringent requirements the pipe ends get post processed to achieve the required dimensions. The relation between the wall thickness of pipe end A and pipe end B can be explained due to the fact that the pipe is made from on sheet of metal and thus large variation in thickness is not expected. Similarly the dependence between the yield stress and the ultimate tensile strength, since both are material strength properties and again only one pipe, or metal sheet, is considered.

Table 4.2: Pearson moment correlations

Variable pair	**Matlab reference**	**Pearson ρ**
Internal diameter Body - Wall thickness A	ID_Body_WT_B	-0.342
Internal diameter Body - Wall thickness B	ID_Body_WT_A	-0.319
Internal diameter Body - Outer diameter B	ID_Body_OD_B	-0.294
Internal diameter Body - Outer diameter A	ID_Body_OD_A	-0.277
Ultimate tensile strength - Internal diameter A	UTS_ID_A	-0.130
Yield stress - Internal diameter A	YS_ID_A	-0.120
Ultimate tensile strength - Outer diameter A	UTS_OD_A	-0.112
Ultimate tensile strength - Outer diameter B	UTS_OD_B	-0.111
Yield stress - Outer diameter A	YS_OD_A	-0.109
Ovality A - Ovality B	Ova_A_Ova_B	0.113
Internal diameter B - Wall thickness A	ID_B_WT_A	0.128
Internal diameter A - Wall thickness A	ID_A_WT_A	0.141
Internal diameter A - Wall thickness B	ID_A_WT_B	0.179
Outer diameter B - Outer diameter Body	OD_B_OD_Body	0.243
Internal diameter B - Outer diameter A	ID_B_OD_A	0.269
Outer diameter Body - Wall thickness B	OD_Body_WT_B	0.273
Outer diameter A - Outer diameter Body	OD_A_OD_Body	0.287
Outer diameter Body - Wall thickness A	OD_Body_WT_A	0.296
Internal diameter A - Outer diameter B	ID_A_OD_B	0.330
Internal diameter A - Internal diameter B	ID_A_ID_B	0.349
Outer diameter B - Wall thickness A	OD_B_WT_A	0.512
Outer diameter A - Wall thickness B	OD_A_WT_B	0.538
Wall thickness A - Wall thickness B	WT_A_WT_B	0.555
Outer diameter A - Outer diameter B	OD_A_OD_B	0.574
Internal diameter A - Outer diameter A	ID_A_OD_A	0.586
Internal diameter B - Outer diameter B	ID_B_OD_B	0.604
Internal diameter Body - Outer diameter Body	ID_Body_OD_Body	0.757
Yield stress - Ultimate tensile strength	YS_UTS	0.800
Outer diameter B - Wall thickness B	OD_B_WT_B	0.847
Outer diameter A - Wall thickness A	OD_A_WT_A	0.885

Table 4.3: Pearson moment correlations

Variable pair	Matlab reference	Pearson ρ
Averaged Wall thickness - Internal diameter Body	WT_ave_ID_Body	-0.375
Averaged internal diameter - Ultimate tensile strength	ID_ave_UTS	-0.132
Averaged outer diameter - Ultimate tensile strength	OD_ave_UTS	-0.126
Averaged outer diameter - Yield stress	OD_ave_YS	-0.115
Averaged internal diameter - Yield stress	ID_ave_YS	-0.111
Wall thickness A & B - Internal diameter A & B	WT_combi_ID_combi	0.102
Averaged Wall thickness - Averaged internal diameter	WT_ave_ID_ave	0.182
Averaged Wall thickness - Outer diameter Body	WT_ave_OD_Body	0.322
Wall thickness A & B - Outer diameter A & B	WT_combi_OD_combi	0.865
Averaged Wall thickness - Averaged outer diameter	WT_ave_OD_ave	0.889

After examining the correlations of all the parameter combinations the expected dependencies for the yield stress and ultimate tensile strength and wall thickness and outer diameter are indeed evident. Note that besides the dependence between these two combinations there is no significant relationship found. This means that in the rest of the report option 2 regarding the wall thickness - outer diameter set will be used, as discussed in subsection 4.1.3.

4.2. Sensitivity analysis

In the following section the sensitivity of the different main parameters of equation 2.19 are analyzed. First the resistance parameters and later the load parameters.

4.2.1. Resistance parameters

For the sake of computational ease in the Monte Carlo simulation variables that cause negligible variation in the outcome can be considered deterministic, as discussed in section 2.5. To determine if the influence of the spread of the variables on the outcome of the unity check is indeed negligible a sensitivity analysis is conducted. The sensitivity analysis is set up as follows:

1. First a reference case is chosen with nominal values for all the basic variables. In this case the load case discussed in chapter 3.
2. From the analysis of the data-set the spread of each variable is known. The domain of each variable is divided in a 15 step vector and serves as input for the model.
3. For each step the unity check is calculated.
4. The variation in unity check outcome is plotted, actual delta and percentual change can be calculated. Relatively over the spread as well as compared to the reference case.

Results of the sensitivity analyses can be found in table 4.4 and figure 4.4. Note that the percentage given in the sensitivity column is the percentual change of the ULSb unity check value over the range of the parameter. Also when the sensitivity of the ovality in this specific case was found to be negligible the water depth was altered to check it's influence in deeper waters.

Table 4.4: Sensitivity analysis resistance parameters

Property	Range in data-set		Range in ULSb	Sensitivity	
Wall thickness	23.9 - 26.3	[mm]	0.90 - 0.71	20.8	[%]
Outer diameter	454 - 460.4	[mm]	0.81 - 0.76	6.5	[%]
Yield stress	451 - 541	[MPa]	0.79 - 0.65	17.3	[%]
Ultimate tensile strength	536 - 589	[MPa]	0.79 - 0.72	9.2	[%]
Ovality (water depth 251 m)	0 - 1.5	[%]	0.79 - 0.79	0.0	[%]
Ovality (water depth 1200 m)	0 - 1.5	[%]	0.91 - 0.99	8.3	[%]

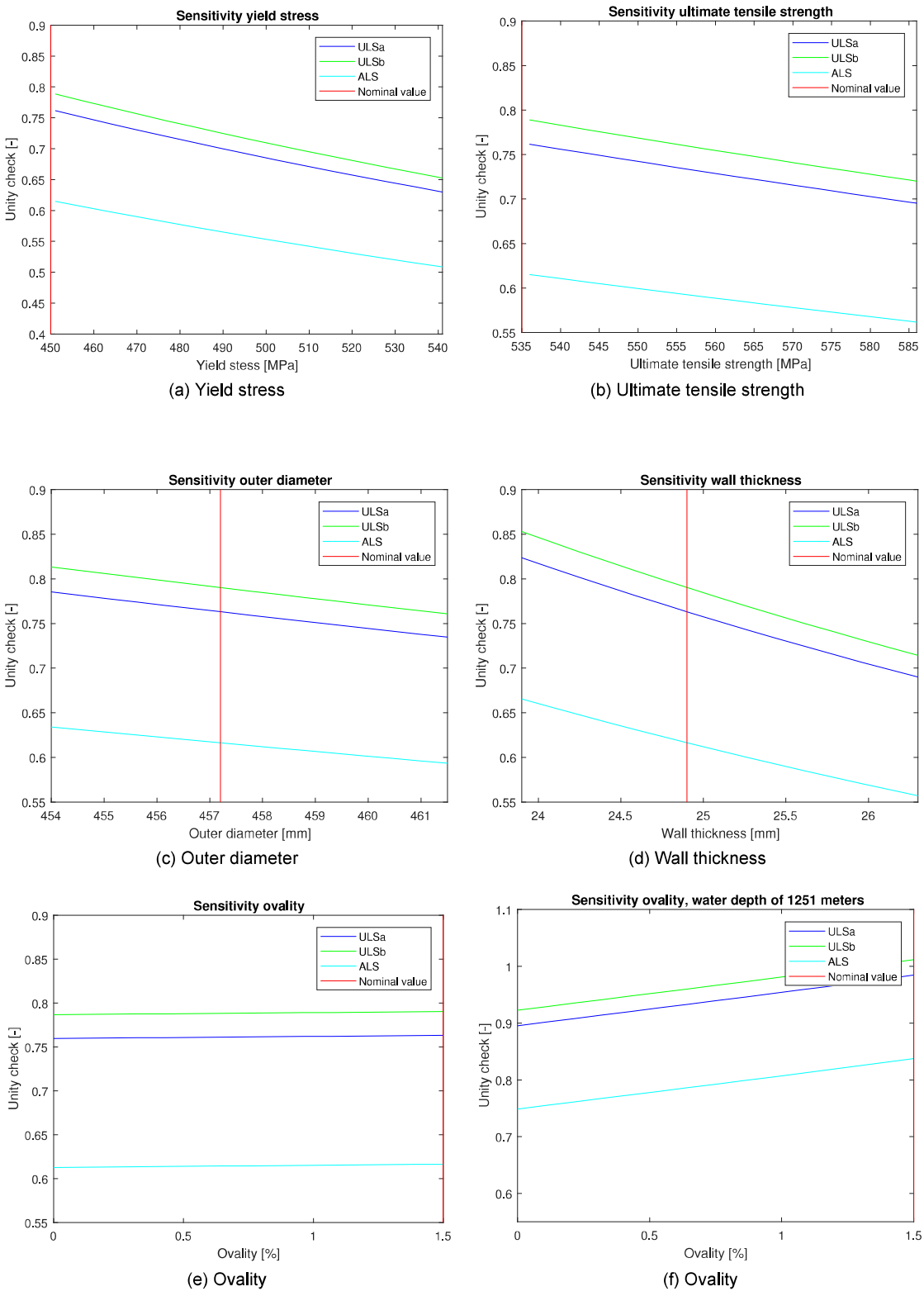

Figure 4.4: Sensitivity analysis resistance parameters

4.2.2. Load parameters

To better understand the influence of the different loads in the combined loading criterion also a sensitivity analyses on the load parameters has been conducted. The sensitivity analyses for the load parameters is set up as follows:

1. Again the load case discussed in chapter 3 is the starting point.
2. Each parameter is, in 15 steps, increased until the unity check reaches a value of 1.
3. For each step the unity check is calculated.
4. The unity check outcome is plotted as a function of the changing load parameter.

The non-linearity of the equation becomes very clear, especially in figure 4.5 a and c. Observe that in cases of the effective axial force and the load moment the ULSb value increases significantly more with respect to the ULSa value. This is directly related to the the load factor γ_E, which differs for the ultimate limit state system check (ULSa), the ultimate limit state local check (ULSb) and the accidental limit state which have values of 0.7, 1.3 and 1.0 respectively as shown in figure A.4. Also it becomes clear that the bending moment is the driving load and that variation in the bending moment has the biggest influence on the final unity check value.

Table 4.5: Sensitivity analysis load parameters

Property	Range		Range in ULSb	Sensitivity
Environmental load moment	243.788 - 400	[kNm]	0.79 - 1.00	most sensitive
Effective axial environmental force	26.295 - 3300	[kN]	0.79 - 1.00	least sensitive
Water depth	251 - 1210	[m]	0.79 - 1.00	-

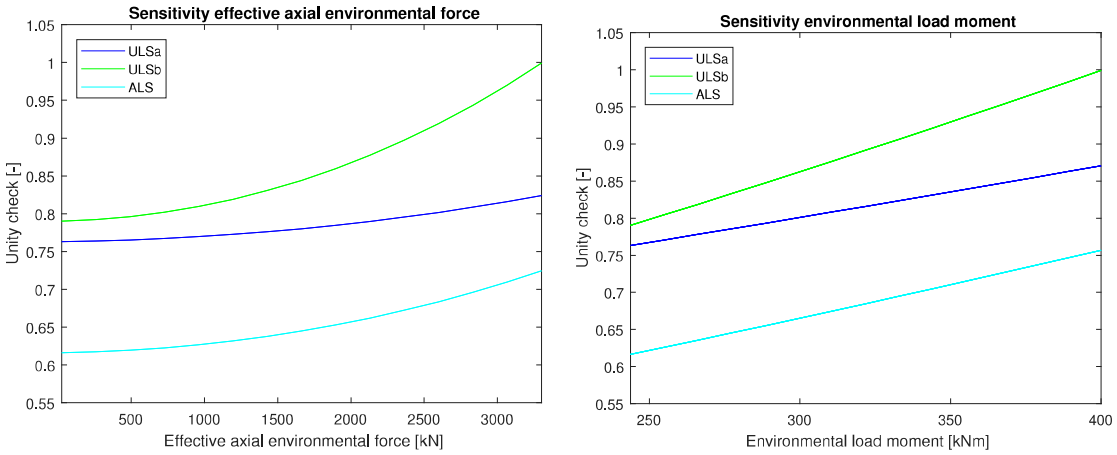

(a) Effective axial force

(b) Bending moment

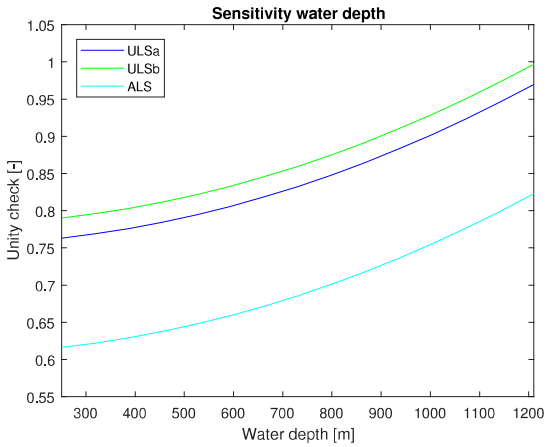

(c) Water depth

Figure 4.5: Sensitivity analysis load parameters

4.3. Variable distributions

After analyzing the dependencies of the different variables and considering the sensitivity analysis it can be concluded that in this specific case it is not necessary to model the ovality as a stochastic variable. The uncertainty in the other variables; Wall thickness, outer diameter, yield stress and ultimate tensile strength do have a significant influence on the unity check so according to their correlations a copula model needs to be fitted. In figure 4.6 scatter plots of both variable pairs can be found. Note that the filtered out data points are depicted in red.

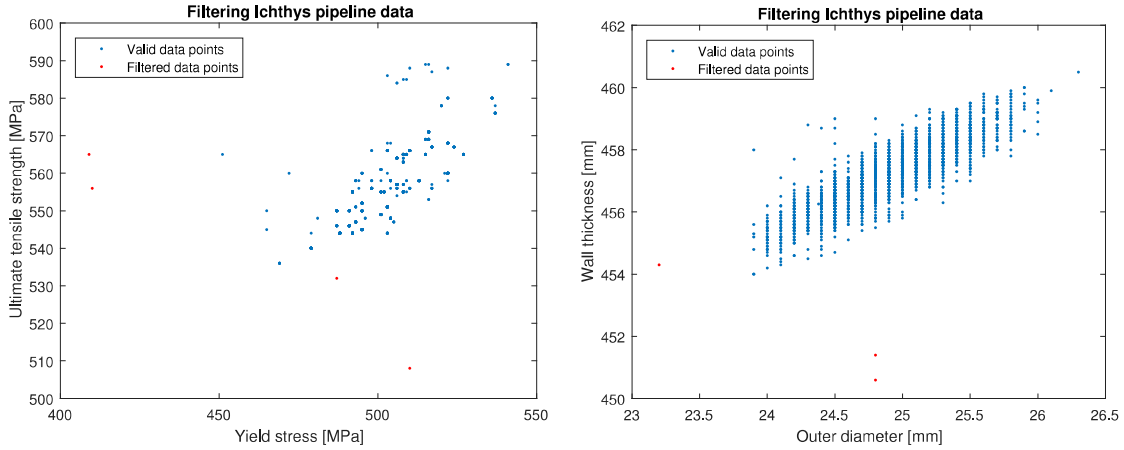

(a) Yield stress - ultimate tensile strength

(b) Wall thickness - outer diameter

Figure 4.6: Filtered data-sets

However, for the sake of completeness a distribution function will be fitted to the ovality. This to be able to conduct a structural reliability assessment in a fictional deep water case and thus be able to give an indication on the influence of the ovality. In the coming sections the copula model will be fitted to the wall thickness - outer diameter dependence model as well as to the yield stress - ultimate tensile strength dependence model. The five different copula models introduced in section 2.9 will be compared to the observed data, using the goodness of fit tests which have been introduced in 2.10.

4.3.1. Wall thickness - outer diameter model

In the coming section the T, Clayton, Frank, Gumbel and Gaussian copula's will be assessed on their goodness of fit. The samples are randomly generated and the copula parameters are calculated using the Spearman rank correlation coefficient of the wall thickness - outer diameter combination, which has a value of 0.86. The degree of freedom for the T copula, the second copula parameter only applicable for the T type copula, is calculated in Matlab using the maximum likelihood estimator and has a value of 11.4. Meaning that the T copula tends towards the Gaussian copula which can also be seen from the semi-correlation values.

Semi-correlations

In table 4.6 the values of the Pearson product moment correlation coefficients of each quadrant can be found. Note that the first column shows values of the Spearman rank correlation and were used as a check to see if the samples indeed had the same rank correlation as the empirical data. It needs to be clear that the south-west quadrant is the most important in this research since in this area low wall thicknesses and small outer diameters are combined, which results in risk of failure when assessing pipe integrity. The samples of the two models that comply best with the measured data, especially in the south-west quadrant, the T and Gaussian copula, are plotted in figure E.1 together with the measured data. Since the relatively high degree of freedom used for the T copula, it hardly differs from the Gaussian copula.

Table 4.6: Semi-correlations wall thickness - outer diameter

	$r_{tot,sp}$	$\rho_{NE,ps}$	$\rho_{NW,ps}$	$\rho_{SE,ps}$	$\rho_{SW,ps}$
Data	0.86	0.70	-0.15	0.10	0.71
T	0.85	0.73	0.15	0.21	0.73
Clayton	0.86	0.33	0.12	0.13	0.91
Frank	0.86	0.54	0.17	0.13	0.55
Gumbel	0.86	0.84	0.04	0.08	0.61
Gaussian	0.86	0.70	0.24	0.22	0.72

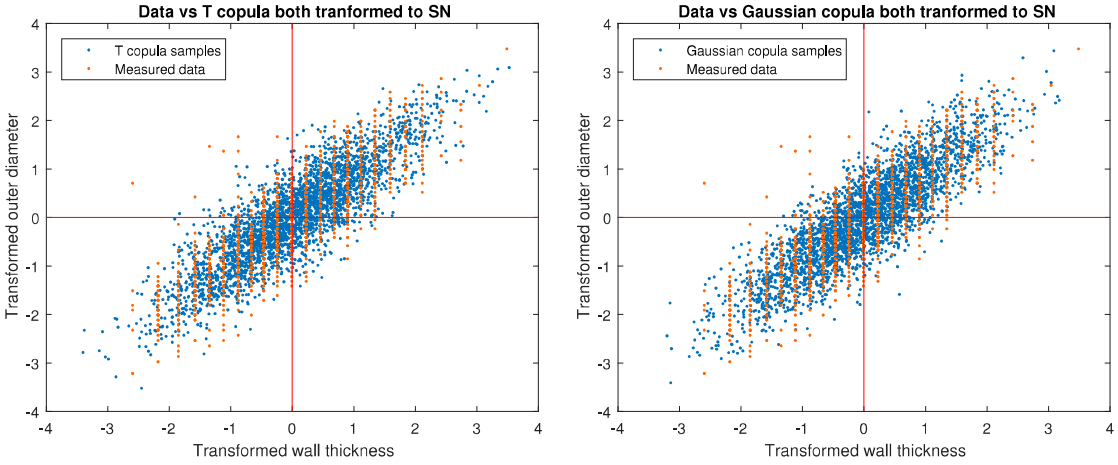

(a) T vs observed data (b) Gaussian vs observed data

Figure 4.7: Model comparison wall thickness outer diameter

Note that all the random samples transformed to standard normal used to calculate the semi-correlations per quadrant can be found in appendix E.

Cramér von Mises

The similar samples that have been used in the semi-correlations comparison have been used to calculate the Cramér von Mises statistic value. First the data needs to be transformed to the copula space, [0,1], after which the empirical copula CDF of the data was calculated using a grid of 11 x 11 bins. Then the same script was used to calculate the empirical copula CDF's of the randomly generated samples of the different copula models. The calculated Cramér von Mises statistic values are stated in 4.7, the lower the CM_n value the better the copula model fits. The absolute difference of the empirical copula's, of the copula models that had the best semi-correlation values, are depicted in figure 4.9. The rest of the empirical copula's and absolute differences can be found in appendix F. The sample size is sufficient since the empirical copula's are smooth and the set is larger than the observed data of the Ichthys set. Increasing the bin size makes the Cramér von Mises statistic value tend to the same value because of the fairly concentrated datapoints, so a bin size needs to be chosen that is fine enough to pick up differences in the two models and rough enough to be able to base decisions on the difference between the values.

Table 4.7: Cramér von Mises statistic value WT-OD

Copula model	CM_n
T	8.6349
Clayton	15.4156
Frank	8.0319
Gumbel	9.2252
Gaussian	7.1109

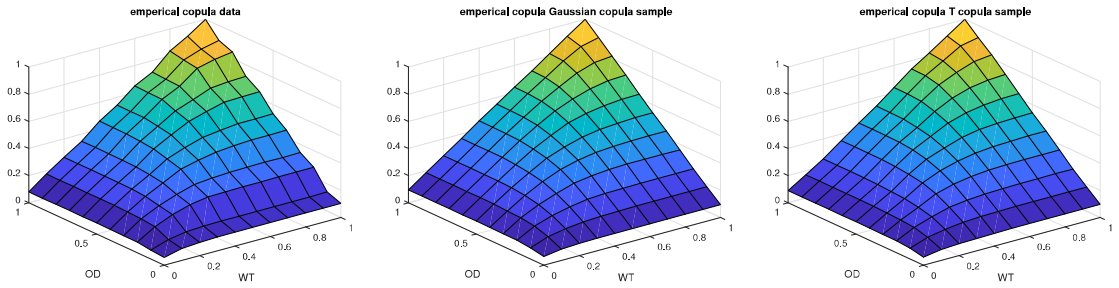

(a) empirical Copula data (b) empirical Copula Gaussian (c) empirical Copula T

Figure 4.8: Model comparison wall thickness outer diameter

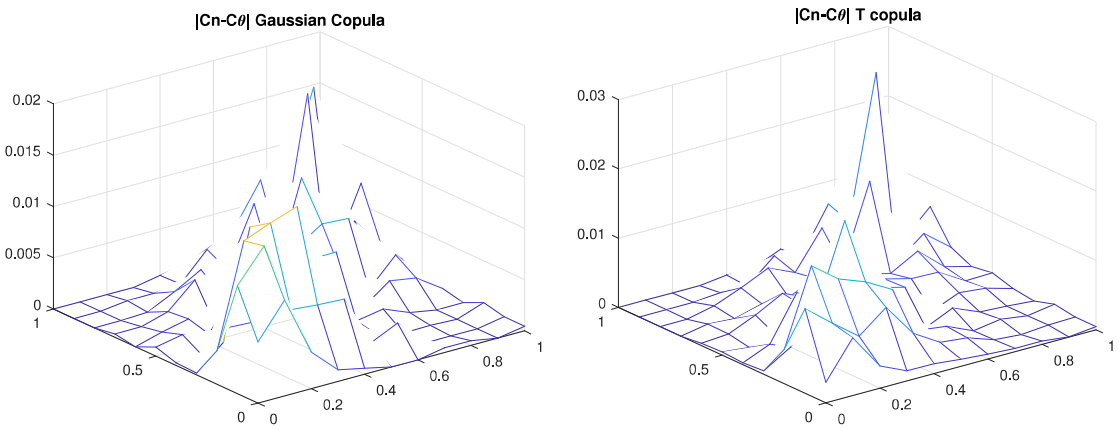

(a) Absolute difference Data - Gaussian copula (b) Absolute difference Data - T copula

Figure 4.9: Absolute difference empirical copulas

Both goodness of fit tests show the same result. The wall thickness - outer diameter dependence model is best represented by a Gaussian Copula.

4.3.2. Yield stress - ultimate tensile strength model

Similar to the procedure followed in the case of the wall thickness - outer diameter model again a randomly generated sample of 3000 points is made from each different copula model calculating the copula parameters according to the Spearman rank correlation coefficient. Which in this case has the value of 0.84. The degree of freedom for the T copula is via the maximum likelihood method calculated to be 8.9.

Semi-correlations

Again the south-west quadrant of the semi-correlation comparison is the most important because similarly to the wall thickness - outer diameter situation low values of yield stress and ultimate tensile strength will lower the pipes structural integrity. In table 4.8 the Pearson moment correlation coefficients of each quadrant can be found.

Table 4.8: Semi correlations yield stress - ultimate tensile strength

	$r_{tot,sp}$	$\rho_{NE,ps}$	$\rho_{NW,ps}$	$\rho_{SE,ps}$	$\rho_{SW,ps}$
Data	0.84	0.49	0.27	0.64	0.65
T	0.83	0.69	0.09	0.16	0.71
Clayton	0.84	0.34	0.06	0.04	0.89
Frank	0.85	0.51	0.17	0.10	0.53
Gumbel	0.83	0.79	0.10	0.07	0.58
Gaussian	0.83	0.67	0.21	0.12	0.67

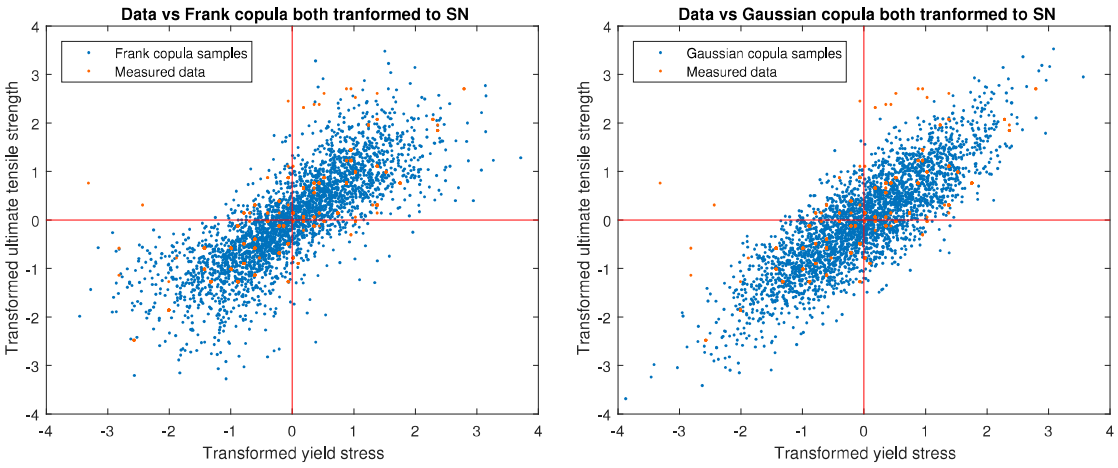

(a) Frank vs observed data (b) Gaussian vs observed data

Figure 4.10: Model comparison yield stress - ultimate tensile strength

Cramér von Mises

Since the data points in the yield stress - ultimate tensile strength data are even more concentrated, some of the plotted dots contain up to five values, the overal values of the Cramér von Mises statistic are a lot higher.

Table 4.9: Cramér von Mises statistic value YS-UTS

Copula model	CM_n
T	30.5038
Clayton	30.8183
Frank	28.8728
Gumbel	31.3830
Gaussian	30.2263

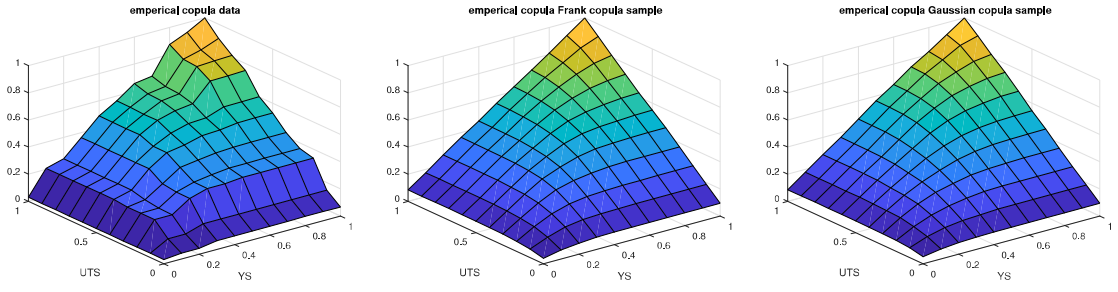

(a) empirical Copula data (b) empirical Copula Gaussian (c) empirical Copula T

Figure 4.11: Model comparison yield stress - ultimate tensile strength

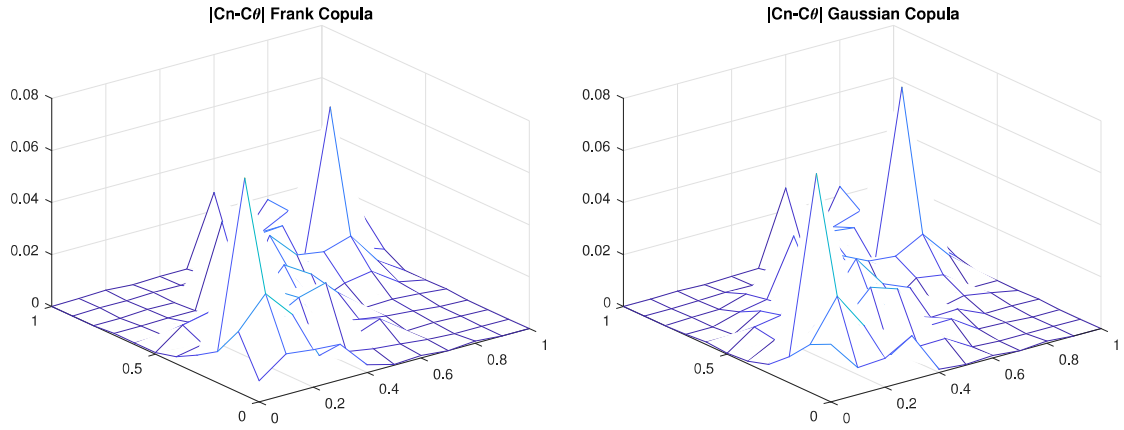

(a) Absolute difference Data - Frank copula (b) Absolute difference Data - Gaussian copula

Figure 4.12: Absolute difference empirical copulas

According to the semi-correlations test the Gaussian copula has the best representation of the observed data in the South-West quadrant. However, the Cramér von Mises statistic value is smaller for the Frank copula. Taking into account the regular project requirements, meaning that values below SMYS 450 MPa and SMTS 535 MPA are not used. As well as the fact that the observed data before filtering also did not show any cases where the the observed pipe had a relatively low yield stress as well as ultimate tensile strength. Meaning that both values are under the requirements. The samples in the Gaussian copula in the lower left corner do not give a good representation of the line pipe used in real life, therefore for in the Monte Carlo simulation the Frank Copula will be used to represent the dependence model for the yield stress - ultimate tensile strength combination. Also note that the absolute difference in figure 4.12 a and b near point (0,0) is smaller for the Frank copula model than for the Gaussian copula model which indicates that for extreme values in this part of the model the Frank copula fits better.

4.3.3. Ovality

To be able to serve as input for the Monte Carlo simulation a probability distribution needs to be fitted to the ovality.

Bayesian Information Criterion

The Bayesian Information Criterion is calculated for a selection of distributions; Beta, Birnbaum-Saunders, Exponential, Extreme value, Gamma, Generalized extreme value, Generalized, Pareto, Inverse Gaussian, Logistic, Log-logistic, Lognormal, Nakagami, Normal, Rayleigh, t location-scale and Weibull. Of all distributions the lowest BIC value was found for the Normal distribution. To maintain the overview in figure 4.13 only six different distributions have been plotted.

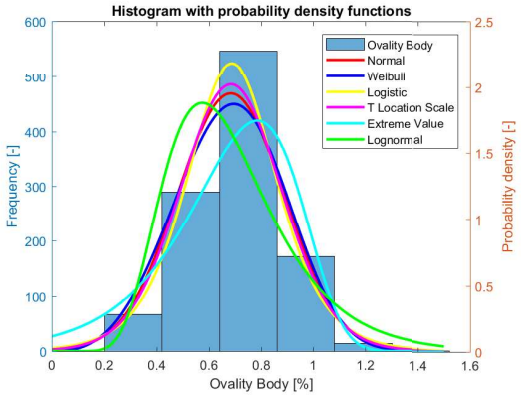

Figure 4.13: Ovality body

Table 4.10: BIC values

Normal	-359.26
Weibull	-357.88
Lognormal	-146.05
Extreme value	-154.25
T Location	-354.87
Logistic	-357.47

Kolmogorov Smirnov Test

According to the Bayesian Information Criterion values the normal distribution is the best fit for the ovality of the body. However visually the fit is not entirely satisfactory. Therefore another goodness of fit test is conducted namely the one-sample Kolmogorov-Smirnov (KS) test. The KS tests the null hypothesis that the data in the sample ovality body, comes from a normal distribution against the alternative that the sample does not come from such a distribution. As discussed in subsection 2.10.2 it is possible to test for any hypothesized distribution. The Kolmogorov-Smirnov test rejects the null hypothesis with a significance level of 5% and thus we can conclude that the fitted normal distribution is a bad representation of the empirical data for the ovality.

Kernel distribution

Since no parametric distribution was found to be able to represent the ovality sample correctly, Kernel density estimation is used to fit a Kernel distribution to the empirical data. Taking the histogram for the ovality of the body into account, when picking the Kernel function and bandwidth the most important is that the final kernel distribution is smooth, unimodal, and has no density around 0 and 1.5%. All four types of Kernel's mentioned in section 2.8 have been tried, however only the Gaussian Kernel resulted in a smooth distribution. In appendix G the Kernel distributions with the uniform, triangular and Epanechnikov Kernels can be found.

In figure 4.14a the Kernel distributions, with a Gaussian Kernel and several different bandwidths are displayed. The blue distribution with bandwidth 0.32 is the default bandwidth that Matlab comes up with. However it has quite some density in the tails which in this case is not favourable since this is not the case in the empirical data. The bandwidth has been varied to create a smooth uni-modal distribution with no or hardly any density at 0 and 1,5 %. The final bandwidth was selected to be 0.10 and the Kernel distribution corresponding to this value is depicted in figure 4.14b.

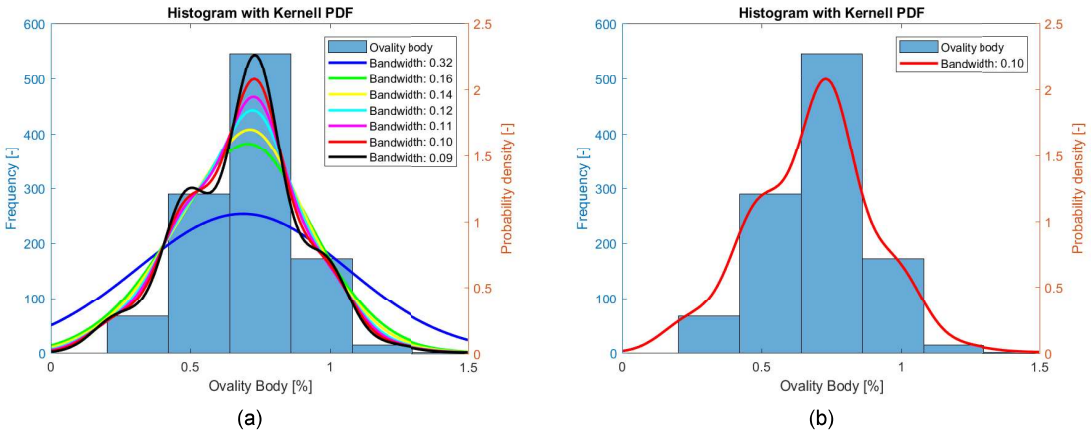

Figure 4.14: Kernel distribution ovality body

4.4. Conclusion

After analyzing the 1106 geometrical and material strength data points of the Ichthys 18" pipeline data set the input for the Monte Carlo simulation has been determined. The wall thickness, outer diameter dependence model is best represented by the use of a Gaussian copula with a copula parameter value of 0.8710. While the yield stress, ultimate tensile strength dependence model is best represented by the use of a Frank copula with a copula parameter value of 9.1115. The ovality probability distribution is defined using Kernel density estimation with a Gaussian Kernel and a bandwidth of 0.10.

5

Structural reliability assessment

In the following chapter the structural reliabity assessment is carried out. In the first section the set-up of the Monte Carlo simulation and the evaluation of the probability of failure is explained. In section 5.2 the different reference and test cases are described. The third section covers the sample size analysis. And finally, in the fourth section, the Monte Carlo simulations are covered.

5.1. Monte Carlo set up

Monte Carlo approaches use random sampling to simulate physical phenomena. In chapter 4 the dependence model for yield stress and ultimate tensile stress and the dependence model for the wall thickness and outer diameter have been described. For the Monte Carlo simulation random samples from these models are generated on the copula scale from zero to one. These random generated values are then transformed back to the original margins of the parameters using using Kernel density estimation and the inverse distribution function. Together with the randomly generated values from the fitted Kernel distribution for the ovality, these values are used to run the Monte Carlo simulation with. As input for the Monte Carlo simulation we have one vector with values for the ovality, a two-column matrix with the values of the yield strength and the ultimate tensile stress and another two-column matrix with the values of the wall thickness and outer diameter.

Whilst running the Monte Carlo simulation the unity check, according to equation 2.19, is calculated in every step. Each successive step using the values in the next row of the described vector and matrices. The result is a vector, with the same length as the vector and matrices that served as input, with unity check values. The target probability of failure aimed for by DNVGL is 10^{-3}, this means that when following the design standard and the unity check value is pushed to it's limit of 1, the pipeline will fail no more then 10^{-3} of the times.

To determine the probability of failure of the test case in the Monte Carlo simulation first a reference case needs to be defined. The unity check value of this reference case serves as the threshold for failure, which is similar to the situation in which the value is pushed to 1. When the Monte Carlo simulation is finished the output, the vector with unity check values, is evaluated according to the unity check value from the reference case. Thus all values above the governing reference case unity check value - ULSa or ULSb depending on which is governing - are considered fails and dividing this number by the sample size of the simulation results in the probability of failure for the specific test case.

This value is expected to be lower than the aimed for probability of failure which in turn would show the conservatism of the situation. Knowing the aimed for probability of failure allows for changing the unity check value according to the results from the Monte Carlo simulation. If we determine the value of the unity check which has $1/1000 \cdot samplesize$ number of unity check values larger then itself, this value is the ULSb value that should be used in order to decrease conservatism and still fulfill the aim of a 10^{-3} probability of failure. When

the adjusted unity check value is known the safety class resistance factor for local buckling can be fine tuned to achieve the same value in the reference case.

5.2. Reference and test cases

For the Monte Carlo simulation 8 reference cases and 14 test cases are defined to assess the influence of the different parameters on the unity check value in different load scenario's. The load case described in chapter 3 serves as the starting point and is represented in reference case 1-a. In reference case 1-b the unity check is calculated with the same load case but the material strength factor is upgraded to 1.

The resistance parameter sensitivity analysis showed that the ovality has no significant influence in a shallow water case like the Ichthys project. To be able to determine the impact of modelling the ovality stochastically, the water depth of the base case, reference case 1, is increased to 1251m. The loads used in this situation have been calculated with Flexcom applying the same sea state and heading that was governing in the base case. The configuration of the pipe string catenary was adjusted to keep the strain of the stem in the static case similar to the base case maintaining the same functional bending moment. Reference case 2 represents this situation and the unity check is calculated for the nominal (2-a) as well as the upgraded material strength factor (2-b). Reducing conservatism is only necessary in situations bordering the limits of structural integrity, e.a. where the unity check has a value close to 1. In reference cases 3a and 3b the significant wave height used, in the base case during the Flexcom dynamic analysis, is increased to the situation where the loads push the unity check of reference case 3-a to a value of around 1. The water depth in this situation is similar to the shallow water base case and has a value of 251 meters.

In reference cases 4-a and 4-b the significant wave height of the sea state is also increased for the deep water case, reference case 2. Table 5.1 gives an overview of the different functional and environmental effective axial tensions and bending moment loads used in the reference cases. Table 5.2 shows, for each reference and test case, if the input of the resistance parameters is modelled deterministic or stochastically, the used material strength factor and the considered water depth. The last column of the table gives the calculated governing unity check value.

Test case 1 to 3 correspond to reference case 1, test case 4 to 8 to reference case 2, test case 8 to 10 to reference case 3 and finally test case 10 to 14 correspond to reference case 4. Note that all loads are calculated using Flexcom during a time domain analysis and thus the values depict a realistic situation with regards to the relationship between the bending moment and tension.

Table 5.1: Loads reference cases

	Functional		Environmental	
	Tension [kN]	**Moment [kNm]**	**Tension [kN]**	**Moment [kNm]**
Reference case 1	130.3	1180	26.295	243.788
Reference case 2	101.5	1180	74.912	147.422
Reference case 3	147.9	1081	104.829	522.896
Reference case 4	87.4	1155	64.897	362.455

Table 5.2: Reference and test cases

	YS -UTS	OD - WT	f0 [%]	α_u	WD [m]	UC
Reference case 1-a	Nominal values	Nominal values	1.50	0.96	251	0.7903
Reference case 1-b	Nominal values	Nominal values	1.50	1	251	0.7284
Reference case 2-a	Nominal values	Nominal values	1.50	0.96	1251	0.8523
Reference case 2-b	Nominal values	Nominal values	1.50	1	1251	0.8476
Reference case 3-a	Nominal values	Nominal values	1.50	0.96	251	1.0546
Reference case 3-b	Nominal values	Nominal values	1.50	1	251	0.9720
Reference case 4-a	Nominal values	Nominal values	1.50	0.96	1251	1.1392
Reference case 4-b	Nominal values	Nominal values	1.50	1	1251	1.0528
Test case 1	Frank copula	Nominal values	1.50	1	251	
Test case 2	Nominal values	Gaussian copula	1.50	1	251	
Test case 3	Frank copula	Gaussian copula	1.50	1	251	
Test case 4	Frank copula	Nominal values	1.50	1	1251	
Test case 5	Nominal values	Gaussian copula	1.50	1	1251	
Test case 6	Nominal values	Nominal values	Distributed	1	1251	
Test case 7	Frank copula	Gaussian copula	Distributed	1	1251	
Test case 8	Frank copula	Nominal values	1.50	1	251	
Test case 9	Nominal values	Gaussian copula	1.50	1	251	
Test case 10	Frank copula	Gaussian copula	1.50	1	251	
Test case 11	Frank copula	Nominal values	1.50	1	1251	
Test case 12	Nominal values	Gaussian copula	1.50	1	1251	
Test case 13	Nominal values	Nominal values	Distributed	1	1251	
Test case 14	Frank copula	Gaussian copula	Distributed	1	1251	

5.3. Sample size analysis

To determine the number of simulations that is needed to get a reliable outcome, different sample sizes are tried in test case 3 until the unity check value and probability of failure converges. The first simulation was run with a sample size of 5K, the sample size in the following simulations increased with steps of 5K until 20K. From 20K to 50K the step size increases with 10K. From 50K to 1000K samples the step size is 50k and finally from 1000K to 5000K the number of samples increases with 500K in every step. The values of this first analysis are stated in table 5.4a. These values are plotted with the blue lines in figures 5.1 and 5.2. Visually speaking both the ULSb value as well as the probability of failure seem to be converged when using at least one million samples. However, the PoF value for two and a half million does pop out. To be certain the sample size is correct different sets of samples with a similar size should be evaluated. For sample sizes 250K, 500K, 1000K, 3000K and 5000K, 10 different sets are randomly generated and used in the same Monte Carlo simulation. The results of using these samples are stated in 5.4b and are plotted in 5.1 and 5.2 with the red dots.

Visually it is clear that the dots move towards each other and thus convergence occurs. To be able to make a decision at what point the values have converged sufficiently the spread in each set of samples is checked. The calculated probability of failure shows the conservatism in the installation analysis. The unity check value is needed to be able to fine tune the safety class resistance factor and is the factor which defines what is allowed by DNVGL and is thus of greater importance. In table 5.3 the smallest value, largest value and the spread of the unity check value for each set of samples is stated. Knowing that in HMC's installation analyses the unity check gets rounded of to two significant digits this is the amount of significant digits needed in this Monte Carlo simulation. It can be concluded that the spread in the set of 3000K samples does not have any influence in a situation where a value gets rounded of to this significance. Meaning that each sample would result in the same unity check value. Thus in the Monte Carlo simulations for test case 1 to 14 a sample size of 3000K will be used.

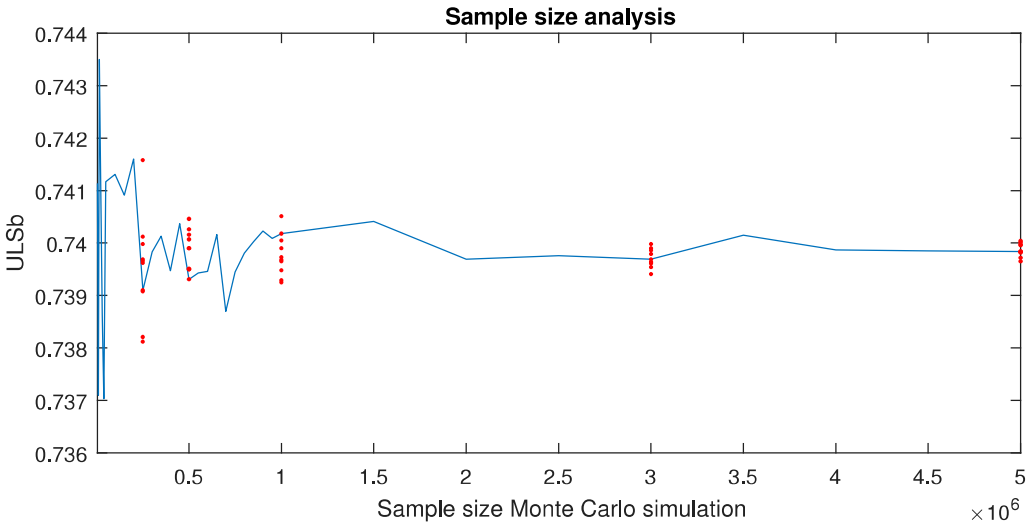

Figure 5.1: Sample size analysis - ULSb

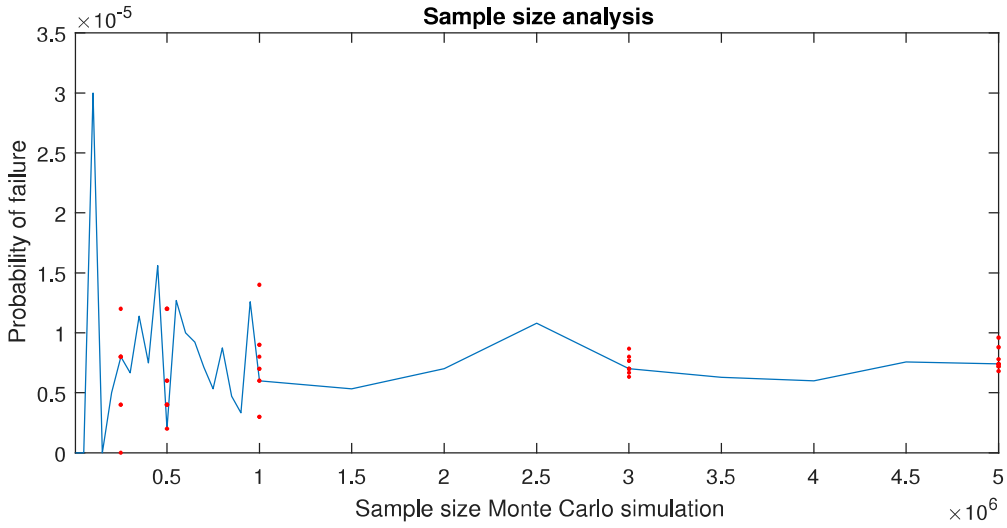

Figure 5.2: Sample size analysis - Probability of failure

Table 5.3: Spread in sample size analysis

	250K	500K	1000K	3000K	5000K
Smallest ULSb	0.73812	0.73931	0.73925	0.73941	0.73965
Largest ULSb	0.74158	0.74046	0.74051	0.73998	0.74004
Spread	0.00346	0.00115	0.00126	0.00057	0.00039

5.4. Monte Carlo simulation

The Monte Carlo simulations for the test cases that have been defined in section 5.2 have been run and the histograms with the calculated unity check values are depicted in figures 5.3 to 5.16. For each simulation the full histogram and a zoomed in figure of the upper tail are showed. Histograms of the input used for Monte Carlo simulations can be found in appendix H.

Table 5.4: Monte Carlo sample size analysis

(a)

n	ULSb	Fails	PoF
5K	0.74114	0	0
10K	0.7371	0	0
15K	0.7435	0	0
20K	0.74178	0	0
30K	0.73864	0	0
40K	0.73703	0	0
50K	0.74117	0	0
100K	0.74131	3	3.00E-05
150K	0.74091	0	0
200K	0.74160	1	5.00E-06
250K	0.73910	2	8.00E-06
300K	0.73983	2	6.67E-06
350K	0.74013	4	1.14E-05
400K	0.73947	3	7.50E-06
450K	0.74037	7	1.56E-05
500K	0.73931	1	2.00E-06
550K	0.73943	7	1.27E-05
600K	0.73946	6	1.00E-05
650K	0.74016	6	9.23E-06
700K	0.73870	5	7.14E-06
750K	0.73945	4	5.33E-06
800K	0.73981	7	8.75E-06
850K	0.74003	4	4.71E-06
900K	0.74023	3	3.33E-06
950K	0.74009	12	1.26E-05
1000K	0.74018	6	6.00E-06
1500K	0.74041	8	5.33E-06
2000K	0.73969	14	7.00E-06
2500K	0.73976	27	1.08E-05
3000K	0.73969	22	7.00E-06
3500K	0.74015	22	6.29E-06
4000K	0.73987	24	6.00E-06
4500K	0.73985	34	7.56E-06
5000K	0.73984	37	7.40E-06

(b)

n	ULSb	Fails	PoF
250K	0.73910	2	8.00E-06
250K	0.73812	2	8.00E-06
250K	0.74158	1	4.00E-06
250K	0.73966	1	4.00E-06
250K	0.73962	1	4.00E-06
250K	0.74012	2	8.00E-06
250K	0.73998	0	0
250K	0.73821	1	4.00E-06
250K	0.73908	3	1.20E-05
250K	0.73969	2	8.00E-06
500K	0.73931	1	2.00E-06
500K	0.7395	2	4.00E-06
500K	0.74026	6	1.20E-05
500K	0.7399	6	1.20E-05
500K	0.74046	3	6.00E-06
500K	0.7399	6	1.20E-05
500K	0.7395	2	4.00E-06
500K	0.74016	3	6.00E-06
500K	0.73951	3	6.00E-06
500K	0.74007	2	4.00E-06
1000K	0.74018	6	6.00E-06
1000K	0.73968	14	1.40E-05
1000K	0.73965	8	8.00E-06
1000K	0.74005	7	7.00E-06
1000K	0.73929	9	9.00E-06
1000K	0.74051	3	3.00E-06
1000K	0.7399	6	6.00E-06
1000K	0.73925	3	3.00E-06
1000K	0.73973	9	9.00E-06
1000K	0.73948	7	7.00E-06
3000K	0.73969	22	7.00E-06
3000K	0.73998	24	8.00E-06
3000K	0.73979	23	7.67E-06
3000K	0.73963	21	7.00E-06
3000K	0.73954	23	7.67E-06
3000K	0.7399	26	8.67E-06
3000K	0.73986	21	7.00E-06
3000K	0.73941	20	6.67E-06
3000K	0.73964	19	6.33E-06
3000K	0.73961	21	7.00E-06
5000K	0.73984	37	7.40E-06
5000K	0.74004	39	7.80E-06
5000K	0.73984	32	6.40E-06
5000K	0.73983	44	8.80E-06
5000K	0.73996	48	9.60E-06
5000K	0.73972	37	7.40E-06
5000K	0.73965	34	6.80E-06
5000K	0.73997	36	7.20E-06
5000K	0.73982	37	7.40E-06
5000K	0.74001	36	7.20E-06

In each figure the red line gives the value of the of the unity check in the corresponding reference case. The green line gives the unity check value according to the Monte Carlo simulation when the target for probability of failure of 10^{-3} is adhered.

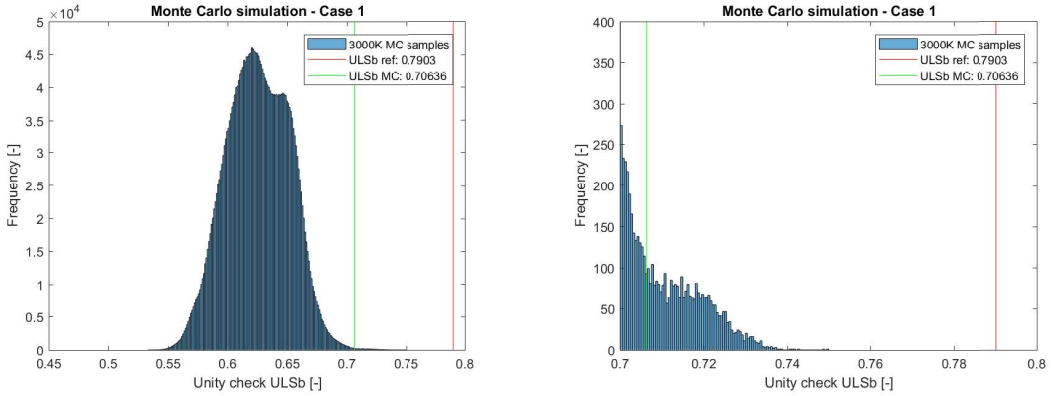

(a) (b)

Figure 5.3: Monte Carlo simulation 3000K samples - Case 1

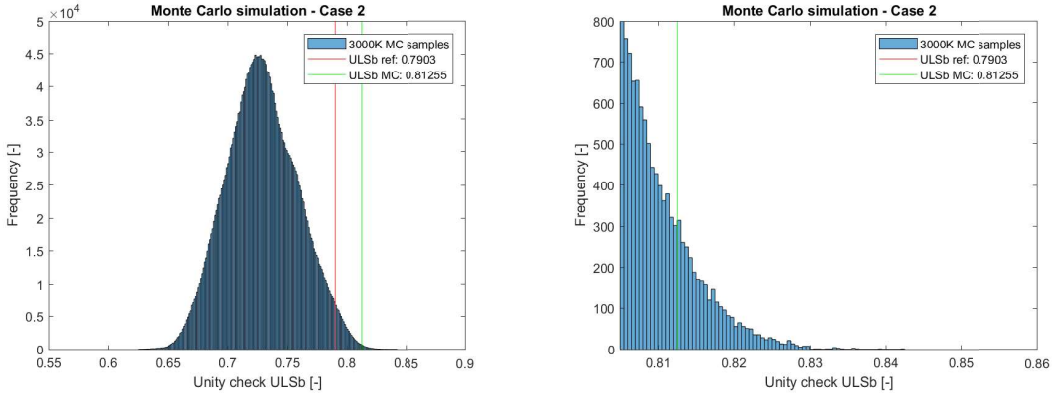

(a) (b)

Figure 5.4: Monte Carlo simulation 3000K samples - Case 2

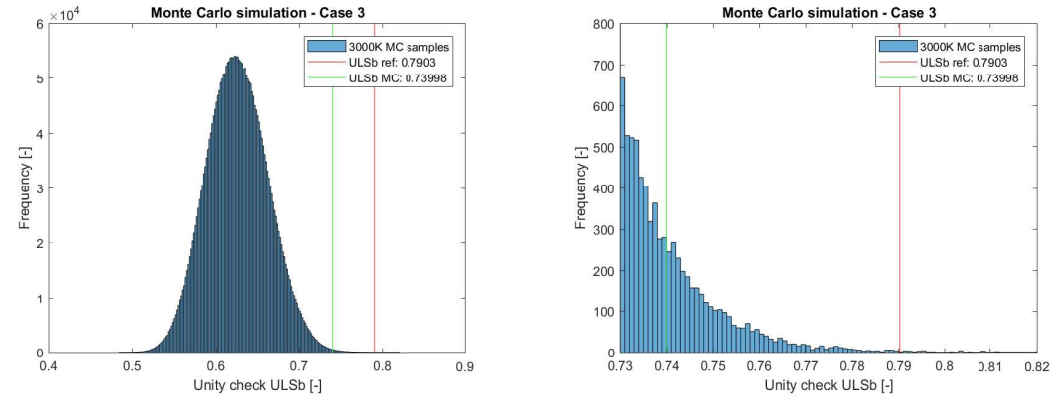

(a) (b)

Figure 5.5: Monte Carlo simulation 3000K samples - Case 3

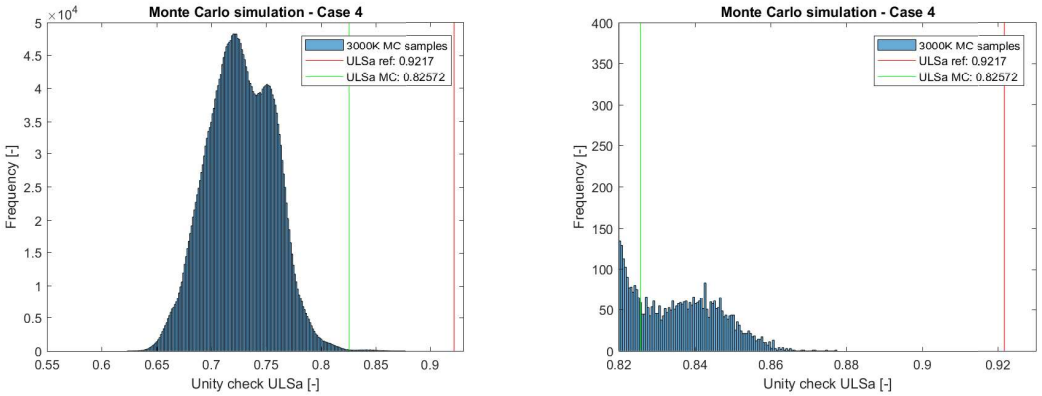

(a) (b)

Figure 5.6: Monte Carlo simulation 3000K samples - Case 4

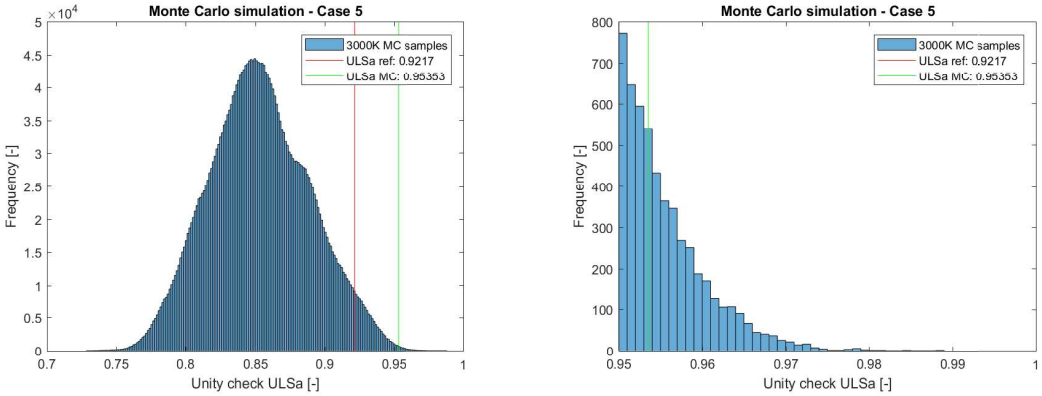

(a) (b)

Figure 5.7: Monte Carlo simulation 3000K samples - Case 5

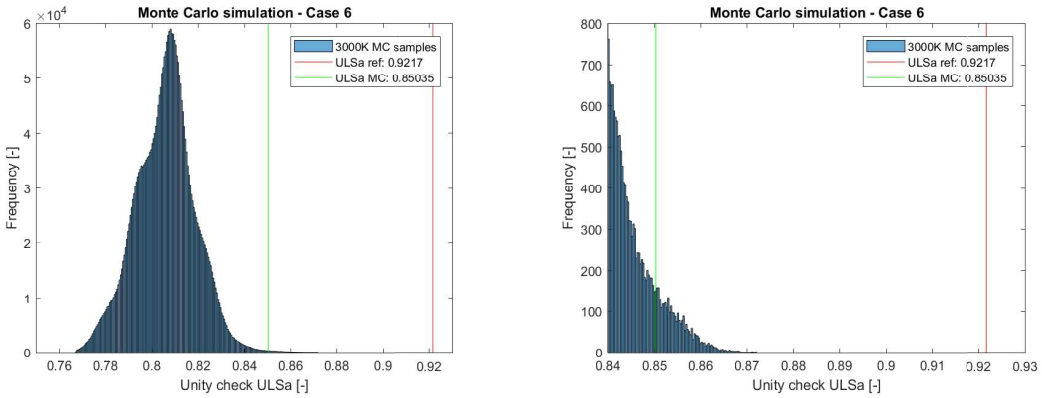

(a) (b)

Figure 5.8: Monte Carlo simulation 3000K samples - Case 6

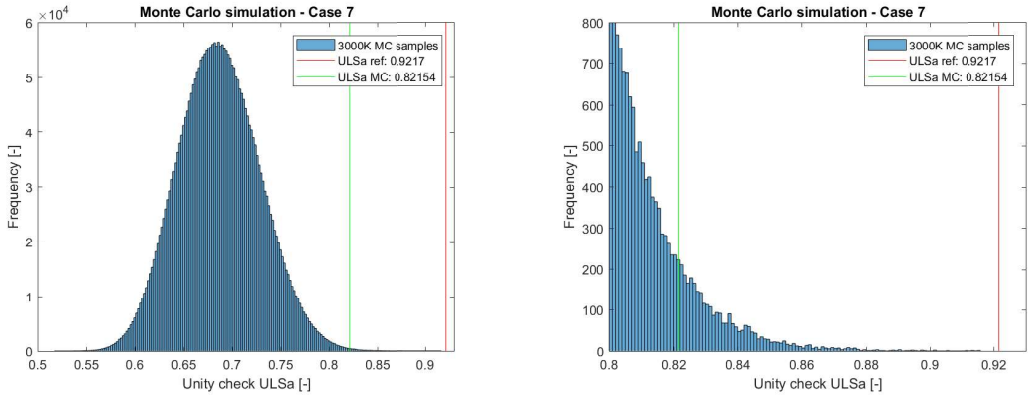

(a) (b)

Figure 5.9: Monte Carlo simulation 3000K samples - Case 7

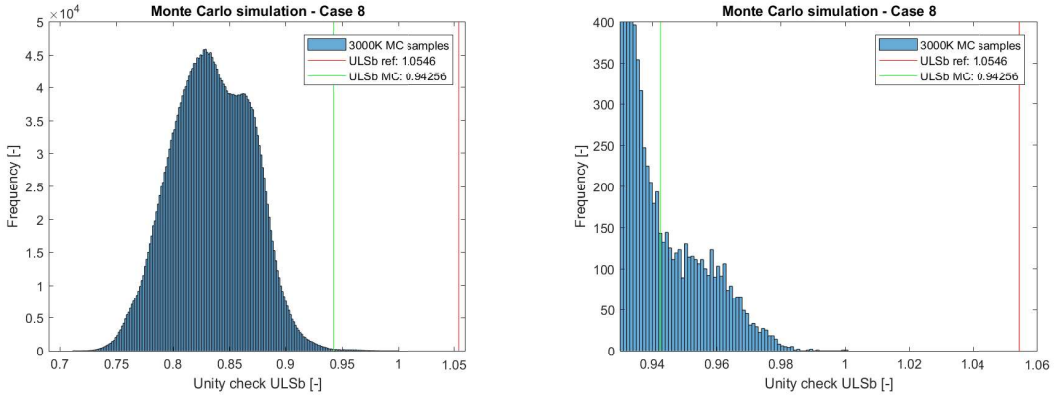

(a) (b)

Figure 5.10: Monte Carlo simulation 3000K samples - Case 8

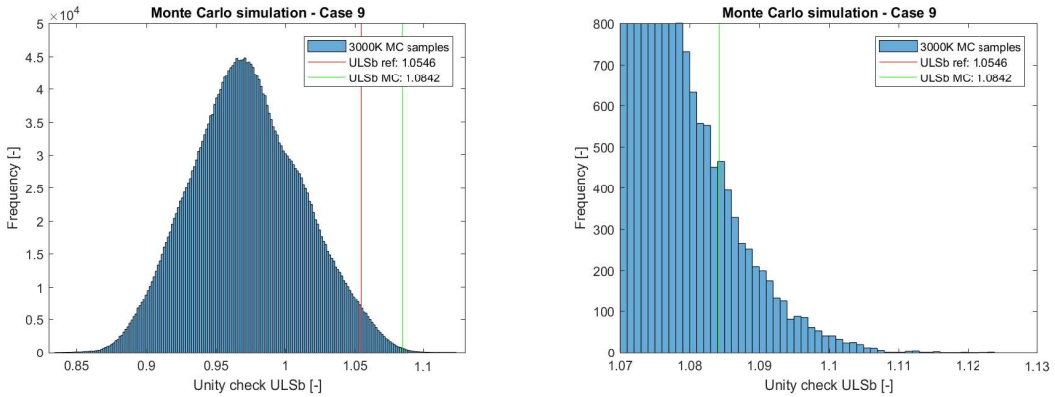

(a) (b)

Figure 5.11: Monte Carlo simulation 3000K samples - Case 9

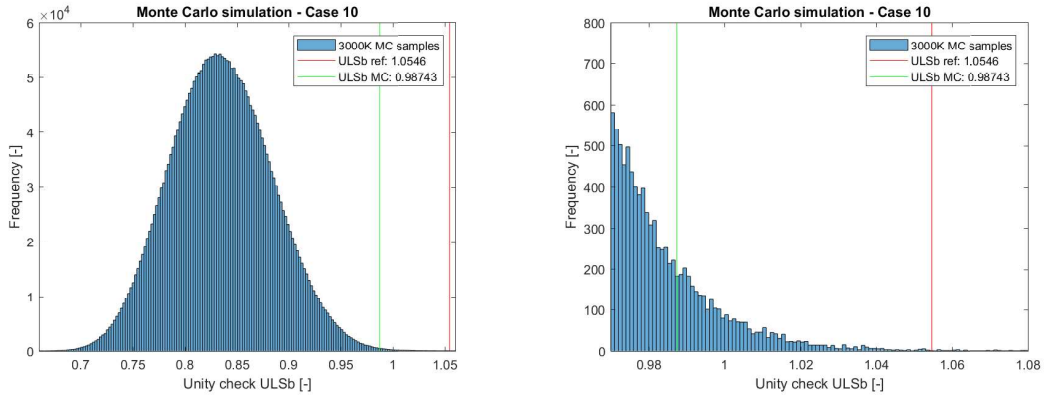

(a) (b)

Figure 5.12: Monte Carlo simulation 3000K samples - Case 10

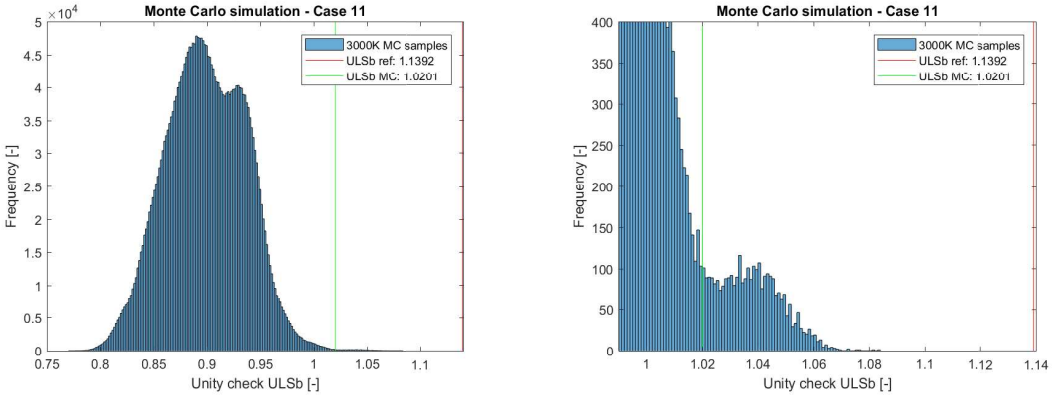

(a) (b)

Figure 5.13: Monte Carlo simulation 3000K samples - Case 11

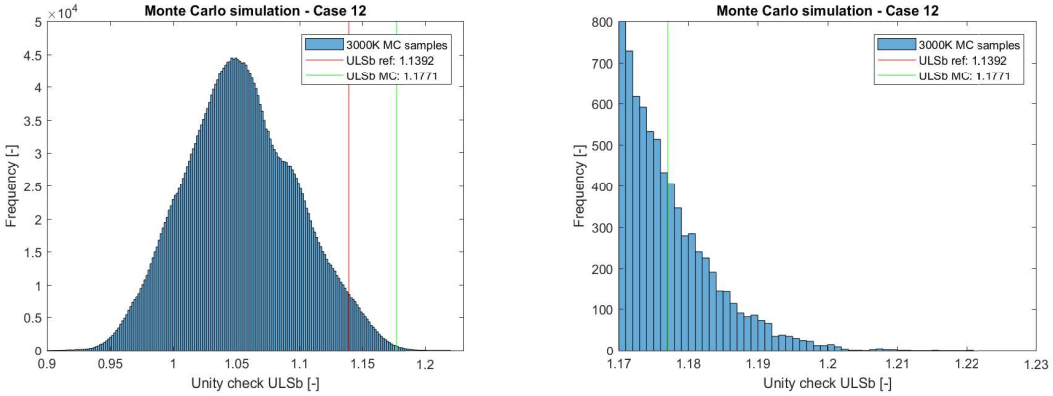

(a) (b)

Figure 5.14: Monte Carlo simulation 3000K samples - Case 12

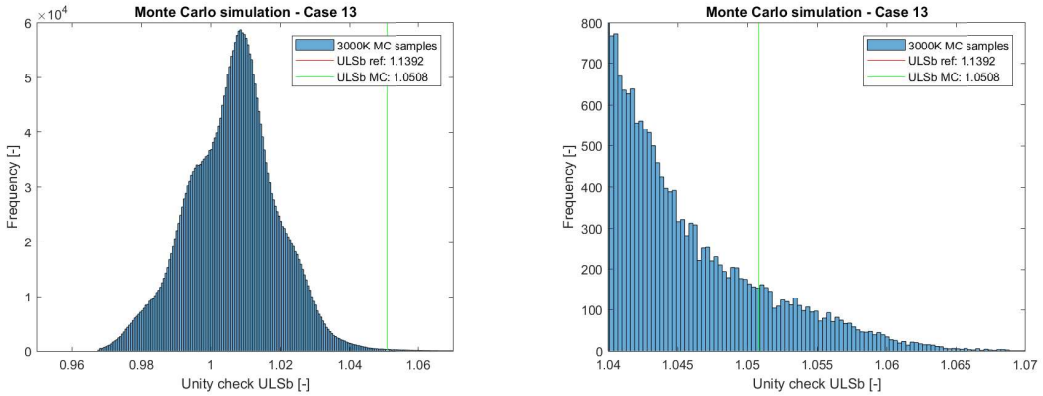

(a) (b)

Figure 5.15: Monte Carlo simulation 3000K samples - Case 13

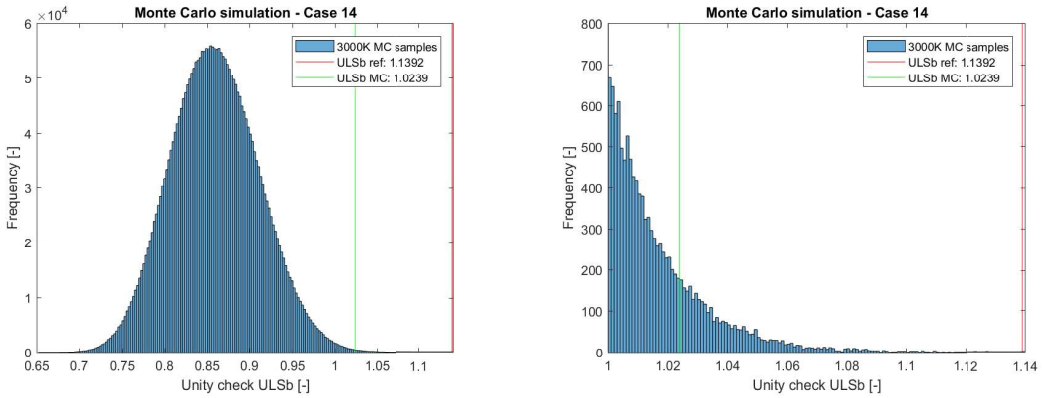

(a) (b)

Figure 5.16: Monte Carlo simulation 3000K samples - Case 14

6

Results

Chapter 6 discusses the results of the structural reliabilty assessment. In the first section the unity check values that have been calculated with the Monte Carlo simulations are summarized and compared to the original values of the reference cases. The second section considers the fine tuning of the safety class resistance factor for local buckling.

6.1. Comparison reference case vs SRA

In table 6.1 the unity check values calculated with the Monte Carlo simulations are stated. Table 6.2 contains the percentual changes of these unity check values with respect to their reference cases.

Table 6.1: Test case UC values

	YS -UTS	OD - WT	f0 [%]	α_u	WD [m]	UC
Reference case 1-a	Nominal values	Nominal values	1.50	0.96	251	0.7903
Reference case 1-b	Nominal values	Nominal values	1.50	1	251	0.7284
Reference case 2-a	Nominal values	Nominal values	1.50	0.96	1251	0.8523
Reference case 2-b	Nominal values	Nominal values	1.50	1	1251	0.8476
Reference case 3-a	Nominal values	Nominal values	1.50	0.96	251	1.0546
Reference case 3-b	Nominal values	Nominal values	1.50	1	251	0.9720
Reference case 4-a	Nominal values	Nominal values	1.50	0.96	1251	1.1392
Reference case 4-b	Nominal values	Nominal values	1.50	1	1251	1.0528
Test case 1	Frank copula	Nominal values	1.50	1	251	0.7064
Test case 2	Nominal values	Gaussian copula	1.50	1	251	0.8126
Test case 3	Frank copula	Gaussian copula	1.50	1	251	0.7400
Test case 4	Frank copula	Nominal values	1.50	1	1251	0.8257
Test case 5	Nominal values	Gaussian copula	1.50	1	1251	0.9535
Test case 6	Nominal values	Nominal values	Distributed	1	1251	0.8505
Test case 7	Frank copula	Gaussian copula	Distributed	1	1251	0.8215
Test case 8	Frank copula	Nominal values	1.50	1	251	0.9246
Test case 9	Nominal values	Gaussian copula	1.50	1	251	1.0842
Test case 10	Frank copula	Gaussian copula	1.50	1	251	0.9874
Test case 11	Frank copula	Nominal values	1.50	1	1251	1.0201
Test case 12	Nominal values	Gaussian copula	1.50	1	1251	1.1771
Test case 13	Nominal values	Nominal values	Distributed	1	1251	1.0508
Test case 14	Frank copula	Gaussian copula	Distributed	1	1251	1.0239

Note that in the shallow water cases the unity check value calculated with the Monte Carlo simulation utilizing all significant resistance parameters is higher than the unity check value in reference cases b.

Table 6.2: PoF and percentual change in UC

	UC	a	b	PoF
Reference case 1		0.7903	0.7284	
Test case 1	0.70636	-10.62%	-3.03%	
Test case 2	0.81255	2.82%	11.55%	
Test case 3	0.73998	-6.37%	1.59%	8.00E-06
Reference case 2		0.9217	0.8467	
Test case 4	0.82572	-10.41%	-3.12%	
Test case 5	0.95353	3.45%	11.88%	
Test case 6	0.85053	-7.72%	-0.21%	
Test case 7	0.82154	-10.87	-3.61%	0
Reference case 3		1.0546	0.972	
Test case 8	0.94256	-10.62%	-3.03%	
Test case 9	1.0842	2.81%	11.54%	
Test case 10	0.98743	-6.37%	1.59%	7.67E-06
Reference case 4		1.1392	1.0528	
Test case 11	1.0201	-10.45%	-3.11%	
Test case 12	1.1771	3.33%	11.81%	
Test case 13	1.0508	-7.76%	-0.19%	
Test case 14	1.0239	-10.12%	-2.75%	6.67E-07

6.2. Fine tuning the safety class resistance factor

With the results of the Monte Carlo simulation it is now possible to fine tune the safety class resistance factor for local buckling. Taking, for each of the load cases, reference case a as a starting point. The safety class resistance factor $\gamma_{SC,LB}$ can be reduced until the unity check value is equal to the unity check value calculated with the Monte Carlo simulation. The values behind the test cases are the safety class resistance factor values used in references cases a to obtain the equal unity check value as calculated with the Monte Carlo simulations. The safety class resistance factor values in blue are the rounded of results which can be used as explained in the next chapter.

Table 6.3: Fine tuning $\gamma_{SC,LC}$

	UC	$\gamma_{SC,LB}$	
Reference case 1a	0.7903	1.04	
Test case 3	0.7400	1.0063	1.01
Reference case 2a	0.9217	1.04	
Test case 7	0.8215	0.9963	1.00
Reference case 3a	1.0546	1.04	
Test case 10	0.9874	1.0063	1.01
Reference case 4a	1.1392	1.04	
Test case 14	1.0239	0.9859	0.99

7

Conclusion and recommendations

7.1. Conclusions

From the results presented in chapter 6 several conclusions can be made. First of all conservatism in current methodology in the case of the Ichthys project is clearly proved. The aimed for probability of failure has a value of 10^{-3} and the calculated probability of failure has a value of at least 10^{-5} for all considered test cases and for the deep water load case in which the UC value was increased to a value above 1 the PoF even reached a value less then 10^{-6}. This situation creates the opportunity to indeed improve the workability in certain project locations when using similar pipes. As discussed it is not possible to make a general statement about the workability since it is very project specific however it is shown that the unity check value can be decreased with 6% in shallow water cases and with 10% in deeper water cases. This percentage is expected to rise in projects where the water depth exceeds the 1251m - which was the deep water depth assessed in this research - because the uncertainty in the ovality starts playing an even bigger role. And as such the significant wave height in the dynamic installation analysis can be increased.

Another very interesting conclusion can be made about the fact that in the Ichthys case the material properties of the pipe batch fulfilled supplementary requirement U. However, when the material strength factor α_u is upgraded from 0.96 to 1.00 the aimed for probability of failure is not reached when the DNVGL code is followed correctly. Table 6.2 shows that the actual unity check value calculated with the Monte Carlo simulation is 1.59% higher than the UC value calculated with the upgraded material strength factor. Meaning that the structural integrity would have been overestimated while completely adhering to the design standard.

Furthermore the results show that the material strength properties of the pipes are a lot better than the nominal values that are used in standard installation analysis calculations. The geometrical properties of the pipes however, are not as good. The Monte Carlo simulations of the test cases in which the uncertainty of the wall thickness and outer diameter where isolated show that they have a negative influence on the final unity check value. This also means that when taking uncertainty in the resistance parameters into account at least yield stress, ultimate tensile strength, wall thickness and outer diameter should be assessed. Only stochastically modeling the yield stress and ultimate tensile strength would overestimate the structural integrity of the pipe. Which would result in not reaching the target probability of failure when the UC value is pushed to reach it's limit.

7.2. Recommendations

Having the knowledge of this research the question remains how to apply the gained insight. It is recommended that for every pipelay project first the necessity of a structural reliability assessment should be examined. Meaning that it should be analyzed if there is a lot to be gained by calculating the situation more precise. For instance does a small increase in significant wave height for a certain sea state improve the workability of the operation

significantly. The fine tuned safety class resistance factor can be used as an ideal tool to quickly, without having to spend a lot of extra resources, investigate certain opportunities. Note that if one would like to conduct a structural reliability assessment or use adjusted safety factors in the final analysis of a commercial project everything needs to be approved by DNVGL. So for projects where more precise calculations are indeed beneficial and the timeline of the project allows it - e.a. the pipe ends are not already produced - the material strength and geometrical data of the pipes should be obtained. And in consultation with DNVGL a structural reliability assessment, similar to the one conducted in this research, should be carried out and approved. Also the adjusted safety factors proposed in this research are specific to the type of pipe used in the Ichthys project. And as such can only be used in similar situations. For this reason it is recommended to keep on expanding the pipeline data base gradually and keep on calculating and adding these fine tuned safety factors, especially for commonly used pipes. This will create a valuable amount of information and one would possibly eventually be able to detect bigger relations. For instance certain pipe mills that always deliver way above specifications or find certain production processes which are considerably better.

In deep water projects, where the ovality of the pipe plays an increasingly important role, a relatively easy way to improve the operability limits of a installation is to measure the ovality of the pipes. Especially when certain installation are found to be critical this opportunity can be ceased relatively last minute.

Lastly for the case of start-up structure installations one should also investigate the possibilities of improving load side of the considered equation. The situation in which the maximum bending moment and maximum effective tension of a certain time domain analysis is picked is not optimal to say the least. However, this is not done easily and is a perfect topic for a new master thesis.

When taking a look at other business units of HMC the decommissioning branch also works a lot with safety factors. Consequently there could also be an opportunity for structural reliability assessments. Taking a learning from the process in this research and having noticed that the HMC pipeline database is not the best organized database. One should investigate the opportunities for the decommissioning work and with this in the back of your mind design the set-up of the database. Determine what significance is needed for the data and standardize as much as possible.

8

Acknowledgements

First of all I would like to thank my company supervisors, Ir. Henk Smienk and Ir. Carel Hoekstra of Heerema Marine Contractors. I have enjoyed the freedom which I was given in the set-up of the research and appreciate the time that they always made available for me effortlessly. Furthermore the support in the decision to continue with the start-up structure installation topic while the subsea department was decided to be closed means a lot to me. Without this support, and thus having to change, would have inevitably delayed my graduation into the next year.

Secondly I would like to thank my academic supervisors, Ir. Andre van der Stap the chairman of the graduation committee, for always creating the overview and pointing me towards the essence of the problem. And Dr. Ir. Oswaldo Morales Napoles for the support regarding the statistics used in this research and showing me that copula's are indeed fun, as mentioned during his lectures.

In addition I would like to express my gratitude towards HMC for the opportunity, the interesting topic and the company resources that have been made available for me the last nine months. And towards my fellow HMC graduation students for the great atmosphere and the LaTeX/Matlab support.

Last but not least, I would like to thank my girlfriend, friends & family, especially my parents, for supporting me not only during this graduation research but throughout my entire student career. Without them this would not have been possible.

K.A.T.J. Franken
Den Haag, December 2018

A

DNVGL-ST-F101 tables

In figures A.1 to A.10 all tables from the DNVGL-ST-F101 design standard needed to determine values used in combined loading criterion are stated.

Table 2-3 Classification of safety classes

Safety class	*Definition*
Low	Where failure implies insignificant risk of human injury and minor environmental and economic consequences.
Medium	Where failure implies low risk of human injury, minor environmental pollution or high economic or political consequences.
High	Classification for operating conditions where failure implies risk of human injury, significant environmental pollution or very high economic or political consequences.

Figure A.1: Classification of safety classes

Table 2-4 Normal classification of safety classes [1)]

Phase	*Fluid category A, C*		*Fluid category B, D and E*	
	Location class		*Location class*	
	1	2	1	2
Temporary[2,3]	Low	Low	-	-
Operational	Low	Medium	Medium	High

1) Other classifications may exist depending on the conditions and criticality of failure the pipeline. For pipelines where some consequences are more severe than normal, i.e. when the table above does not apply, the selection of a higher safety class shall also consider the implication, on the total gained safety. If the total safety increase is marginal, the selection of a higher safety class may not be justified.
2) Installation until pre-commissioning (temporary phase) should be classified as safety class Low.
3) For safety classification of temporary phases after commissioning, special consideration shall be made to the consequences of failure, i.e. giving a higher safety class than Low.

Figure A.2: Normal classification of safety classes

Table 2-5 Nominal annual target failure probabilities per pipeline vs. safety classes[5)]

Limit state category	*Limit state*	*Safety classes*			
		Low	*Medium*	*High*	*Very high[4)]*
SLS	All	10^{-2}	10^{-3}	10^{-3}	10^{-4}
ULS	Pressure containment[1)]	10^{-4} to 10^{-5}	10^{-5} to 10^{-6}	10^{-6} to 10^{-7}	10^{-7} to 10^{-8}
ALS					
ULS	All other	10^{-3}	10^{-4}	10^{-5}	10^{-6}
FLS[2)]					
ALS[3)]					

1) The failure probability for the pressure containment (wall thickness design) is one to two order of magnitudes lower than the general ULS criterion given in this table, in accordance with industry practice and reflected by the ISO requirements.
2) The failure probability will effectively be governed by the last year in operation or prior to inspection depending on the adopted inspection philosophy.
3) Nominal target failure probabilities can alternatively be one order of magnitude less (e.g. 10^{-4} per pipeline to 10^{-5} per km) for any running km if the consequences are local and caused by local factors.
4) See Table F-2.
5) The target shall be interpret as probability that a failure occurs in the period of one year.

Figure A.3: Target failure probabilities

Table 4-4 Load effect factor combinations

Limit state/load combination	*Load effect combination*		*Functional loads* [1)]	*Environmental load*	*Interference loads*	*Accidental loads*
			γ_F	γ_E	γ_F	γ_A
ULS	*a*	System check[2)]	1.2	0.7		
	b	Local check	1.1	1.3	1.1	
FLS	*c*		1.0	1.0	1.0	
ALS	*d*		1.0	1.0	1.0	1.0

1) If the functional load effect reduces the combined load effects, γ_F shall be taken as 1/1.1.
2) This load effect factor combination shall only be checked when system effects are present, i.e. when the major part of the pipeline is exposed to the same functional load. This will typically only apply to pipeline installation.

Figure A.4: Load effect factor combinations

Table 4-5 Condition load effect factors, γ_c

Condition	γ_c
Pipeline resting on uneven seabed	1.07
J-tube pull-in [1]	0.82
System pressure test	0.93
S-lay installation; Local buckling load control check on stinger[2]	0.80
Reeling installation; Displacement controlled check, seamless pipes[2]	0.77
Reeling installation; Displacement controlled check, welded pipes[2,3]	0.82
Otherwise	1.00

1) Load combination a needs not to be analysed
2) For installation both load combination a and b shall always be analysed, see also [5.8.2]
3) This factor has not been re-assessed but reflects the less uniform material properties around the circumference

Figure A.5: Condition load effect factors

Table 5-1 Material resistance factor, γ_m

Limit state category[1)]	*SLS/ULS/ALS*	*FLS*
γ_m	1.15	1.00
1) The limit states (SLS, ULS, ALS and FLS) are defined in [5.4].		

Figure A.6: Material resistance factor

Table 5-3 Material strength factor, α_U

Loading scenario	α_U	
	Normal	*Supplementary requirement U*
System pressure test	1.00	1.00
Other	0.96	1.00

Figure A.7: Material strength factor

Table 5-4 Maximum fabrication factor, α_{fab}

Pipe	*Seamless*	*UO, TRB, ERW and HFW*	*UOE*
α_{fab}	1.00	0.93	0.85

Figure A.8: Maximum fabrication factor

Table 5-5 Characteristic wall thickness

Characteristic thickness	*Prior to operation*[1)]	*Operation*[2)]
t_1	$t\text{-}t_{fab}$	$t\text{-}t_{fab}\text{-}t_{corr}$
t_2	t	$t\text{-}t_{corr}$

1) Is intended when there is negligible corrosion (mill pressure test, construction (installation) and system pressure test condition). If corrosion exist, this shall be subtracted similar to as for operation.
2) Is intended when there is corrosion.

Figure A.9: Characteristic wall thickness

Table 5-7 Typical link between scenarios and limit states

Scenario	*Ultimate limit states*							*Serviceability limit states*			
	Fracture			*Instability*							
				Local buckling							
	Pressure containment	Fatigue	Fracture	System collapse	Propagating buckling	Combined loading	Global buckling	Dent	Ovalisation	Accumulated deformation	Displacement
Wall thickness design	X			X	X						
Installation		X	X	X	X	X			X		X
Free-span	(X)	X	X			X					
Trawling/3rd party	(X)					X		X			
On bottom stability	(X)	(X)	(X)			(X)		(X)	(X)		X[1]
Pipeline Walking						X					
Global Buckling	(X)	X	X			X				X	

1) Typically applied as a simplified way to avoid checking each relevant limit state

Figure A.10: Link between scenarios and limit states

B

Collapse pressure

The analytical solution for the collapse pressure, as used in the Matlab script, is given below.

$$p_c = y - \frac{1}{3}b \tag{B.1}$$

Where:

$$b = -p_{el}(t) \tag{B.2}$$

$$c = p_p(t)^2 + p_p(t) \cdot p_{el} \cdot O_0 \cdot \frac{D}{t} \tag{B.3}$$

$$d = p_{el}(t)p_p(t)^2 \tag{B.4}$$

$$u = \frac{1}{3}\left(-\frac{1}{3}b^2 + c\right) \tag{B.5}$$

$$v = \frac{1}{2}\left(\frac{2}{27}b^3 - \frac{1}{3}bc + d\right) \tag{B.6}$$

$$\Phi = cos^{-}1\left(\frac{-v}{\sqrt{-u^3}}\right) \tag{B.7}$$

$$y = -2\sqrt{-u} \cdot cos\left(\frac{\Phi}{3} + \frac{60\pi}{180}\right) \tag{B.8}$$

C

Copula models

Elliptical copula's [21]
Normal copula

$$C_\rho(u,v) = \int_{-\infty}^{\Phi^{-1}(u)} \int_{-\infty}^{\Phi^{-1}(v)} \frac{1}{2\pi\,(1-\rho^2)^{\frac{1}{2}}} exp\left\{-\frac{x^2-2\rho xy+y^2}{2\,(1-\rho^2)}\right\} dxdy \tag{C.1}$$

Where Φ^{-1} is the inverse of the univariate standard Normal distribution and ρ, the linear correlation coefficient, is the copula parameter.
Student-T copula

$$C_{\rho,\nu}(u,v) = \int_{-\infty}^{t_\nu^{-1}(u)} \int_{-\infty}^{t_\nu^{-1}(v)} \frac{1}{2\pi\,(1-\rho^2)^{\frac{1}{2}}} \left\{1+\frac{x^2-2\rho xy+y^2}{\nu(1-\rho^2)}\right\}^{-(\nu+2)/2} \tag{C.2}$$

Where ν, the number of degrees of freedom, and ρ, the linear correlation coefficient, are the copula parameters.

Archimedean copula's [20]
Clayton copula

$$C_\alpha(u,v) = max\left(\left[u^{-\alpha}+v^{-\alpha}-1\right]^{\frac{-1}{\alpha}}, 0\right) \tag{C.3}$$

Where: $\alpha \in [-1,\infty)\backslash\{0\}$

Frank copula

$$C_\alpha(u,v) = -\frac{1}{\alpha} ln\left(1+\frac{(e^{-\alpha u}-1)\,(e^{-\alpha v}-1)}{e^{-\alpha}-1}\right) \tag{C.4}$$

Where: $\alpha \in (-\infty,\infty)\backslash\{0\}$

Gumbel copula

$$C_\alpha(u,v) = exp\left\{-\left[(-lnu)^\alpha+(-lnv)^\alpha\right]^{\frac{1}{\alpha}}\right\} \tag{C.5}$$

Where: $\alpha \in [1,\infty)$

The copula parameters α control the degree of dependence between u and v and are related to the rank correlation.

D

Statistical analysis

D.1. Correlations

Table D.1: Pearson moment correlations

Variable pair	**Matlab reference**	**Pearson ρ**
Internal diameter Body - Wall thickness A	ID_Body_WT_B	-0.342
Internal diameter Body - Wall thickness B	ID_Body_WT_A	-0.319
Internal diameter Body - Outer diameter B	ID_Body_OD_B	-0.294
Internal diameter Body - Outer diameter A	ID_Body_OD_A	-0.277
Ultimate tensile strength - Internal diameter A	UTS_ID_A	-0.130
Yield strength - Internal diameter A	YS_ID_A	-0.120
Ultimate tensile strength - Outer diameter A	UTS_OD_A	-0.112
Ultimate tensile strength - Outer diameter B	UTS_OD_B	-0.111
Yield strength - Outer diameter A	YS_OD_A	-0.109
Yield strength - Outer diameter B	YS_OD_B	-0.096
Ultimate tensile strength - Internal diameter B	UTS_ID_B	-0.090
Internal diameter A - Out of roundness Body	ID_A_OoR_Body	-0.087
Internal diameter A - Ovality Body	ID_A_Ova_Body	-0.087
Ultimate tensile strength - Wall thickness B	UTS_WT_B	-0.079
Yield strength - Wall thickness B	YS_WT_B	-0.076
Out of roundness B - Ovality Body	OoR_B_Ova_Body	-0.070
Ovality B - Ovality Body	Ova_B_Ova_Body	-0.070
Out of roundness B - Out of roundness Body	OoR_B_OoR_Body	-0.069
Out of roundness Body - Ovality B	OoR_Body_Ova_B	-0.069
Yield strength - Internal diameter B	YS_ID_B	-0.066
Yield strength - Wall thickness A	YS_WT_A	-0.064
Ultimate tensile strength - Wall thickness A	UTS_WT_A	-0.062
Internal diameter B - Internal diameter Body	ID_B_ID_Body	-0.039
Out of roundness A - Ovality Body	OoR_A_Ova_Body	-0.035
Ovality A - Ovality Body	Ova_A_Ova_Body	-0.034
Out of roundness A - Out of roundness Body	OoR_A_OoR_Body	-0.034
Out of roundness Body - Ovality A	OoR_Body_Ova_A	-0.033
Internal diameter A - Internal diameter Body	ID_A_ID_Body	-0.033
Internal diameter B - Out of roundness Body	ID_B_OoR_Body	-0.025
Internal diameter B - Ovality Body	ID_B_Ova_Body	-0.025
Outer diameter B - Out of roundness Body	OD_B_OoR_Body	-0.020
Outer diameter B - Ovality Body	OD_B_Ova_Body	-0.017
Ovality B - Wall thickness A	Ova_B_WT_A	-0.015
Out of roundness B - Wall thickness A	OoR_B_WT_A	-0.015
Internal diameter B - Ovality B	ID_B_Ova_B	-0.013
Internal diameter A - Ovality A	ID_A_Ova_A	-0.011
Out of roundness Body - Wall thickness B	OoR_Body_WT_B	-0.008
Internal diameter B - Out of roundness B	ID_B_OoR_B	-0.007
Internal diameter A - Out of roundness A	ID_A_OoR_A	-0.007
Ovality Body - Wall thickness B	Ova_Body_WT_B	-0.005
Internal diameter Body - Ovality Body	ID_Body_Ova_Body	-0.003
Outer diameter A - Ovality B	OD_A_Ova_B	-0.003

Table D.1: Pearson moment correlations

Variable pair	**Matlab reference**	**Pearson ρ**
Outer diameter A - Out of roundness B	OD_A_OoR_B	-0.001
Outer diameter A - Out of roundness Body	OD_A_OoR_Body	0.001
Outer diameter A - Ovality Body	OD_A_Ova_Body	0.004
Outer diameter A - Ovality A	OD_A_Ova_A	0.006
Internal diameter Body - Out of roundness Body	ID_Body_OoR_Body	0.006
Outer diameter A - Out of roundness A	OD_A_OoR_A	0.009
Internal diameter B - Ovality A	ID_B_Ova_A	0.012
Internal diameter B - Out of roundness A	ID_B_OoR_A	0.014
Ovality A - Wall thickness A	Ova_A_WT_A	0.014
Yield strength - Ovality Body	YS_Ova_Body	0.014
Out of roundness A - Wall thickness A	OoR_A_WT_A	0.015
Yield strength - Out of roundness Body	YS_OoR_Body	0.015
Outer diameter B - Ovality B	OD_B_Ova_B	0.015
Outer diameter Body - Ovality Body	OD_Body_Ova_Body	0.017
Outer diameter B - Out of roundness B	OD_B_OoR_B	0.019
Internal diameter A - Ovality B	ID_A_Ova_B	0.021
Internal diameter A - Out of roundness B	ID_A_OoR_B	0.023
Outer diameter Body - Out of roundness Body	OD_Body_OoR_Body	0.024
Ultimate tensile strength - Ovality Body	UTS_Ova_Body	0.025
Ultimate tensile strength - Out of roundness Body	UTS_OoR_Body	0.026
Yield strength - Out of roundness A	YS_OoR_A	0.027
Ovality A - Wall thickness B	Ova_A_WT_B	0.027
Yield strength - Ovality A	YS_Ova_A	0.027
Ovality B - Wall thickness B	Ova_B_WT_B	0.028
Out of roundness A - Wall thickness B	OoR_A_WT_B	0.028
Outer diameter B - Ovality A	OD_B_Ova_A	0.028
Out of roundness B - Wall thickness B	OoR_B_WT_B	0.028
Outer diameter B - Out of roundness A	OD_B_OoR_A	0.030
Yield strength - Outer diameter Body	YS_OD_Body	0.033
Ultimate tensile strength - Outer diameter Body	UTS_OD_Body	0.039
Ultimate tensile strength - Out of roundness A	UTS_OoR_A	0.042
Internal diameter Body - Out of roundness B	ID_Body_OoR_B	0.042
Ultimate tensile strength - Ovality A	UTS_Ova_A	0.042
Internal diameter Body - Ovality B	ID_Body_Ova_B	0.042
Internal diameter B - Outer diameter Body	ID_B_OD_Body	0.047
Ultimate tensile strength - Out of roundness B	UTS_OoR_B	0.047
Yield strength - Out of roundness B	YS_OoR_B	0.048
Ultimate tensile strength - Ovality B	UTS_Ova_B	0.048
Yield strength - Ovality B	YS_Ova_B	0.048
Outer diameter Body - Ovality B	OD_Body_Ova_B	0.048
Outer diameter Body - Out of roundness B	OD_Body_OoR_B	0.048
Out of roundness Body - Wall thickness A	OoR_Body_WT_A	0.052
Ovality Body - Wall thickness A	Ova_Body_WT_A	0.055
Internal diameter Body - Out of roundness A	ID_Body_OoR_A	0.080
Internal diameter Body - Ovality A	ID_Body_Ova_A	0.080
Yield strength - Internal diameter B	YS_ID_Body	0.087
Internal diameter B - Wall thickness B	ID_B_WT_B	0.089
Ultimate tensile strength - Internal diameter Body	UTS_ID_Body	0.094
Internal diameter A - Outer diameter Body	ID_A_OD_Body	0.094
Outer diameter Body - Ovality A	OD_Body_Ova_A	0.098
Outer diameter Body - Out of roundness A	OD_Body_OoR_A	0.099
Ovality A - Ovality B	Ova_A_Ova_B	0.113
Out of roundness B - Ovality A	OoR_B_Ova_A	0.113
Out of roundness A - Ovality B	OoR_A_Ova_B	0.113
Out of roundness A - Out of roundness B	OoR_A_OoR_B	0.113
Internal diameter B - Wall thickness A	ID_B_WT_A	0.128
Internal diameter A - Wall thickness A	ID_A_WT_A	0.141
Internal diameter A - Wall thickness B	ID_A_WT_B	0.179
Outer diameter B - Outer diameter Body	OD_B_OD_Body	0.243
Internal diameter B - Outer diameter A	ID_B_OD_A	0.269
Outer diameter Body - Wall thickness B	OD_Body_WT_B	0.273
Outer diameter A - Outer diameter Body	OD_A_OD_Body	0.287
Outer diameter Body - Wall thickness A	OD_Body_WT_A	0.296
Internal diameter A - Outer diameter B	ID_A_OD_B	0.330

Table D.1: Pearson moment correlations

Variable pair	**Matlab reference**	**Pearson ρ**
Internal diameter A - Internal diameter B	ID_A_ID_B	0.349
Outer diameter B - Wall thickness A	OD_B_WT_A	0.512
Outer diameter A - Wall thickness B	OD_A_WT_B	0.538
Wall thickness A - Wall thickness B	WT_A_WT_B	0.555
Outer diameter A - Outer diameter B	OD_A_OD_B	0.574
Internal diameter A - Outer diameter A	ID_A_OD_A	0.586
Internal diameter B - Outer diameter B	ID_B_OD_B	0.604
Internal diameter Body - Outer diameter Body	ID_Body_OD_Body	0.757
Yield strength - Ultimate tensile strength	YS_UTS	0.800
Outer diameter B - Wall thickness B	OD_B_WT_B	0.847
Outer diameter A - Wall thickness A	OD_A_WT_A	0.885
Out of roundness Body - Ovality Body	OoR_Body_Ova_Body	1.000
Out of roundness B - Ovality B	OoR_B_Ova_B	1.000
Out of roundness A - Ovality A	OoR_A_Ova_A	1.000

Table D.2: Pearson moment correlations

Variable pair	**Matlab reference**	**Pearson ρ**
Averaged wall thickness - Internal diameter Body	WT_ave_ID_Body	-0.375
Averaged internal diameter - Ultimate tensile strength	ID_ave_UTS	-0.132
Averaged outer diameter - Ultimate tensile strength	OD_ave_UTS	-0.126
Averaged outer diameter - Yield stress	OD_ave_YS	-0.115
Averaged internal diameter - Yield stress	ID_ave_YS	-0.111
Averaged wall thickness - Ultimate tensile strength	WT_ave_UTS	-0.080
Averaged wall thickness - Yield stress	WT_ave_YS	-0.079
Averaged internal diameter - Out of roundness Body	ID_ave_OoR_Body	-0.066
Averaged internal diameter - Ovality Body	ID_ave_Ova_Body	-0.065
Averaged outer diameter - Out of roundness Body	OD_ave_OoR_Body	-0.010
Averaged outer diameter - Ovality Body	OD_ave_Ova_Body	-0.007
Averaged internal diameter - Ovality A	ID_ave_Ova_A	0.001
Averaged internal diameter - Ovality B	ID_ave_Ova_B	0.003
Averaged internal diameter - Out of roundness A	ID_ave_OoR_A	0.005
Averaged wall thickness - Ovality B	WT_ave_Ova_B	0.007
Averaged outer diameter - Ovality B	OD_ave_Ova_B	0.007
Averaged wall thickness - Out of roundness B	WT_ave_OoR_B	0.008
Averaged internal diameter - Out of roundness B	ID_ave_OoR_B	0.008
Averaged outer diameter - Out of roundness B	OD_ave_OoR_B	0.010
Averaged outer diameter - Ovality A	OD_ave_Ova_A	0.019
Averaged outer diameter - Out of roundness A	OD_ave_OoR_A	0.022
Averaged wall thickness - Ovality A	WT_ave_Ova_A	0.023
Averaged wall thickness - Out of roundness A	WT_ave_OoR_A	0.024
Averaged wall thickness - Out of roundness Body	WT_ave_OoR_Body	0.025
Averaged wall thickness - Ovality Body	WT_ave_Ova_Body	0.028
Wall thickness A & B combined - Inner diameter A & B combined	WT_combi_ID_combi	0.102
Averaged wall thickness - Averaged internal diameter	WT_ave_ID_ave	0.182
Averaged wall thickness - Outer diameter Body	WT_ave_OD_Body	0.322
Wall thickness A & B combined - Outer diameter A & B combined	WT_combi_OD_combi	0.865
Averaged wall thickness - Averaged outer diameter	WT_ave_OD_ave	0.889

D.2. Filtering

Table D.3: Filtered outliers

ID A	OD A	ID Body	OD Body	ID B	OD B	WT A	WT B	OoR A	Ova A	OoR B	Ova B	OoR Body	Ova Body	YS	UTS
407.9	454.3	408.4	456.6	407.5	457.5	23.2	25	1.6	0.39	1.4	0.34	2	0.49	493	547
407.8	458.2	409.2	459.8	408	458.8	25.2	25.4	2.3	0.56	2.6	0.64	3	0.73	409	565
407.4	456.8	410.1	459.6	407	456.6	24.7	24.8	2.6	0.64	2.6	0.64	3	0.73	410	556
407.9	457.9	408.9	459	408.6	458.8	25	25.1	2.7	0.66	1.2	0.29	2	0.49	510	508
406.4	456.6	409.1	458.3	408	456.2	25.1	24.1	1.6	0.39	1.3	0.32	3	0.73	487	532
407.9	457.5	408.6	458	407.7	456.9	24.8	24.6	1.4	0.34	2.6	0.64	3	0.73	487	532
408.1	456.9	408.9	458.2	408.2	458	24.4	24.9	2	0.49	1.8	0.44	3	0.73	487	532
407.2	456.2	408	457.6	407.1	457.3	24.5	25.1	2.2	0.54	1.4	0.34	3	0.74	487	532
407.8	458.6	408.9	458.9	408.2	457.4	25.4	24.6	1.4	0.34	1.90	0.47	6.6	1.61	487	550
401.8	451.4	410	459.7	407.8	457.6	24.8	24.9	2.3	0.57	2.2	0.54	4	0.98	495	552
407.8	456.8	409.2	458.5	401	450.6	24.5	24.8	2.6	0.64	2.7	0.67	1.5	0.37	488	544
407.5	457.1	nan	nan	408.2	456.8	24.8	24.3	1.6	0.39	2	0.49	3	nan	501	549
40.7	90.1	408.2	457.9	407.9	457.9	24.7	25	1.5	3.69	2.1	0.51	3	0.73	491	546
407.5	457.1	408.9	436.2	407.5	412.5	24.8	2.5	1.9	0.47	2.7	0.66	3	0.73	508	555

Internal Diameter pipe end A [mm]
Outer Diameter pipe end A [mm]
Internal Diameter Body [mm]
Outer Diameter Body [mm]
Internal Diameter pipe end B [mm]
Outer Diameter pipe end B [mm]
Wall Thickness pipe end A [mm]
Wall Thickness pipe end B [mm]
Out of Roundness pipe end A [mm]
Ovality A [%]
Out of Roundness pipe end B [mm]
Ovality pipe end B [%]
Out of Roundness Body [mm]
Ovality Body [%]
Yield Strength [MPa]
Ultimate Tensile Stress [MPa]

E

Semi-correlations

Table E.1: Semi-correlations wall thickness - outer diameter

	$r_{tot,sp}$	$\rho_{NE,ps}$	$\rho_{NW,ps}$	$\rho_{SE,ps}$	$\rho_{SW,ps}$
Data	0.86	0.70	-0.15	0.10	0.71
T	0.85	0.73	0.15	0.21	0.73
Clayton	0.86	0.33	0.12	0.13	0.91
Frank	0.86	0.54	0.17	0.13	0.55
Gumbel	0.86	0.84	0.04	0.08	0.61
Gaussian	0.86	0.70	0.24	0.22	0.72

Table E.2: Semi-correlations yield stress - ultimate tensile strength

	$r_{tot,sp}$	$\rho_{NE,ps}$	$\rho_{NW,ps}$	$\rho_{SE,ps}$	$\rho_{SW,ps}$
Data	0.84	0.48	0.08	0.26	0.51
T	0.82	0.71	0.11	0.15	0.66
Clayton	0.85	0.30	0.14	0.13	0.89
Frank	0.83	0.50	0.13	0.10	0.51
Gumbel	0.84	0.82	0.07	-0.03	0.50
Gaussian	0.84	0.65	0.22	0.26	0.68

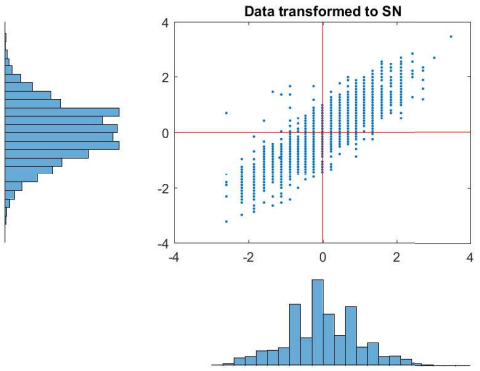

(a) Observed data

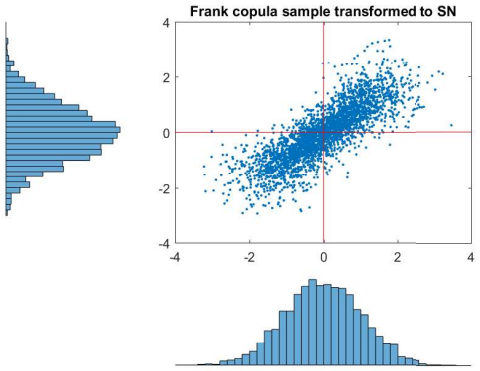

(b) Frank

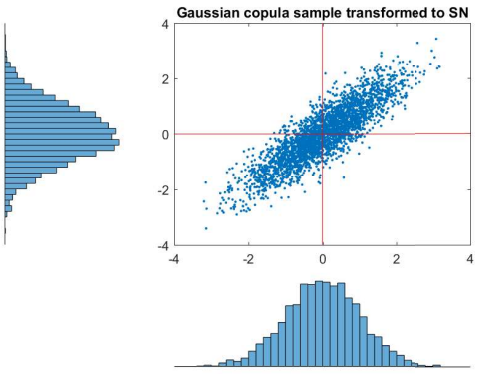

(c) Gaussian

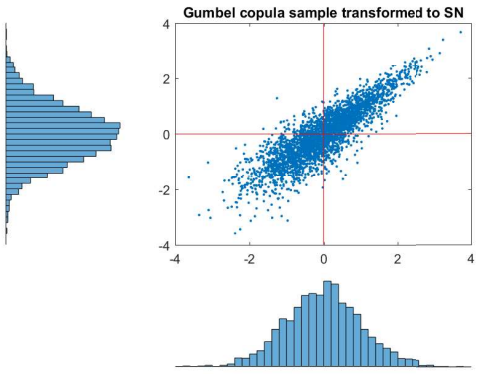

(d) Gumbel

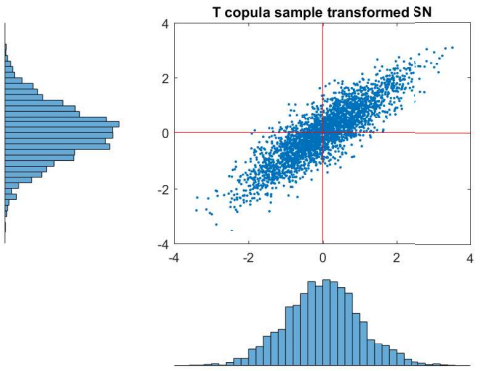

(e) T

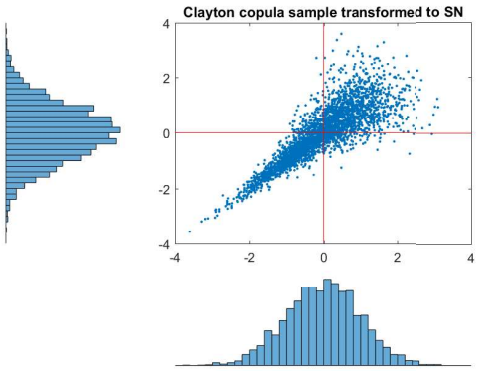

(f) Clayton

Figure E.1: Semi-correlations wall thickness - outer diameter copula models

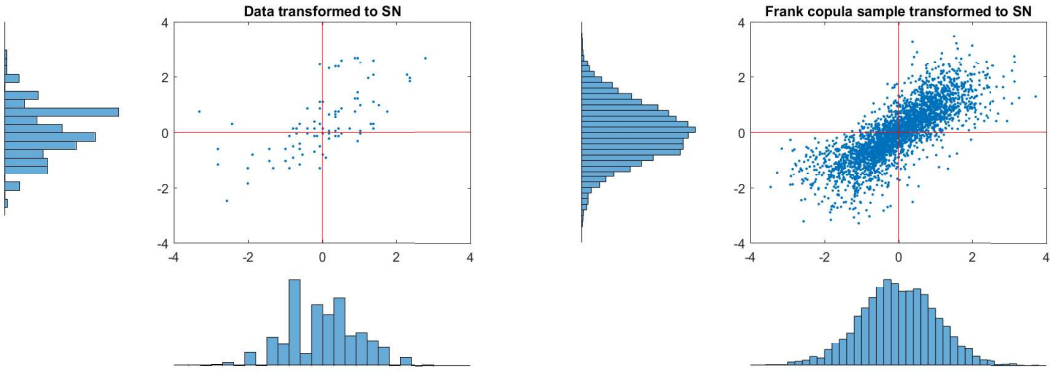

(a) Observed data

(b) Frank

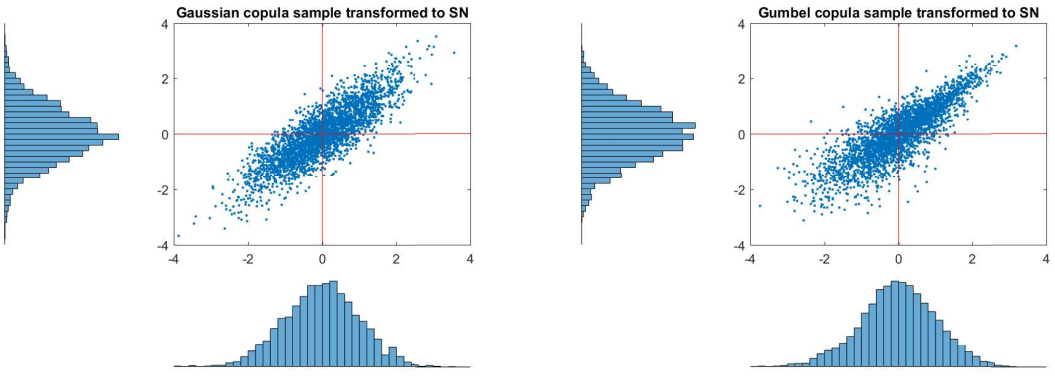

(c) Gaussian

(d) Gumbel

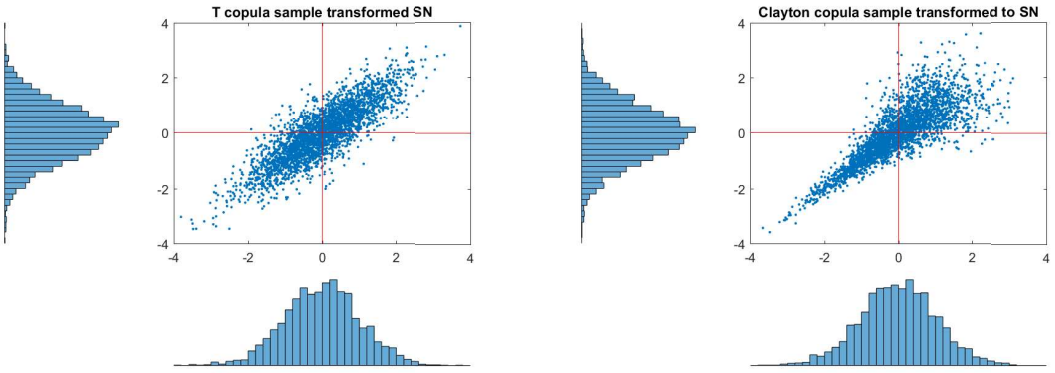

(e) T

(f) Clayton

Figure E.2: Semi-correlations yield stress - ultimate tensile strength copula models

F

Cramér von Mises

Table F.1: Cramér von Mises statistic value WT - OD

Copula model	CM_n
T	8.6349
Clayton	15.4156
Frank	8.0319
Gumbel	9.2252
Gaussian	7.1109

Table F.2: Cramér von Mises statistic value YS - UTS

Copula model	CM_n
T	30.5038
Clayton	30.8183
Frank	28.8728
Gumbel	31.3830
Gaussian	30.2263

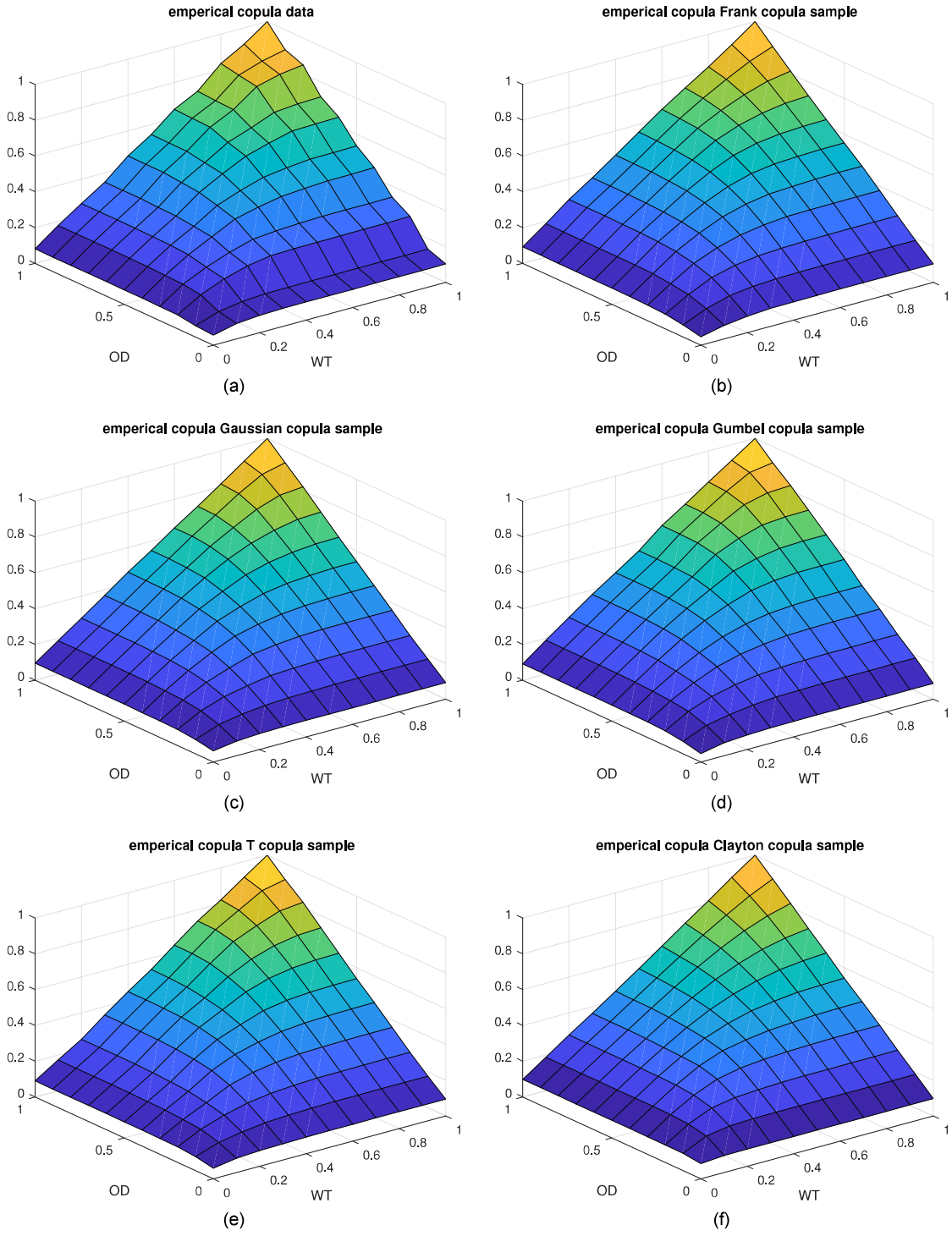

Figure F.1: Empirical copulas different copula models WT - OD

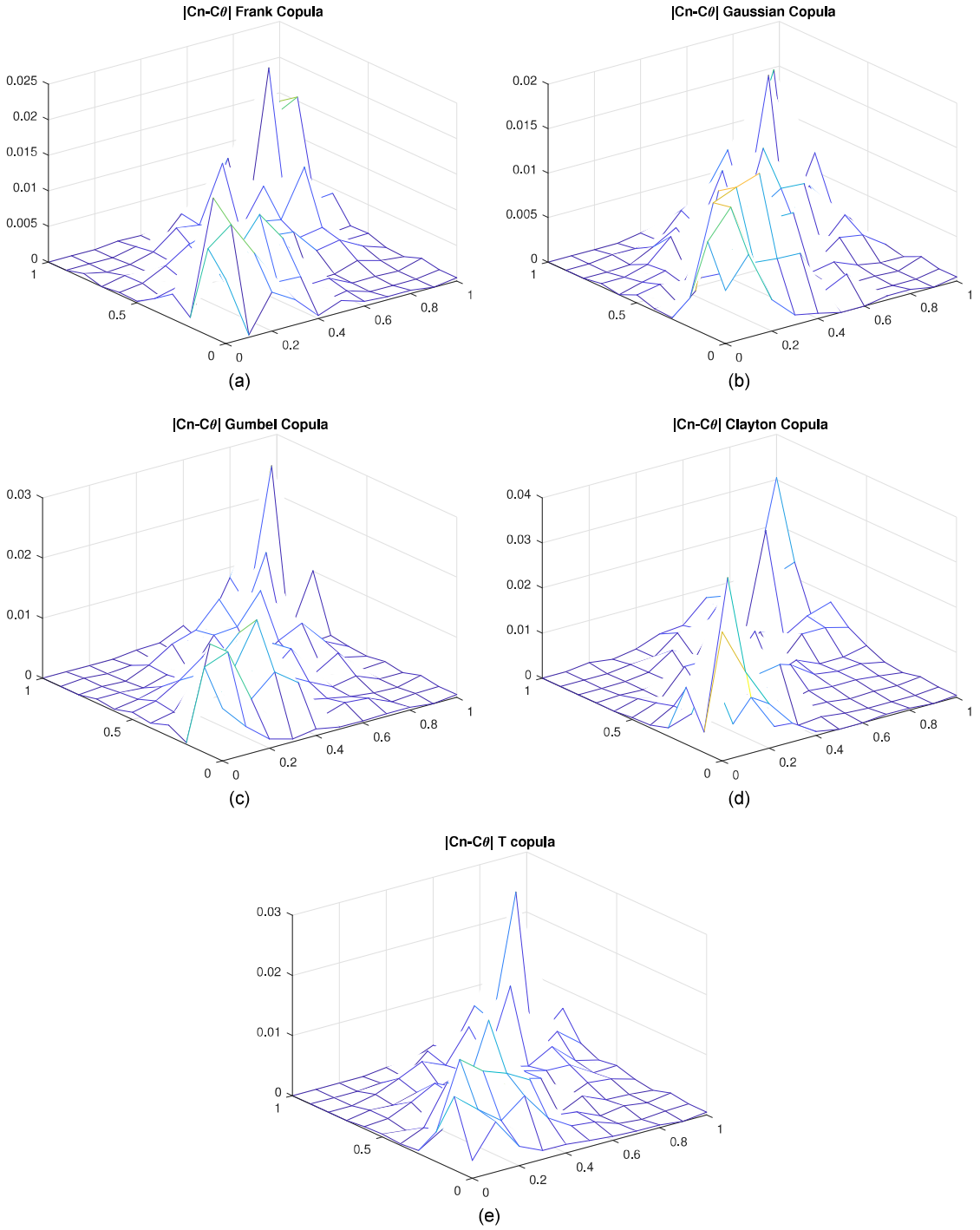

Figure F.2: Absolute difference Empirical copula and different copula models WT - OD

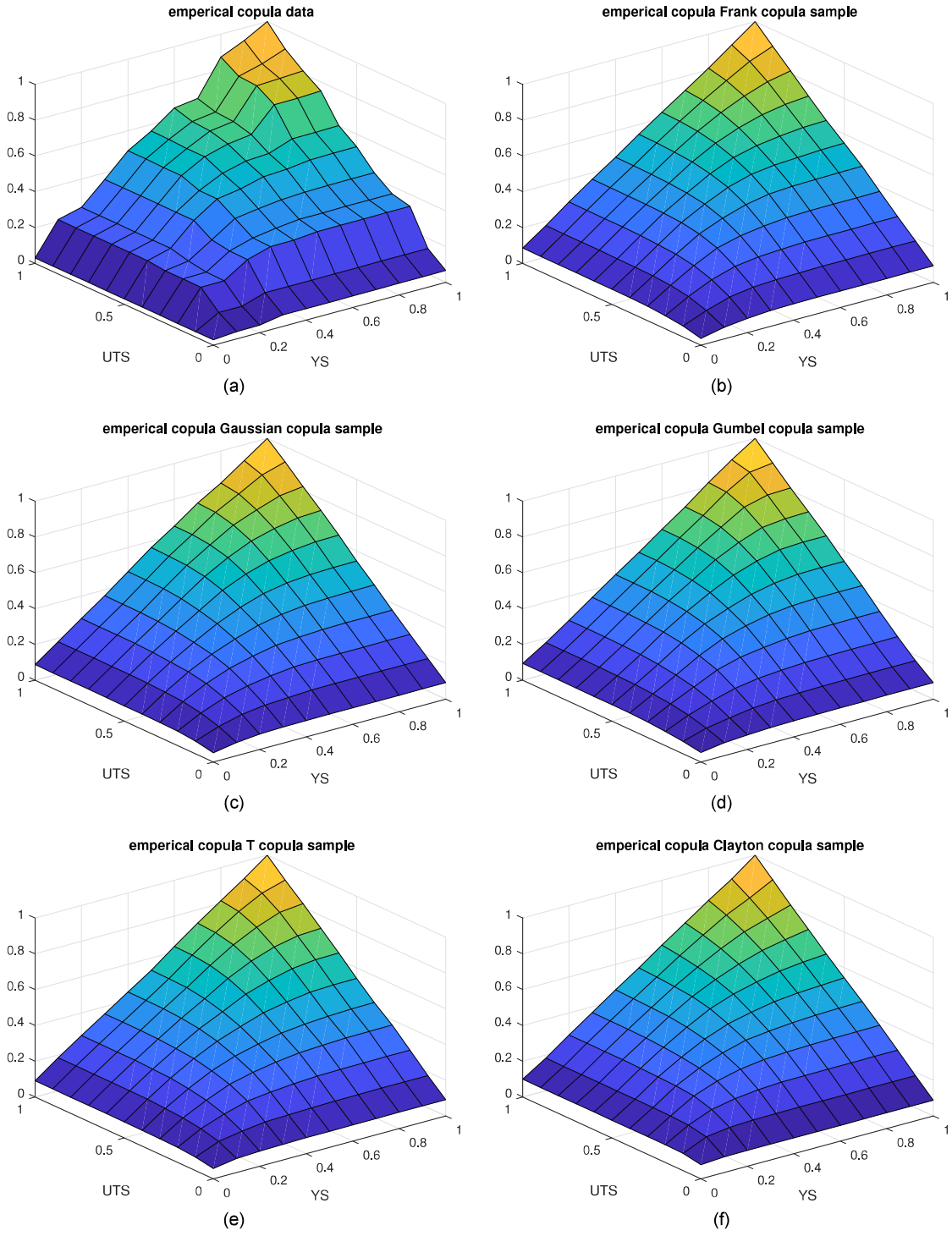

Figure F.3: Empirical copulas different copula models YS - UTS

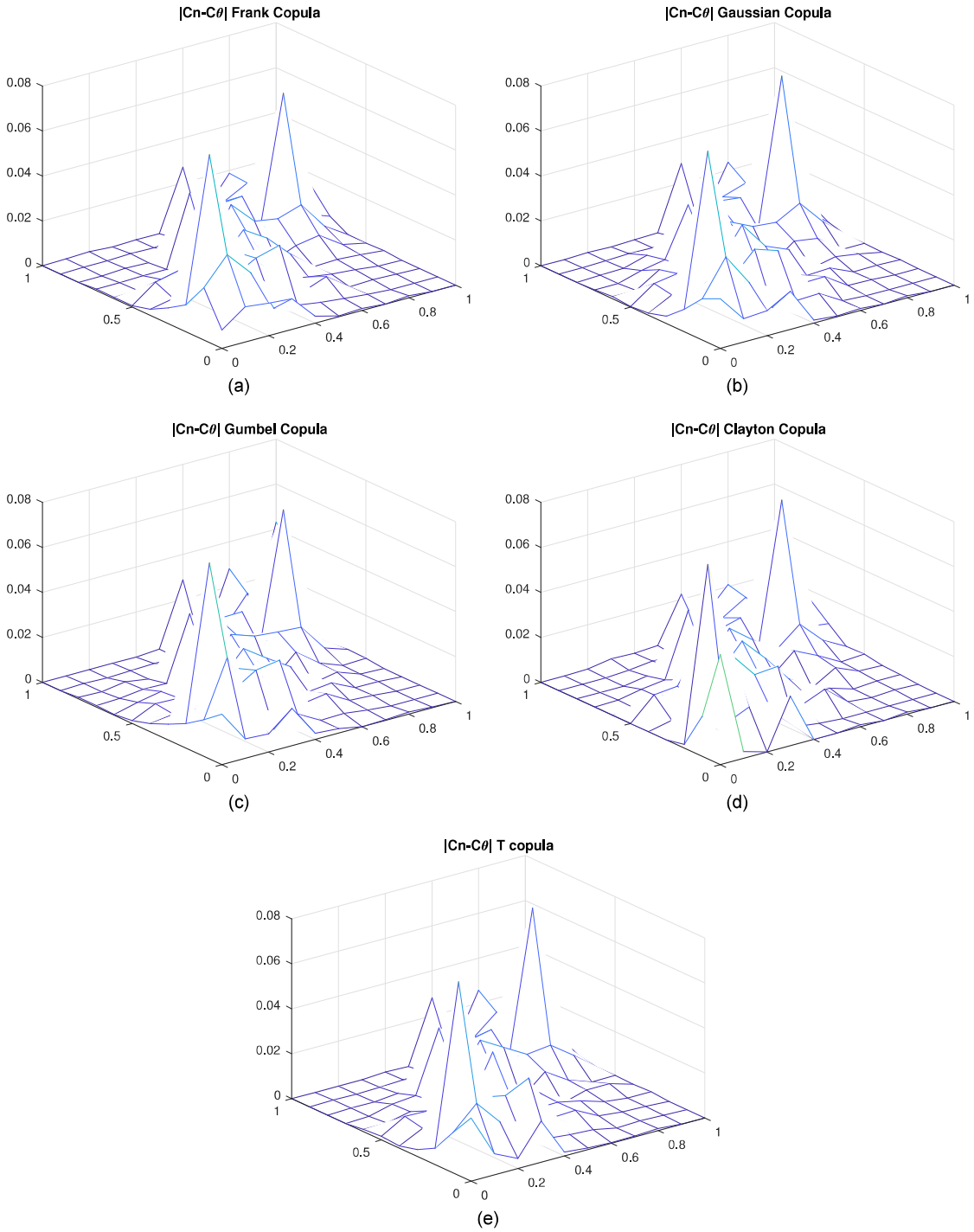

Figure F.4: Absolute difference Empirical copula and different copula models YS-UTS

Ovality

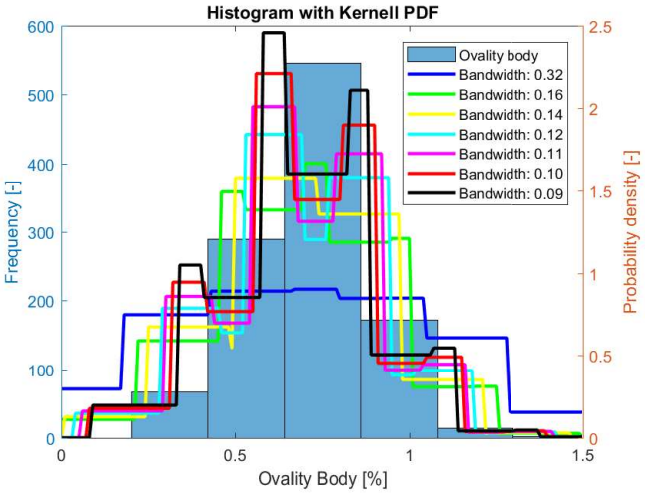

Figure G.1: Kernel distribution - Uniform Kernel

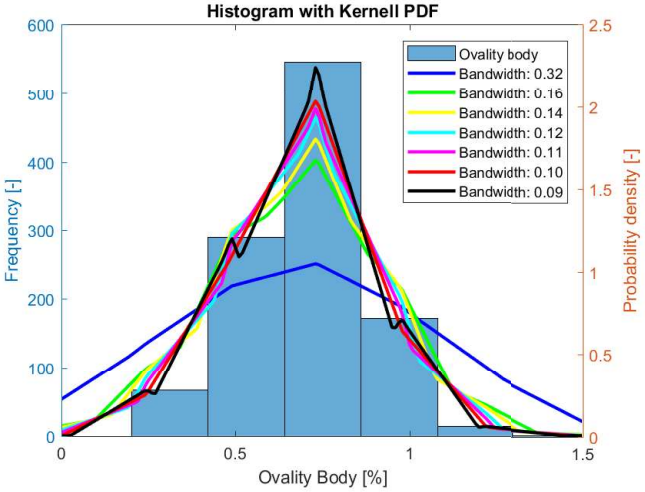

Figure G.2: Kernel distribution - Triangular Kernel

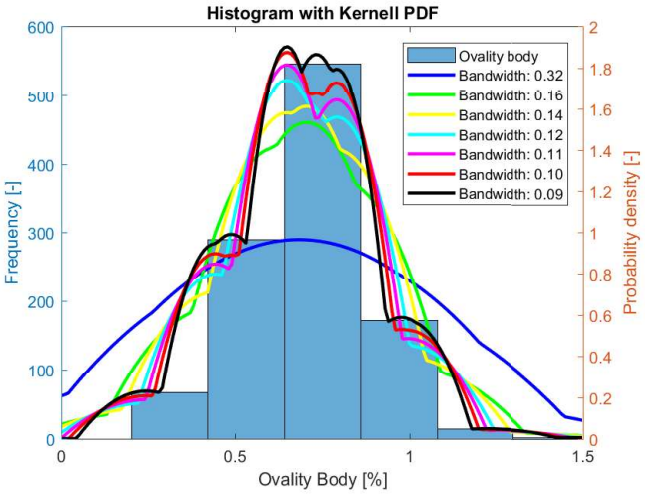

Figure G.3: Kernel distribution - Epanechnikov Kernel

H

Monte Carlo input

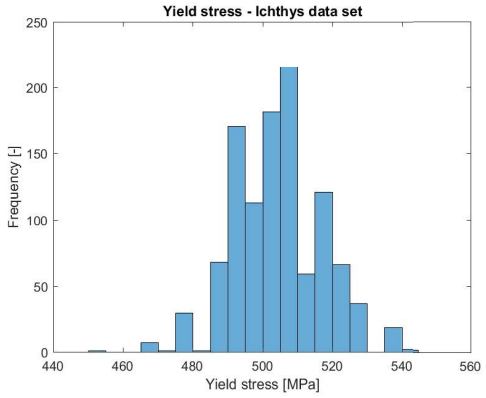

(a) Ichthys data

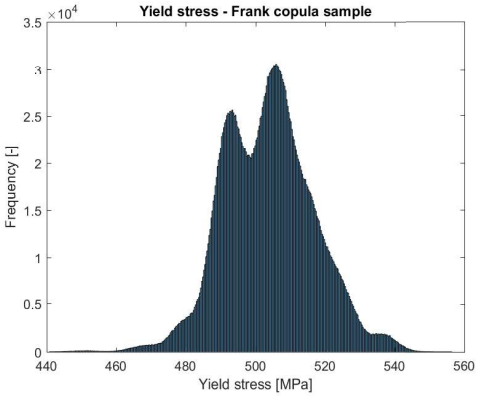

(b) Frank copula sample

Figure H.1: Yield stress empirical data and sample

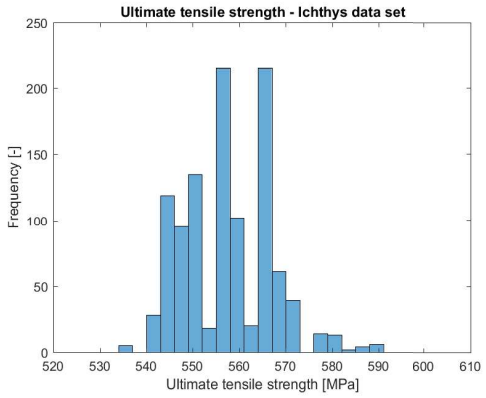

(a) Ichthys data

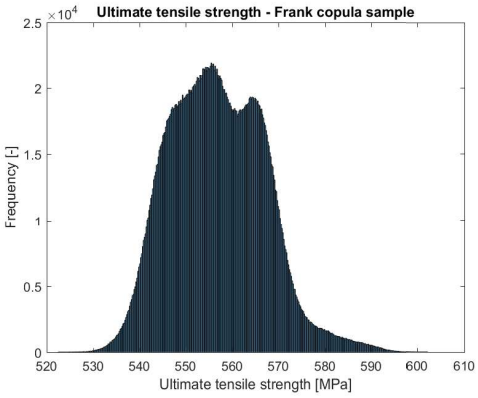

(b) Frank copula sample

Figure H.2: Ultimate tensile strength empirical data and sample

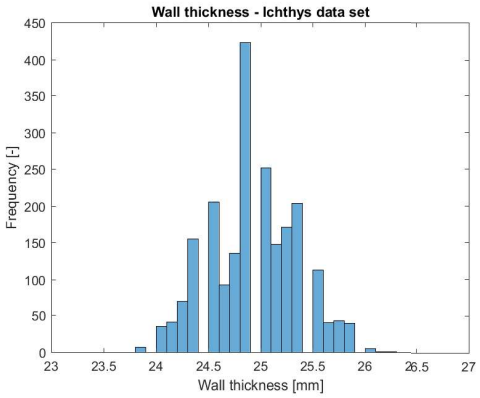

(a) Ichthys data

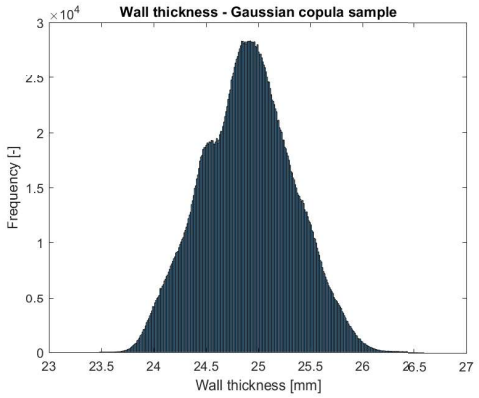

(b) Gaussian copula sample

Figure H.3: Wall thickness empirical data and sample

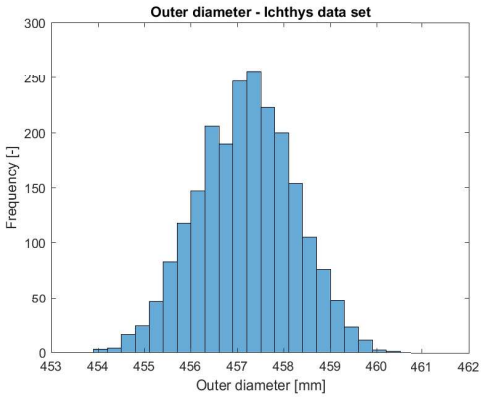

(a) Ichthys data

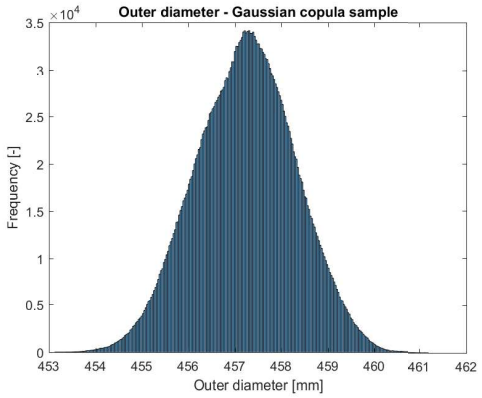

(b) Gaussian copula sample

Figure H.4: Outer diameter empirical data and sample

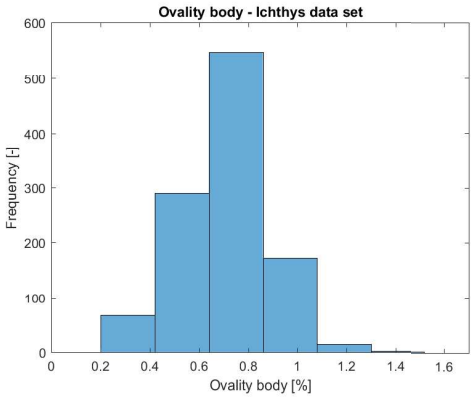

(a) Ichthys data

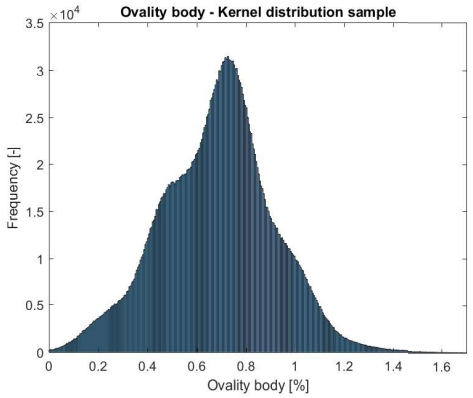

(b) Kernel distribution sample

Figure H.5: Ovality empirical data and sample

Bibliography

[1] Olav Aamlid and DNV GL. R31333-MDR-DNV-CCQ-0057 FE Analysis of Allowable Bending Strains for 18" Lined Pipe. Technical report, 2014.

[2] API. API RP 1111 Design, Construction, Operation and Maintenance of Offshore Hydrocarbon Pipelines (Limit State Design). Technical Report September, 2015.

[3] Butting Germany. 18" LINED LINEPIP DELIVERY - BATCH 1B - DAT BREDERO KUANTAN. Technical report, 2013.

[4] Butting Germany. Clad pipes. *Butting company brochure*, pages 1–12, 2014.

[5] CEN European Committee for Standardization. EN 1990:2002 E, Eurocode - Basis of Structural Design. Technical report, 2001.

[6] DNV GL. DNVGL-ST-F101 Submarine pipeline systems. Technical Report October, 2017. URL https://img1.wsimg.com/blobby/go/34c443fd-26d6-4847-82b6-c31392e5b94d/downloads/1c2g8im4v_104651.pdf.

[7] Christian Genest and Anne-Catherine Favre. Everything You Always Wanted to Know about Copula Modeling but Were Afraid to Ask. *Journal of Hydrologic Engineering*, 12(4):347–368, 2007. ISSN 1084-0699. doi: 10.1061/(ASCE)1084-0699(2007)12:4(347). URL http://ascelibrary.org/doi/10.1061/%28ASCE%291084-0699%282007%2912%3A4%28347%29.

[8] Shanhong; Chacko Jacob; Ghalambor Ali Guo, Boyun; Song. *Offshore Pipelines*. Elsevier, 2005. ISBN 978-0-7506-7847-6.

[9] Heerema Marine Contractors and McDermott. HMC - Flowline Installation - 18" Production 1st End Flet - Installation Analysis. Technical report, 2014.

[10] INPEX. The Ichthys LNG project. Technical report, 2016.

[11] International Energy Agency. World Energy Investment 2017. *International Energy Agency*, 2017. URL https://www.iea.org/publications/wei2017/.

[12] ISO. ISO 13623 Petroleum and natural gas industries - Pipeline transportation systems. Technical Report June, 2009.

[13] S N Jonkman, A C W M Vrouwenvelder, R D J M Steenbergen, O Morales-nápoles, and J K Vrijling. *Probabilistic Design : Risk and Reliability Analysis in Civil Engineering*. 2015.

[14] R R Julien. *Statistical approaches to copula model selection*. PhD thesis, 2015.

[15] Robert E. Kass and Adrian E. Raftery. Bayes Factors. *Journal of the American Statistical Association*, 90(430):773–795, 1995. ISSN 1077-5730. doi: 10.1108/10775730610619007. URL http://www.emeraldinsight.com/doi/10.1108/10775730610619007.

[16] Frank J. Massey. The Kolmogorov-Smirnov Test for Goodness of Fit Author (s): Frank J . Massey , Jr . Published by : Taylor & Francis , Ltd . on behalf of the American Statistical Association Stable URL : http://www.jstor.org/stable/2280095 Accessed : 30-06-2016 18 : 58. *Journal of the American Statistical Association*, 46(253):68–78, 1951.

[17] Gerard Poort and Heerema Marine Contractors. MEM-094 - FE Analysis of Allowable Bending Strains for 18" Lined Pipe. 2014.

[18] Stefanie Scheid. Introduction to kernel smoothing, 2004. URL http://compdiag.molgen.mpg.de/docs/talk_05_01_04_stefanie.pdf%0A%0A.

[19] Tenaris. Welded pipe manufacturing, 2014. URL http://www.tenaris.com/en/AboutUs/ProductionProcesses.aspx.

[20] Vose Software. Archimedean copulas - Clayton, Frank and Gumbel, . URL https://www.vosesoftware.com/riskwiki/Archimedeancopulas-theClaytonFrankandGumbel.php.

[21] Vose Software. Elliptical copulas - Normal and T, . URL https://www.vosesoftware.com/riskwiki/Ellipticalcopulas-NormalandT.php.

[22] Wood Group. Flexcom Brochure 2018, 2018.